Coupled magnetic and structural transitions in high-purity Dy and $Gd_5Sb_xGe_{4-x}$

by

Alexander S. Chernyshov

A dissertation submitted to the graduate faculty

in partial fulfillment of the requirements for the degree of

DOCTOR OF PHILOSOPHY

Major: Materials Science and Engineering

Program of Study Committee:
Vitalij K. Pecharsky, Co-major Professor
Karl A. Gschneidner, Jr., Co-major Professor
R. William McCallum
Robert J. McQueeney
Xiaoli Tan

Iowa State University

Ames, Iowa

2006

Copyright © Alexander Chernyshov, 2006. All rights reserved.

Graduate College
Iowa State University

This is to certify that the doctoral dissertation of

Alexander S. Chernyshov

has met the dissertation requirements of Iowa State University

Co-major Professor

Co-major Professor

For the Major Program

TABLE OF CONTENTS

ABSTRACT v

CHAPTER 1: INTRODUCTION 1

Literature review 2
Dysprosium 2
Expected crystal and magnetic structures of the $Gd_5Sb_xGe_{4-x}$ system 5
Dissertation organization 7
References 8

CHAPTER 2: MAGNETIC AND MAGNETOCALORIC PROPERTIES, AND MAGNETIC PHASE DIAGRAM OF SINGLE CRYSTAL DYSPRODIUM 11

Abstract 11
Introduction 12
Experimental details 17
Results 20
Magnetic properties 20
Magnetothermal properties 26
AFM $\rightarrow$ FM phase transition 31
Commensurability effects 32
The fan phase 41
The vicinity of Neél and tri-critical points 44
Impurity effects 46
Magnetocaloric effect 48
Conclusion 53
Acknowledgements 53
References 54

CHAPTER 3 CRYSTALLOGRAPHIC STUDY OF DYSPROSIUM 57

Abstract 57
Introduction 58
Experimental details 60
Results 62
Discussion 70
Conclusion 73
Acknowledgements 73
References 73

CHAPTER 4: STRUCTURAL AND MAGNETO-THERMAL PROPERTIES OF THE $Gd_5Sb_xGe_{4-x}$ SYSTEM 75

Abstract 75
Introduction 76
Experimental details 76
Results 77
Discussion 81
Conclusion 82
Acknowledgements 82
References 82

CHAPTER 5: CRYSTALLOGRAPHIC AND MAGNETIC PROPERTIES OF THE $Gd_5Sb_{0.5}Ge_{3.5}$ SINGLE CRYSTAL 84

Abstract 84
Introduction 85
Experimental details 88
Results 90
Discussion 100
Coupled magnetic-structural transition in $Gd_5Sb_{0.5}Ge_{3.5}$ 101
Appearance of a Griffiths-like phase in $Gd_5Sb_{0.5}Ge_{3.5}$ 102
Model of the electronic transition in Gd_5Ge_4 and $Gd_5Sb_{0.5}Ge_{3.5}$ 104
Conclusion 114
Acknowledgements 115
References 115

GENERAL CONCLUSIONS 118

Dysprosium 118
$Gd_5Sb_xGe_{4-x}$ 119
Recommendations for future work 121

ACKNOWLEDGEMENTS 123

APPENDIX: MAGNETIC STRUCTURES OF DYSPROSIUM 124

IS-T 2567

ABSTRACT

Magnetic materials exhibiting magnetic phase transitions simultaneously with structural rearrangements of their crystal lattices hold a promise for numerous applications including magnetic refrigeration, magnetomechanical devices and sensors.

We undertook a detailed study of a single crystal of dysprosium metal, which is a classical example of a system where magnetic and crystallographic sublattices can be either coupled or decoupled from one another. Magnetocaloric effect, magnetization, ac magnetic susceptibility, and heat capacity of high purity single crystals of dysprosium have been investigated over broad temperature and magnetic field intervals with the magnetic field vector parallel to either the *a*- or *c*-axes of the crystal. Notable differences in the behavior of the physical properties when compared to Dy samples studied in the past have been observed between 110 K and 125 K, and between 178 K and ~210 K. A plausible mechanism based on the formation of antiferromagnetic clusters in the impure Dy has been suggested in order to explain the reduction of the magnetocaloric effect in the vicinity of the Neél point. Experimental and theoretical investigations of the influence of commensurability effects on the magnetic phase diagram and the value of the magnetocaloric effect have been conducted. The presence of newly found anomalies in the physical properties has been considered as evidence of previously unreported states of Dy. The refined magnetic phase diagram of dysprosium with the magnetic field vector parallel to the *a*-axis of a crystal has been constructed and discussed.

The magnetic and crystallographic properties of $Gd_5Sb_xGe_{4-x}$ pseudo-binary system were studied by x-ray diffraction (at room temperature), heat capacity, ac- magnetic susceptibility, and magnetization in the temperature interval 5-320 K in magnetic fields up to 100 kOe. The magnetic properties of three composition (x = 0.5, 1, 2) were examined in detail. The $Gd_5Sb_2Ge_2$ compound that adopts $Tm_5Sb_2Si_2$-type of structure (space group is Cmca), shows a second order FM-PM transition at 200 K, whereas $Gd_5Sb_xGe_{4-x}$ compounds for x=0.5 and x=1 (Sm_5Ge_4-type of structure, space group is Pnma) exhibit first order phase transformations at 45 K and 37 K, respectively.

The detailed investigation of crystallographic, magnetic, thermal and electronic properties of $Gd_5Sb_{0.5}Ge_{3.5}$ single crystal shows that the compound undergoes a coupled magnetic-structural transition at 40 - 70 K and an electronic transition around 60 K. The low temperature crystallographic study shows that unlike in other 5:4 materials with such a large volume change (0.5 %), the coupled magnetic structural transition in $Gd_5Sb_{0.5}Ge_{3.5}$ occurs without changing symmetry of the lattice. The magnetic and structural properties exhibit a narrower temperature and magnetic field hystereses associated with a first order transition compared to $Gd_5(Si_xGe_{1-x})_4$, which may be important for practical applications. Low magnetic field data show a clear presence of a complicated short range magnetic ordering ("Griffiths" phase) in the temperature interval from 40 to 250 K. The model that quantitatively describes electronic transition in $Gd_5Sb_{0.5}Ge_{3.5}$ and Gd_5Ge_4 is proposed.

CHAPTER 1: INTRODUCTION

In the past, the magnetic and thermal properties of single crystal Dy were studied by various authors using different samples, and often low purity; sometimes impurities and their contents have not been quantified. Consequently, it is rather difficult to compare the results obtained by various authors in an attempt to develop a clear picture describing the nature of multiple phase transitions observed in the elemental Dy as a function of temperature and magnetic field. To the best of our knowledge, a thorough investigation of the magnetothermal properties of this lanthanide metal employing a variety of experimental techniques with the magnetic field applied along different crystallographic directions in the same quality crystals obtained from a single initial batch of Dy was not conducted heretofore.

The magnetic properties of $R_5(Si_xGe_{1-x})_4$ system, where R-is a lanthanide metal, have been extensively studied since 1997 when V.K. Pecharsky and K.A.Gschneidner, Jr. (Ref 1) discovered the giant magnetocaloric effect in $Gd_5Si_2Ge_2$ compound. Due to the first order coupled structural magnetic phase transitions in the $R_5(Si_xGe_{1-x})_4$ compounds a series of extraordinary magnetic phenomena, such as a giant magnetostriction[2] and giant magnetoresistance,[3] have been observed in addition to the giant magnetocaloric effect. Interest in these materials is strong because of future economical benefits, i.e. potential application of $Gd_5Ge_2Si_2$ and related compounds in room temperature magnetic refrigeration. Later studies of $Gd_5(Ge_xGa_{1-x})_4$ system[4] showed similar mechanism of martensitic/magnetic transition as in case of $Gd_5Ge_2Si_2$ (see Ref 5) due to partially broken interlayer T-T bonds, where T is a statistical mixture of (Ge, Si) or (Ge, Ga). Reference 4 also suggested that lack of one electron in the outer shell of Ga (3 valence electrons for Ga instead of 4 for Si) drives the phase transformation in $Gd_5(Ge_xGa_{1-x})_4$ system by changing valence electron concentration. Therefore it is natural to try to shift valence electron concentration in the opposite direction by adding 5 valence electrons antimony instead of four valent silicon. The other advantage of an additional electron might be improvement of mechanical, thermal and electrical properties.

Literature review

Dysprosium

A comprehensive investigation of the magnetic and thermal properties of high purity single crystals of Dy has considerable fundamental importance because the nature of magnetic phase transitions may be strongly affected by the presence of H, C, N, O, and/or F in the studied material.[6] As we will show below, the magnetic phase diagram constructed using the results obtained from a high purity Dy contains several anomalous features and phases that were likely masked by interstitial impurities, and therefore, left undetected in previous studies. Future theoretical investigations and neutron and/or x-ray scattering experiments should be conducted to gain a better understanding of the nature and behavior of the magnetic structure of Dy in these regions of temperature and magnetic fields. Such studies are especially important because it is also known that in low-purity single crystals of Dy, magnetic phase transitions have features typical of the coexisting first- and second-order phase transformations.

In addition to furthering basic understanding of the relationships between structure and magnetism, Dy may be considered a classical example of a magnetic material where in certain regions of temperature and magnetic fields, a first-order magnetic phase transition coincides with a first-order structural transformation (in a zero magnetic field both transitions occur at ~90 K). Recent advancements in understanding complex intermetallic compounds[7] indicate that materials with combined magnetic-crystallographic transformations have a potential for practical applications, e.g., in energy efficient and environmentally benign magnetic refrigeration. Presently, compounds with coupled magnetic and structural phase changes are believed to be the most promising class of materials[8, 9, 10, 11] for future applications in magnetic cooling and heating.

The rare-earth metal dysprosium (Dy) has one of the largest magnetic moments in the lanthanide series, which for the free trivalent ion reaches $p_{eff} = g\sqrt{J(J+1)} = 10.65\mu_B$, where g is the gyromagnetic factor, J is the total angular momentum quantum number and μ_B is the Bohr magneton. In the ferromagnetically ordered state, the spontaneous magnetic

moment of Dy is slightly lower, i.e., $m = gJ = 10\mu_B$. The metal exhibits numerous magnetic phase transitions as temperature and/or magnetic field vary. In a zero magnetic field, Dy is in the paramagnetic (PM) state above its Neél temperature, $T_N \cong 180$ K. At ~180 K, elemental Dy transforms into a helical antiferromagnetic (AFM) phase (see Fig. 1 in the Appendix), which is stable between ~90 K and ~180 K. At the Curie temperature, $T_C \cong 90$ K, the metal orders ferromagnetically (FM) and remains in this state down to the lowest reported temperature of 4.2 K.[12, 13, 14, 15] The transition between the AFM and FM phases at the Curie temperature is first-order, while that between the AFM and PM states at the Neél point is a second-order transformation. The intermediate fan magnetic structure (Fig. 1, Appendix) emerges between the AFM and FM phases in a certain range of non-zero magnetic fields between ~127 K and ~180 K. [15] A tri-critical point on the phase diagram, where, in agreement with the Landau theory, the nature of the AFM ↔ fan transition changes from first- to second-order, is located near 165 K.[16]

In a zero magnetic field, the first-order phase transition from a helical AFM to a collinear FM state occurs simultaneously with the orthorhombic distortion of the hexagonal close-packed structure of the metal.[17] Above the Neél point, no short range magnetic order has been observed by neutron scattering.[18, 19] The x-ray diffraction investigation in low magnetic fields ($H \leq 1$ kOe), carried out in the vicinities of both the Curie and Neél temperatures, revealed a broad region where the AFM and FM phases coexist.[20] Kida *et al.*[21] reported similar observations in magnetic fields higher than 1 kOe. The crystallographic transition in Dy is preserved in non-zero magnetic fields, but according to Vorob'ev *et al.*,[20] the structural distortion is shifted to a higher temperature by ~3 K in a 1 kOe magnetic field when compared to that in a zero field. This result agrees with both the magnetization [15] and magnetocaloric effect (MCE)[16] data.

Thermal expansion[22, 23] and heat capacity[24] measured in a zero magnetic field reveal additional anomalies, such as steps and sudden slope changes, which were explained by temperature dependent changes in the commensurability between the magnetic and crystallographic lattices. The correspondence between the anomalies and commensurability points was considered by Greenough *et al.*[25] with the objective to understand the nature of

the complex temperature dependence of the thermal expansion and elastic constants in a zero magnetic field, and to relate the changes of the magnetic structure studied by neutron scattering with the elastic properties of Dy.

As mentioned above, the AFM ↔ PM magnetic transition in Dy is a second-order transformation, in agreement with the conventional theory of phase transformations. It is supported by the following experimental observations.

i. The H–T diagram of Dy contains a tricritical point at $T = \sim 165$ K and $H = \sim 11$ kOe, where the first-order AFM ↔ FM (or AFM ↔ fan) transition becomes a second-order transformation. Thus, at least the boundary of the AFM ↔ fan transition approaches the zero magnetic field Neél point as a second-order transformation.

ii. The AFM ↔ fan transition takes place over a broad range of magnetic fields, and therefore, has a continuous character.

iii. The magnetic field hysteresis is absent in the range from the tricritical point (~165 K) to the Neél temperature (180 K).

Nevertheless, the presence of temperature hysteresis near the AFM ↔ PM phase transition, detected by heat capacity [24] and other properties measurements, including magnetic field hysteresis of the magnetization in pulsed magnetic fields near the Neél temperature,[26] points to a mixed character of this phase transition. The presence of the extended temperature hysteresis in the paramagnetic region supports the notion about the existence of AFM clusters in the PM phase matrix. Both the amount and size of these clusters decrease with the increasing temperature, and the paramagnetic phase becomes uniform and homogeneous only at temperatures approximately 30 K to 50 K above the Neél point.[27]

The most recent magnetic phase diagrams of Dy [24] indicate the presence of an unknown magnetic phase (the so called "fan II" phase) inside the well-known fan phase region in the temperature interval from ~170 K to ~180 K and in magnetic fields between 12 kOe and 25 kOe. The x-ray diffraction investigations [21] revealed anomalies of the temperature dependence of the c-axis and thermal expansion in this region, but both of them

can be explained without assuming the presence of an additional phase. Neutron scattering data reveal differences in scattering from the conventional "fan" and the new "fan II" phases.[28]

Expected crystal and magnetic structures of the $Gd_5Sb_xGe_{4-x}$ system

Taking into account that no literature data have been found on $Gd_5Sb_xGe_{4-x}$ pseudo-binary system, we will discuss below the known crystallographic and magnetic properties observed in of the $Gd_5(Si_xGe_{1-x})_4$ and $Gd_5(Ga_xGe_{1-x})_4$ systems.

Three different crystal structures are found in $Gd_5(Si_xGe_{1-x})_4$ pseudo-binary system. They are presented in Fig. 1:

(1) an orthorhombic Sm_5Ge_4-type (space group is Pnma) with all of the T-T dimers between ${}^{2}_{\infty}[Gd_5T_4]$ slabs broken (see Fig. 1. (a)), where T is a statistical mixture of Ge and Si and the top ${}^{2}_{\infty}[Gd_5T_4]$ slab is marked by a shaded rectangle in $Gd_5(Si_xGe_{1-x})_4$).

(2) a monoclinic $Gd_5Ge_2Si_2$-structure type (space group is $P112_1/a$) with half of the T-T interslab dimers broken (see Fig. 1. (b)).

(3) an orthorhombic Gd_5Si_4-structure type (space group is Pnma) with T-T interslab dimers between ${}^{2}_{\infty}[Gd_5T_4]$ slabs (see Fig. 1. (c).

Changing concentration (the Si to Ge atoms ratio), temperature, pressure, or magnetic field [5,2,7] half or all of the interslab T-T dimers may break or reform, driving reversible first order structural phase transformations between the above mentioned crystal structures. The structural transformation is strongly coupled with drastic changes in the magnetic properties because of a Ruderman-Kittel-Kasuya-Yoshida (RKKY) exchange between Gd atoms. The RKKY exchange is known to have an oscillating character depending on distances between magnetic atoms and, therefore, it is very sensitive to any changes in crystal structure[5]. Thus, coupling between magnetic and crystal structures brings about some extreme magnetic effects, such as the giant magnetocaloric effect[1], giant magnetostriction [2], and giant magnetoresistance [3].

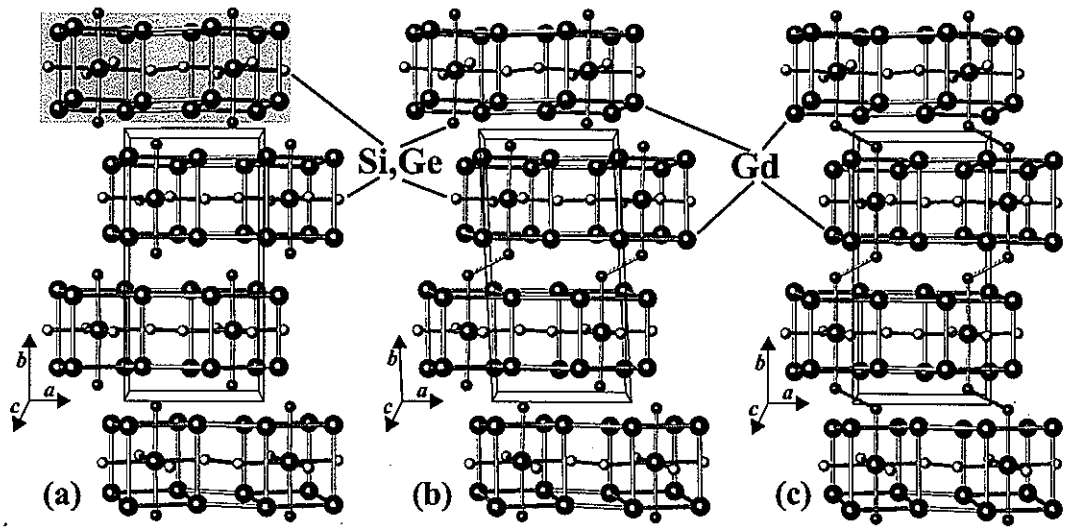

FIG. 1. -- Three types of crystal structure in the $Gd_5(Si_xGe_{1-x})_4$ system: (a) Sm_5Ge_4-type, (b) $Gd_5(Si_2Ge_2)$-type, (c) Gd_5Si_4-type. A shaded rectangle marks a ${}^{2}_{\infty}[Gd_5T_4]$ slab. Large black spheres represent Gd atoms, small gray spheres represent interslab Si and/or Ge atoms (the T-atoms, see text), small black spheres represent the T atoms, which are responsible for the interslab bonds.

Recent studies of the $Gd_5(Ga_xGe_{1-x})_4$ system [4] showed that replacement of 4-valent silicon by 3-valent Ga affects the interslab T-T interactions and, consequently, the inter-atomic distances and crystal structure themselves. It drives a phase transformation from the orthorombic Sm_5Ge_4-type (stable at 30-31 electrons per formula unit) to orthorhombic Gd_5Si_4-type (with 29-30 electrons per formula unit) by creating additional T-T bonds. Actually, tight-binding linear-muffin-tin-orbital calculations [4] showed that the trivalent Ga decreases and that the tetravalent Ge increases population of the antibonding states within the dimers, and consequently increasing the valence electron count results in the breaking of dimers. Thus, it was interesting to check the influence of increasing the number of valence electrons in a Gd_5T_4 system by substitution of the 4-valent Ge by the semi-metallic 5-valent electrons antimony. Of course, germanium can be replaced by arsenic, which has a closer atomic radius to the one of Ge, but arsenic is toxic, so we decided to work with a safer antimony instead of arsenic.

The crystallographic study of some $R_5(Sb,\{Si,Ge\})_4$ compounds[29], were R- is a rare-earth metal, showed the existence of a new, higher symmetry structure type in the $R_5(T,Sb)_4$ systems, called $Tm_5Sb_2Si_2$ – type structure. It adopts an orthorhombic symmetry with the space group Cmca. The $Tm_5Sb_2Si_2$ – type structure is close to Sm_5Ge_4 –type structure, but it has a higher symmetry. Authors [29] reported a variety of compounds with heavy rare-earth metals, however they did not observe a $Gd_5Sb_xGe_{4-x}$ solid solution, probably because of low purity of their Gd metal.

Dissertation organization

This dissertation is written in an alternate format composed of original published papers or already drafted, preceded with a general introduction and conclusion chapters. References cited within each chapter have been placed immediately after the chapter.

The first paper, presented in Chapter 2, "Magnetic and magnetocaloric properties, and magnetic phase diagram of single crystal dysprosium" was published in *Physical Review B* in 2005. The authors were A.S. Chernyshov (graduate student and primary researcher at the Materials Science and Engineering Department of Iowa State University and the Ames Laboratory of the U.S. Department of Energy (DOE)), A.O. Tsokol (assistant scientist at the Ames Laboratory of the U.S. DOE), A.M. Tishin (Leading scientist, department of physics, M.V. Lomonosov Moscow State University), K.A. Gschneidner, Jr. (graduate advisor at the Materials Science and Engineering Department of Iowa State University and senior metallurgist at the Ames Laboratory of the U.S. DOE) and V.K. Pecharsky (graduate advisor at the Materials Science and Engineering Department of Iowa State University and senior scientist at the Ames Laboratory of the U.S. DOE). This paper presents the results of detailed investigation of magnetic and thermal properties of a high-purity single crystal.

The second manuscript, presented in Chapter 3, "Crystallographic study of dysprosium" has been prepared for publication. The authors are A.S. Chernyshov, Ya.S. Mudryk (assistant scientist at the Ames Laboratory of the U.S. DOE), V.K. Pecharsky and K.A. Gschneidner, Jr.. This manuscript presents the results of X-ray powder diffraction study of Dy at low temperatures in applied magnetic fields.

The third paper, presented in Chapter 4, "Structural and magneto-thermal properties of the $Gd_5Sb_xGe_{4-x}$ system" was published in the *Journal of Applied Physics* and is based on the poster presentation given by A.S. Chernyshov at the 50-th Magnetism and Magnetic Materials Conference in November of 2005. The authors were A.S. Chernyshov, Ya.S. Mudryk, V.K. Pecharsky and K.A. Gschneidner, Jr. This manuscript presents the results of a study of the structural, magnetic and thermal properties of the $Gd_5Sb_xGe_{4-x}$ system.

The fourth manuscript, presented in Chapter 5, "Crystallographic, magnetic and electronic properties of $Gd_5Sb_{0.5}Ge_{3.5}$ single crystal" has been prepared for publication. The authors are A.S. Chernyshov, Ya.S. Mudryk, V.K. Pecharsky and K.A. Gschneidner, Jr. This manuscript presents the results of a low temperature X-ray powder diffraction study, electrical resistivity and magnetic measurements on a $Gd_5Sb_{0.5}Ge_{3.5}$ single crystal in applied magnetic fields.

References

[1] V.K. Pecharsky, K.A. Gschneidner, Jr., Phys. Rev. Lett. **78**, 4494 (1997)

[2] L. Morellon, P.A. Algarabel, M.R. Ibarra, J. Blasco, B. Garcia-Landa, Z. Arnold, and F. Albertini, Phys. Rev. B **58**, R14721-R14724 (1998)

[3] E.M. Levin, A.O. Pecharsky, V.K. Pecharsky, and K.A. Gschneidner, Jr., Phys. Rev. B **63**, 064426/1-064426/10 (2001)

[4] Yurij Mozharivskyj, Wonyoung Choe, Alexandra O. Pecharsky, and Gordon J. Miller, J. Amer. Chem. Soc. **125**, 15183(2203).

[5] W. Choe, V.K. Pecharsky, A.O. Pecharsky, K.A. Gschneidner, Jr., V.G. Young, Jr., G.J. Miller, Phys. Rev. Lett. **84**, 4617(2000)

[6] K. A. Gschneidner, Jr., J. Alloys Compds. **193**, 1 (1993).

[7] V. K. Pecharsky and K. A. Gschneidner, Jr., Adv. Mater. **13**, 683 (2001).

[8] K. A. Gschneidner, Jr. and V. K. Pecharsky, in *Intermetallic Compounds. Principles and Practice*, edited by J. H. Westbrook and R.L. Fleischer (John Wiley & Sons, New York, 2002), Vol. **3**, p.519.

[9] V. K. Pecharsky, A. P. Holm, K. A. Gschneidner, Jr., and R. Rink, Phys. Rev. Lett. **91**, 197204 (2003).

[10] L. Morellon, Z. Arnold, C. Magen, C. Ritter, O. Prokhnenko, Y. Skorokhod, P. A. Algarabel, M. R. Ibarra, and J. Kamarad, Phys. Rev. Lett. **93**, 137201 (2004).

[11] A. M. Tishin and Y. I. Spichkin, *The Magnetocaloric Effect and its Applications* (Institute of Physics, Bristol and Philadeplphia, 2003), 475 pp.

[12] J. Jensen and A. R. Mackintosh, *Rare earth magnetism: structure and excitations* (Clarendon Press, Oxford, 1991), 12 pp.

[13] S. Legvold, in *Ferromagnetic Materials*, edited by E. P. Wohlfarth (North-Holland, Amsterdam, 1980), Vol. **1**, Chap. 3, p.183.

[14] K. A. McEwen, in *Handbook on the Physics and Chemistry of Rare Earths*, edited by K. A. Gschneidner, Jr. and L. Eyring (North-Holland, Amsterdam, 1978), Vol. **1**, Chap. 6, p.411.

[15] R Hertz and H. Kronmüller, J.Magn. Magn. Mater. **9**, 273 (1978).

[16] S. A. Nikitin, A. S. Andreenko, and V. A. Pronin, Fiz. Tverd. Tela (Leningrad) **21**, 2808 (1979).

[17] V. A. Finkel, *The structure of rare earths* (Metallurgiya, Moscow, 1978), 6 pp.

[18] V. G. Bessergenev, V. V. Gogava, Yu. A. Kovalevskaya, A. G. Mandzhavidze, V. M. Fedorov, and S. I. Shilo, Pis'ma Zh. Eksp. Teor. Fiz. **42**, 412 (1985).

[19] V. G. Bessergenev, V. V. Gogava, A. G. Mandzhavidze, V. M. Fedorov, and S. I. Shilo, Pis'ma Zh. Eksp. Teor. Fiz. **47**, 92 (1988).

[20] V. V. Vorob'ev, M. Ya. Krupotkin, and V. A. Finkel, Sov. Phys. JETP **61**, 1056 (1985).

[21] Y. Kida, K. Tajima, Y. Shinoda, K. Hayashi, and H. Ohsumi, J. Phys. Soc. Jpn. **68**, 650 (1999).

[22] E. B. Amitin, V. G. Bessergenev, and Yu. A. Kovalevskaya, J. Phys. F **14**, 2935 (1984).

[23] Y. Shinoda and K. Tajima, J. Phys. Soc. Jpn. **65**, 2367 (1996).

[24] H. U. Astrom and G. Benediktson, J. Phys. F 18 **18**, 2113 (1988).

[25] R. D. Greenough, G. N. Blackie, and S. B. Palmer, J. Phys. C **14**, 9 (1981).

[26] S. Yu. Dan'kov, Y. F. Popov, and A. M. Tishin, Vestnik Moskovskogo Universteta **35**, 98 (1994).

[27] N. F. Hettiarachi, R. D. Greenough, D. Fort, and D. W. Jones, J. Magn. Magn. Mater. **25**, 310 (1981).

[28] N. Wakabayashi, J. W. Cable, and J. L. Robertson, Physica B **241-243**, 517 (1998).

[29] A.Yu. Kozlov, V.V. Pavlyuk, V.M. Davydov, Intermetallics **12**, 151(2004)

CHAPTER 2: MAGNETIC AND MAGNETOCALORIC PROPERTIES, AND MAGNETIC PHASE DIAGRAM OF SINGLE CRYSTAL DYSPRODIUM

A paper published in *Physical Review B* [1]

A.S. Chernyshov,[2,3] A.O. Tsokol,[3] A.M. Tishin,[4] K.A. Gschneidner, Jr.,[2,3] and V.K. Pecharsky[2,3]

Abstract

Magnetic materials exhibiting magnetic phase transitions simultaneously with structural rearrangements of their crystalline lattices hold promise for numerous practical applications including magnetic refrigeration, magnetomechanical devices and sensors. We undertook a detailed study of a single crystal of dysprosium metal, which is a classical example of a system where magnetic and crystallographic sublattices can be either coupled or decoupled from one another. Magnetocaloric effect, magnetization, ac magnetic susceptibility, and heat capacity of high purity single crystals of dysprosium have been investigated over broad temperature and magnetic field intervals with the magnetic field vector parallel to either the *a*- or *c*-axes of the crystal. Notable differences in the behavior of the physical properties when compared to Dy samples studied in the past have been observed between 110 K and 125 K, and between 178 K and ~210 K. A plausible mechanism based on the formation of antiferromagnetic clusters in the impure Dy has been suggested in order to explain the reduction of the magnetocaloric effect in the vicinity of the Neél point of

---

[1] Physical Review B, 2005, **71**, 184410

[2] Department of Materials Science and Engineering, Iowa State University, Ames, IA 50011-2300, USA

[3] Materials and Engineering Physics Program, Ames Laboratory of the U. S. Department of Energy, Iowa State University, Ames, IA 50011-3020, USA

[4] Department of Physics, M.V. Lomonosov Moscow State University, 119899 Moscow, Russia

relatively impure samples. Experimental and theoretical investigations of the influence of commensurability effects on the magnetic phase diagram and the value of the magnetocaloric effect have been conducted. The presence of newly found anomalies in the physical properties has been considered as evidence of previously unreported states of Dy. The refined magnetic phase diagram of dysprosium with the magnetic field vector parallel to the *a*-axis of a crystal has been constructed and discussed.

Introduction

The rare-earth metal dysprosium (Dy) has one of the largest magnetic moments in the lanthanide series, which for the free trivalent ion reaches $p_{eff} = g\sqrt{J(J+1)} = 10.65\mu_B$, where g is the gyromagnetic factor, J is the total angular momentum quantum number and μ_B is the Bohr magneton. In the ferromagnetically ordered state, the spontaneous magnetic moment of Dy is slightly lower, i.e., $m = gJ = 10\mu_B$. The metal exhibits numerous magnetic phase transitions as temperature and/or magnetic field vary. In a zero magnetic field, Dy is in the paramagnetic (PM) state above its Neél temperature, $T_N \cong 180$ K. At ~180 K, elemental Dy transforms into a helical antiferromagnetic (AFM) phase, which is stable between ~90 K and ~180 K. At the Curie temperature, $T_C \cong 90$ K, the metal orders ferromagnetically (FM) and remains in this state down to the lowest reported temperature of 4.2 K.[1,2,3,4] The transition between the AFM and FM phases at the Curie temperature is first-order, while that between the AFM and PM states at the Neél point is a second-order transformation. The intermediate fan magnetic structure emerges between the AFM and FM phases in a certain range of non-zero magnetic fields between ~127 K and ~180 K.[4] A tri-critical point on the phase diagram, where, in agreement with the Landau theory, the nature of the AFM $\leftrightarrow$ fan transition changes from first- to second-order, is located near 165 K.[5]

In a zero magnetic field, the first-order phase transition from a helical AFM to a collinear FM state occurs simultaneously with the orthorhombic distortion of the hexagonal close-packed structure of the metal.[6] Above the Neél point, no short range magnetic order has been observed by neutron scattering.[7,8] The x-ray diffraction investigation in low magnetic fields ($H \leq 1$ kOe), carried out in the vicinities of both the Curie and Neél

temperatures, revealed a broad region where the AFM and FM phases coexist.[9] Kida *et al.*[10] reported similar observations in magnetic fields higher than 1 kOe. The crystallographic transition in Dy is preserved in non-zero magnetic fields, but according to Vorob'ev *et al.*,[9] the structural distortion is shifted to a higher temperature by ~3 K in a 1 kOe magnetic field when compared to that in a zero field. This result agrees with both the magnetization[4] and magnetocaloric effect (MCE) (Ref. 5) data.

Thermal expansion[11, 12] and heat capacity[13] measured in a zero magnetic field reveal additional anomalies, such as steps and sudden slope changes, which were explained by temperature dependent changes in the commensurability between the magnetic and crystallographic lattices. The correspondence between the anomalies and commensurability points was considered by Greenough *et al.*[14] with the objective to understand the nature of the complex temperature dependence of the thermal expansion and elastic constants in a zero magnetic field, and to relate the changes of the magnetic structure studied by neutron scattering with the elastic properties of Dy.

The investigation of the magnetization in magnetic fields ranging from 0 to 20 kOe applied along the hard magnetization direction, i.e., along the *c*-axis of a crystal in a temperature interval from 4 K to 300 K was carried out by Jordan and Lee.[15] Magnetization, resistance and thermal expansion studies conducted between 4 K and 6.5 K enabled Wills and Ali[16, 17] to conclude that a component of the magnetic moment along the *c*-axis is likely present at low temperatures.

The magnetic phase diagram with the magnetic field applied along the *a*-axis (the easy magnetization direction) has been constructed using different experimental methods. These include magnetization data,[4] ultrasonic measurements,[18] ac calorimetry,[13] magnetocaloric effect,[5, 19] and Young's modulus.[19] Even though the magnetic and thermal properties of single crystalline Dy have been thoroughly studied, additional features in the magnetism and the need to revise the arrangement of phase fields in the vicinity of the Neél point were noted in Refs. 13, 20, 21, 22, and 23. Some of the anomalies can be explained by the occurrence of the intermediate vortex state, the presence of which in a narrow temperature range was predicted theoretically by Kosevich *et al.*[24] in the case of the magnetic

field vector parallel to the *c*-axis. As noted in Ref. 24, Dy – which is an easy plane magnetic material – may be unstable with respect to a transformation of the original magnetic phase into a vortex magnetic state perpendicular to the basal *ab*-plane. Amitin *et al.*[25] suggested that the anomalous features of thermal expansion can be understood assuming the appearance of an intermediate vortex structure and by considering Dy as a two-dimensional magnetic system. The presence of the vortex state was experimentally verified by neutron scattering[7] in a zero magnetic field. The location of this additional magnetic phase on the *H–T* diagram with the magnetic field vector parallel to the $[11\bar{2}0]$ direction has been investigated by Alkhafaji and Ali[26] using magnetization measurements.

As mentioned above, the AFM ↔ PM magnetic transition in Dy is a second-order transformation, in agreement with the conventional theory of phase transformations. It is supported by the following experimental observations.

i. The *H–T* diagram of Dy contains a tricritical point at $T = \sim 165$ K and $H = \sim 11$ kOe, where the first-order AFM ↔ FM (or AFM ↔ fan) transition becomes a second-order transformation. Thus, at least the boundary of the AFM ↔ fan transition approaches the zero magnetic field Neél point as a second-order transformation.

ii. The AFM ↔ fan transition takes place over a broad range of magnetic fields, and therefore, has a continuous character.

iii. The magnetic field hysteresis is absent in the range from the tricritical point (~165 K) to the Neél temperature (180 K).

Nevertheless, the presence of temperature hysteresis near the AFM ↔ PM phase transition, detected by heat capacity[13] and other properties[19] measurements, including magnetic field hysteresis of the magnetization in pulsed magnetic fields near the Neél temperature,[27] points to a mixed character of this phase transition. The presence of the extended temperature hysteresis in the paramagnetic region supports the notion about the existence of AFM clusters in the PM phase matrix. Both the amount and size of these clusters decrease with the increasing temperature, and the paramagnetic phase becomes

uniform and homogeneous only at temperatures approximately 30 K to 50 K above the Neél point.[19, 28]

Since the behavior of the heat capacity at constant pressure, $C_p(H, T)$, as a function of temperature and magnetic field can be used to examine the nature of magnetic phase transitions, several sets of experimental investigations of the heat capacity of Dy have been reported to date. Specific heat was investigated by ac calorimetry from 80 K to 130 K in a zero magnetic field[13] and in magnetic fields up to 17 kOe[19] applied along the easy magnetization direction (*a*-axis). Unusual superheating during a first-order FM → AFM transformation in a zero magnetic field was observed by Pecharsky et al.[29] and by Gschneidner et al.[30] for a solid-state electrolysis purified polycrystalline Dy.

The most recent magnetic phase diagrams of Dy[13,26] indicate the presence of an unknown magnetic phase (the so called "fan II" phase) inside the well-known fan phase region in the temperature interval from ~170 K to ~180 K and in magnetic fields between 12 kOe and 25 kOe. The x-ray diffraction investigations[10] revealed anomalies of the temperature dependence of the *c*-axis and thermal expansion in this region, but both of them can be explained without assuming the presence of an additional phase. Neutron scattering data reveal differences in scattering between the conventional "fan" and the new "fan II" phases.[31]

In the past, the magnetic and thermal properties of single crystal Dy were studied by various authors using different quality samples. The majority of known investigations were performed using specimens of different, and often low purity; sometimes impurities and their contents have not been quantified. Consequently, it is rather difficult to compare the results obtained by various authors in an attempt to develop a clear picture describing the nature of multiple phase transitions observed in elemental Dy as a function of temperature and magnetic field. To the best of our knowledge, a thorough investigation of the magnetothermal properties of this lanthanide metal employing a variety of experimental techniques with the magnetic field applied along different crystallographic directions in the same quality crystals obtained from a single initial batch of Dy was not conducted heretofore.

A comprehensive investigation of the impact of purity of Dy single crystals on their magnetic and thermal properties has considerable fundamental importance because the nature of magnetic phase transitions may be strongly affected by the presence of H, C, O, N, and/or F in the studied material.[32] As we will show below, the magnetic phase diagram constructed using the results obtained from a high purity Dy crystal contains several anomalous features and phases that were likely masked by interstitial impurities, and therefore, left undetected in previous studies. Future theoretical investigations and neutron and/or x-ray scattering experiments should be conducted to gain a better understanding of the nature and behavior of the magnetic structure of Dy in these regions of temperature and magnetic fields. Such studies are especially important because it is also known that in low-purity single crystals of Dy, magnetic phase transitions have features typical of the coexisting first- and second-order phase transformations.[19]

In addition to furthering basic understanding of the relationships between structure and magnetism, Dy may be considered a classical example of a magnetic material where in certain regions of temperature and magnetic fields, a first-order magnetic phase transition coincides with a first-order structural transformation (in a zero magnetic field both transitions occur at ~90 K). Recent advancements in understanding complex intermetallic compounds[33] indicate that materials with combined magnetic-crystallographic transformations have a potential for practical applications, e.g., in energy efficient and environmentally benign magnetic refrigeration. Presently, compounds with coupled magnetic and structural phase changes are believed to be the most promising class of materials[34, 35, 36, 37] for future applications in magnetic cooling and heating.

In this paper, we report a variety of experimental measurements, including dc magnetization, ac magnetic susceptibility, magnetocaloric effect, and heat capacity, all as functions of temperature and magnetic field, performed using the identical quality Dy single crystals with magnetic field applied parallel to either the *a*- or *c*-axes of the crystal. The obtained results have been compared with previously known data and utilized in an attempt to explain the nature of the anomalies recently reported in Refs. 13 and 31.

Experimental details

The single crystal of Dy investigated in this work was prepared by the Materials Preparation Center at the Ames Laboratory. The major impurities in the polycrystalline metal used to grow the single crystal *via* a strain-anneal process were as follows (in *ppm atomic*): O – 600, C – 190, F – 110, Fe – 60, and N – 50, thus the starting material was approximately 99.89 at.% (99.98 wt.%) pure. The specimens for the dc magnetization and ac magnetic susceptibility measurements were cut by using the spark-eroding technique from a large grain and shaped as parallelepipeds with the approximate dimensions $2\times2\times4$ mm^3. The longest axes of the parallelepipeds were parallel to either the *a*- or *c*-crystallographic axes of Dy. The samples for the heat capacity measurements, also extracted from a large grain, were approximately cylindrically shaped with the height of the cylinder around 3 mm, and its diameter approximately 10 mm; the *a*- and *c*-crystallographic axes were parallel to the shortest dimensions of the two different samples. Crystallographic directions were determined using the back reflection Laue technique. The combined accuracy of the alignment of the crystallographic axes with the direction of the magnetic field vector was $\pm5^{\circ}$. All isothermal magnetization measurements reported in this paper have been corrected for demagnetization. The value of the demagnetization factor used for recalculating the magnetization was 0.2.

The dc magnetization and ac magnetic susceptibility data were measured using a Lake Shore ac/dc susceptometer/magnetometer, model 7225. Magnetic measurements were carried out in the range of external magnetic fields varying from 0 to 56 kOe and in the temperature interval from 4.5 K to 300 K. The rms amplitudes of the ac magnetic fields varied from 2.5 Oe to 10 Oe, and the range of the ac magnetic fields' frequencies was from 55 Hz to 1000 Hz. The accuracy of the magnetic measurements, derived from measuring a Pt standard, appears to be better than 1%.

The heat capacity in constant magnetic fields ranging from 0 to 100 kOe was measured between ~4 K and 350 K in a semiadiabatic heat pulse calorimeter, which has been described elsewhere.[38] The accuracy of the heat capacity data was better than ~0.6 % in the

temperature interval from 20 K to 350 K and better than ~1 % in the temperature range 4 K – 20 K.

The isothermal magnetic entropy change as a function of temperature was calculated from magnetization data by using the Maxwell relation

$$\Delta S_{mag}(T) = \int_0^{H_0} \left(\frac{\partial M}{\partial T} \right)_H dH . \tag{1}$$

The experimental isofield heat capacity data, $C_P(T, H_i)$, (usually a total of ~300 data points for each value of the external magnetic field) were used to calculate the total entropies, $S_{total}(T, H_i)$, where H_i is a fixed magnetic field:

$$S_{total}(T, H_i) = \int_0^T \frac{C_P(T, H_i)}{T} dT . \tag{2}$$

In Eq. 2, the zero temperature entropy is assumed to be zero and independent of the magnetic field. In order to reduce the influence of a small variance in temperature at which the measurements in different H_i were initiated, the numerical integration of Eq. 2 was performed beginning at a common lowest temperature, $T_{\min}$, for all magnetic fields. Hence, the total entropy was calculated, as follows:

$$S_{total}(T, H_i) = \int_0^{T_{\min}} \frac{C'_P(T, H_i)}{T} dT + \int_{T_{\min}}^{T} \frac{C_P(T, H_i)}{T} dT . \tag{3}$$

The heat capacity, $C'_P(T, H_i)$, was extrapolated from $T = T_{min}$ to $T = 0$ using the experimental data in the temperature interval from ~3.5 K to ~8 K and assuming that the total heat capacity is the sum of the lattice, electronic, and magnetic contributions. It was also assumed that at low temperature and far way from the nearest magnetic phase transition ($T_C \cong 90$ K), the contributions from the electronic (γT) and lattice (βT^3) heat capacities are magnetic field independent. Hence, magnetic field affects only the magnetic part of the heat capacity, $C_M = BT^n$, where $n = 1.5$, and B is a parameter determined from a least squares fit of the heat capacity data from T_{min} to ~8 K. Thus, the determined γ, B and β were used in the

interpolation from $T = T_{min}$ to $T = 0$ K using $C'_P(T, H_i) = \gamma T + B_{Hi}T^{1.5} + \beta T_3$. The magnetocaloric effect was determined as the isothermal (ΔS_M) and the isentropic differences (ΔT_{ad}) between the two entropy functions: $S_{total}(T, H_i \neq 0)$ and $S_{total}(T, H_i = 0)$.

The magnetocaloric effect, ΔT_{ad}, was also measured directly from ~77 K to 300 K in quasi-static magnetic fields using a home-built apparatus. The magnetic field changes ranged from 2 kOe to 14 kOe and the magnetic field was generated by an electromagnet. Due to the relatively large magnetic induction of the coil, the time of the field sweep from 0 to 14 kOe was $\tau \cong 2$ sec. The measurements were made on thermally insulated samples in a vacuum of ~10^{-3} torr to minimize the heat exchange between the specimen and the surroundings. The MCE data were usually recorded as follows. First, the temperature of the specimen was stabilized after either cooling from ~200 K or heating from ~80 K to the target temperature in a zero magnetic field. Second, the MCE measurements were carried out by changing the magnetic field between zero and the desired value (and then back to zero) beginning from small magnetic field increments and ending with the largest ΔH. The zero-magnetic field temperature of the specimen was kept constant during each series of measurements. We will refer to these data as the MCE measured isothermally. In another approach, which we call isofield measurements and which may yield different results because some phase transitions of Dy are first-order and hysteretic, the MCE data were recorded after sample temperature was stabilized as described above before each magnetic field sweep. The magnetic field change was always from zero to the same non-zero field value. The equilibrium temperature of the specimen was measured using a copper-constantan thermocouple before and after the magnetic field sweeps. The magnetocaloric effect was determined as the difference between the two equilibrium temperatures with ~7 % to ~10 % accuracy.

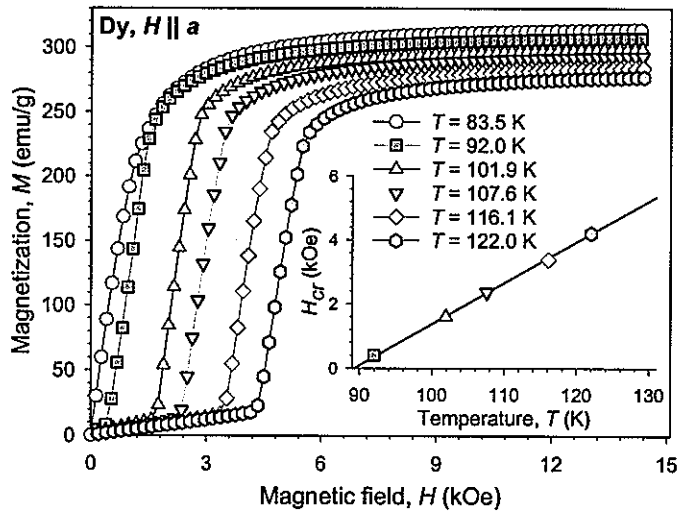

Fig. 1. Isothermal magnetization of Dy measured between 83.5 K and 122 K with the magnetic field vector parallel to the *a*-axis. The inset shows the critical magnetic fields as a function of temperature. The sample was heated to 250 K (i.e., the paramagnetic state) and then cooled down in a zero magnetic field to the temperature of each measurement.

Results

Magnetic properties

The isothermal dependencies of the magnetization of the Dy single crystal measured in low magnetic fields in the temperature interval from 83.5 K to 122 K with the magnetic field applied parallel to the *a*-axis are shown in Fig. 1. Distinct metamagnetic-like steps in the magnetization corresponding to the magnetic field-induced first-order AFM → FM transformation are observed at all temperatures exceeding 90 K. The critical magnetic field, H_{cr}, increases nearly linearly with temperature at a rate (dH_{cr}/dT) of 0.13 kOe/K, see inset in Fig. 1.

The magnetic field dependencies of the magnetization along the same crystallographic axis at higher temperatures and higher magnetic fields are shown in Fig. 2. The critical magnetic field required to induce the AFM → FM transformation continues to increase nearly linearly from ~4 kOe to ~11 kOe with increasing temperature and then saturates at $H_{cr} \cong 11$ kOe at $T \geq 165$ K. A step-like increase in the magnetization is clearly

observed even at 177 K (not shown in Fig. 2). At 180 K, the step becomes nearly indistinguishable and the anomaly is reduced to a change of slope of the $M(H)_T$ function, which presumably corresponds to a second-order magnetic field-induced AFM → fan transition. This behavior is in good agreement with the results reported in Ref. 2. In higher magnetic fields (11 kOe to 22 kOe) and just below 180 K, Dy becomes ferromagnetic due to the magnetic field induced fan → FM transition. The magnetic field induced anomaly similar to that shown for the 180 K isotherm in Fig. 2 disappears above 181.5 K. The behavior of the magnetization becomes nearly linear with field as Dy adopts the paramagnetic state.

The magnetization along the *c*-axis (Fig. 3) displays quite a different behavior, which is consistent with a hard magnetization direction. Between 120 K and 180 K, anomalous but minor slope changes are observed in magnetic fields below 15 kOe. With increasing temperature, the location of this slope anomaly moves towards the higher values of the magnetic field in a nearly linear fashion.

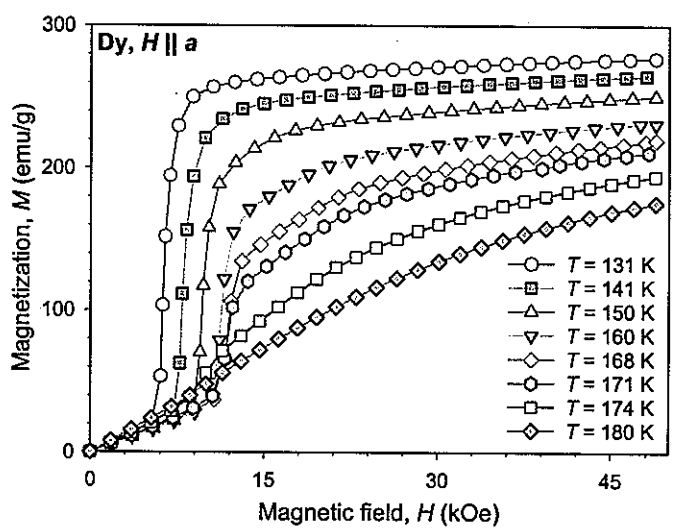

Fig. 2. Isothermal magnetization of Dy measured between 135 K and 180 K with the magnetic field vector parallel to the *a*-axis. The sample was heated to 250 K (i.e., the paramagnetic state) and then cooled down in a zero magnetic field to the temperature of each measurement.

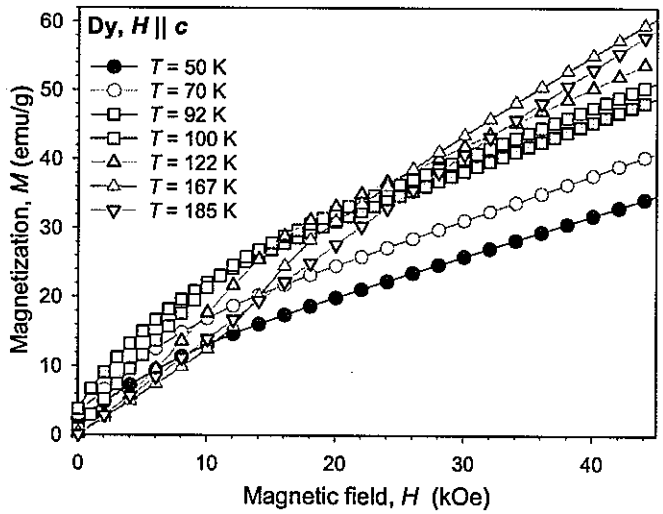

Fig. 3. Isothermal magnetization of Dy measured between 50 K and 185 K with the magnetic field vector parallel to the *c*-axis. The sample was heated to 250 K (i.e., the paramagnetic state) and then cooled down in a zero magnetic field to the temperature of each measurement.

The temperature dependencies of the magnetization along the *a*-axis measured in several different dc magnetic fields are shown in Fig. 4. Sharp reductions of the magnetization observed on heating in 3 kOe, 6 kOe and 10 kOe magnetic fields correspond to the temperature induced first-order FM → AFM magnetic phase transitions. The cusps, seen near 180 K, correspond to second-order AFM → PM transitions. A weak anomaly is also observed in the vicinity of 100 K in low magnetic fields, which is better visualized as the derivative of the magnetization with respect to temperature (e.g., in a 6 kOe magnetic field see inset in Fig. 4). The presence of the anomalies around 100 K may be explained by the proximity of the point where magnetic and crystal structures become commensurate with one another. Similar anomalies have been confirmed by our magnetocaloric effect measurements (see below), which also reveal the existence of an additional critical field in the temperature interval from 110 K to 125 K.

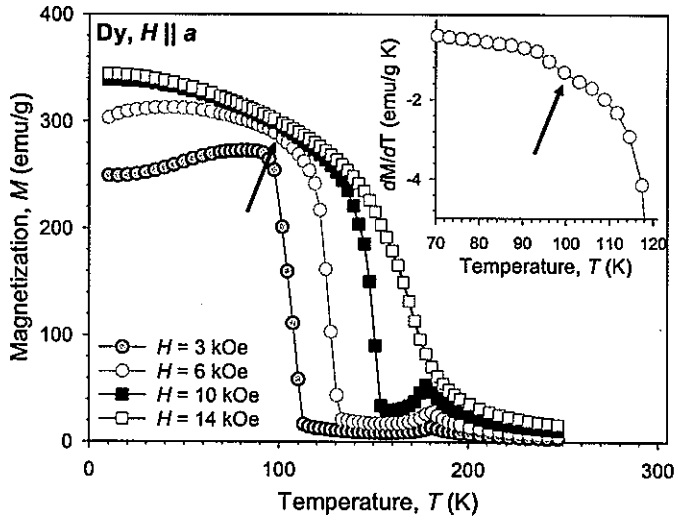

Fig. 4. Isofield magnetization of Dy measured during heating of a zero magnetic field cooled sample from 4.5 K to 250 K with the magnetic field vector parallel to the *a*-axis. The inset shows the derivative of the magnetization with respect to temperature between 70 and 120 K when H = 6 kOe. The arrows point to a minor anomaly observed near 100 K in a 6 kOe magnetic field.

The isofield magnetization measurements along the *c*-axis in the temperature interval from 50 K to 250 K and applied magnetic fields of 5 kOe and 15 kOe are illustrated in Fig. 5. Both curves behave anomalously between 80 K and 90 K (the Curie point) and around 180 K (the Neél point). The step-like decrease of the magnetization at ~80 K reflects the first-order FM → AFM transition occurring on heating. The maximum of the magnetization at ~180 K coincides with the Neél point, where a second-order transition from the AFM to the PM phase occurs.

The temperature dependencies of the ac magnetic susceptibility measured along the easy magnetization axis with dc magnetic fields of 5 kOe and 10 kOe applied along the *a*-axis of the crystal are presented in Fig. 6. The anomalies observed when the sample was biased by a 5 kOe dc magnetic field (a minimum at 106.7 K, a maximum at 124.7 K, and a maximum at 180.2 K) correspond to the anomalies in the MCE (see below) and the dc magnetization (see Fig. 13) in this region of temperatures and magnetic fields. The minimum at 106.7 K is related to an intermediate magnetic phase. In the dc magnetic field of 10 kOe, the minimum of the ac susceptibility transforms into a weak step-like anomaly (see inset in Fig. 6). There are also anomalies related to the second-order phase

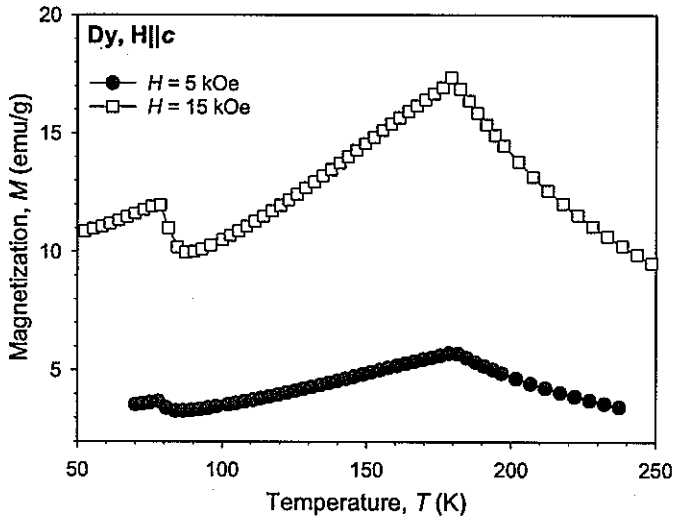

Fig. 5. Isofield magnetization of Dy measured on heating of a zero magnetic field cooled sample from ~50 K to ~250 K with a magnetic field vector parallel to the *c*-axis.

transition between ferromagnetic and fan phases ($T \cong 140$ K), the first-order AFM-FM magnetic phase transition ($T \cong 153$ K) and the second-order transition between AFM and PM phases ($T \cong 175$ K) when the ac susceptibility measurements are biased by a 10 kOe dc magnetic field.

The $\chi'_{ac}(T)$ data along the *c*-axis measured in a zero external dc magnetic field, have two peaks approximately corresponding to the locations of the Curie and Neél points (see Fig. 8). Additional steps appear in the applied dc magnetic fields of 5 kOe, 8 kOe and 10 kOe (only the 10 kOe curve is shown in Fig. 8), and their locations on the temperature scale ascend in a linear fashion with the increasing magnetic field. In a 20 kOe magnetic field, the temperature dependence of the ac susceptibility has a characteristic maximum related to the position of the AFM ↔ PM transition and a step in the vicinity of the Curie temperature.

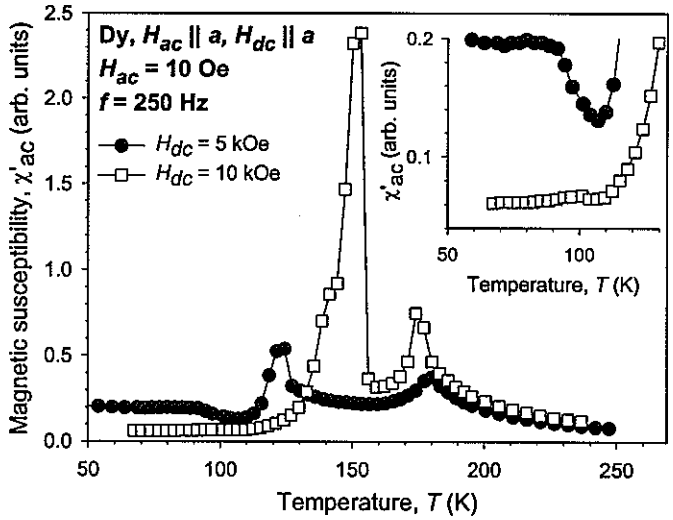

Fig. 6. The real component of the ac magnetic susceptibility of Dy measured on heating of the zero magnetic field cooled sample from 50 K to 250 K with both the ac and dc magnetic field vectors parallel to the *a*-axis. The inset clarifies details around 100 K.

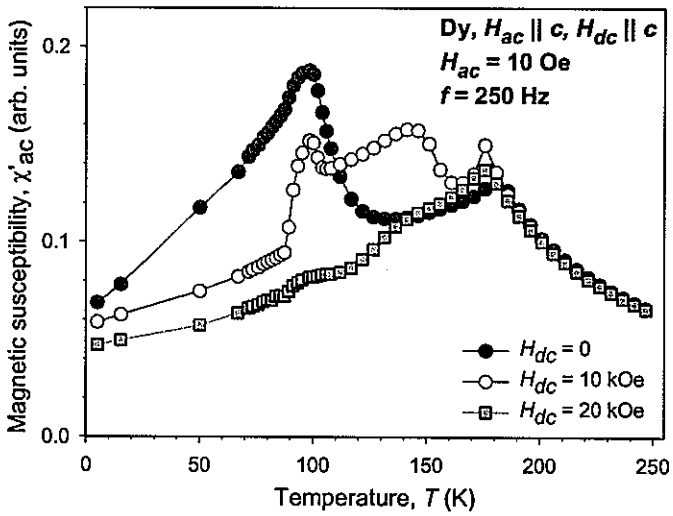

Fig. 7. The real component of the ac magnetic susceptibility of Dy measured on heating of a zero magnetic field cooled sample from 5 K to 250 K with both the ac and dc magnetic field vectors parallel to the *c*-axis.

Magnetothermal properties

The heat capacity of single crystalline Dy in a zero magnetic field (see Fig. 8) agrees with the previous measurements.[13] A sharp peak at ~90 K corresponds to the first-order AFM → FM transition and the characteristic λ-type anomaly at ~180 K reflects a second-order AFM → PM transformation. Upon application of the magnetic field parallel to the easy magnetization direction, the behavior of the heat capacity changes considerably. The temperature of the sharp peak at 90 K remains nearly constant in magnetic fields between 3 and 15 kOe but its magnitude is gradually suppressed, especially in a 15 kOe field. The peak completely disappears in a 20 kOe magnetic field (not shown in Fig. 8). A second low temperature feature – a small cusp – develops above 90 K in low magnetic fields, and it quickly shifts towards higher temperature as the magnetic field increases (see the inset in Fig. 8). The location of the cusp approximately corresponds to the magnetic field induced AFM → FM transitions (see Fig. 1 and Fig. 2). The high temperature anomaly splits into two when the magnetic field is in the range of 15 to 25 kOe (only the 15 kOe data are shown in Fig. 8).

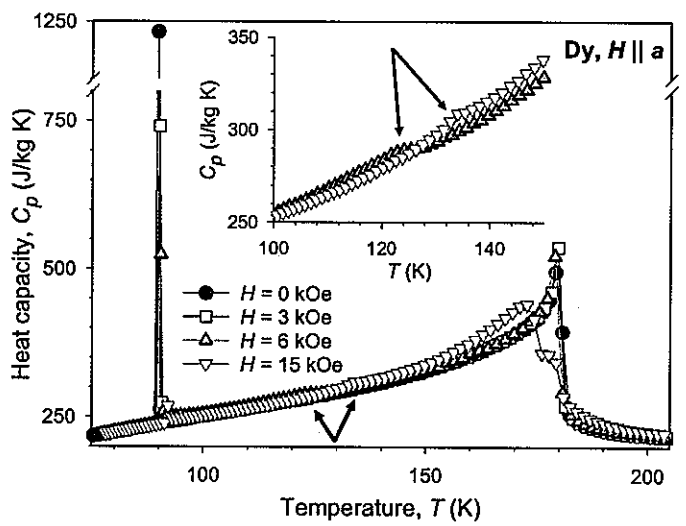

Fig. 8. The heat capacity of Dy between ~70 K and 250 K measured on heating of a zero field cooled sample in low magnetic fields with the magnetic field vector parallel to the *a*-axis. The inset clarifies the behavior between 100 and 150 K at 6 kOe and 15 kOe. The cusps, which develop in these magnetic fields, are indicated by arrows.

The heat capacity measured with the magnetic field applied along the *c*-axis in the temperature interval 70 K to 200 K in the range of magnetic fields up to 15 kOe is shown in Fig. 9. Unlike when the magnetic field is applied parallel to the *a*-axis, the data presented in Fig. 9 has only two anomalies. The sharp peak at ~90 K corresponds to a first-order phase transition. The magnitude of this peak decreases with increasing magnetic field, however, the suppression is not as drastic as in the case when magnetic field vector coincides with the easy magnetization direction. As long as the magnetic field is less than or equal to 20 kOe, its influence on the heat capacity around $T_N = 180$ K is nearly negligible.

The isothermal dependencies of the magnetocaloric effect in the region from ~111 K to ~122 K are presented in Fig. 10. Each curve displays two step-like anomalies. The low-field steps correspond to the magnetic field induced AFM → FM transitions. Additional steps occur at slightly larger magnetic fields and they are observed in the temperature interval from 105 K to 125 K. The difference between the values of the critical fields corresponding to the first step, measured after heating and after cooling of the sample, shows temperature hysteresis, which is consistent with the first-order nature of the AFM → FM transition. The second steps have little, if any hysteresis, thus indicating a second-order nature of the underlying transformation (also see below).

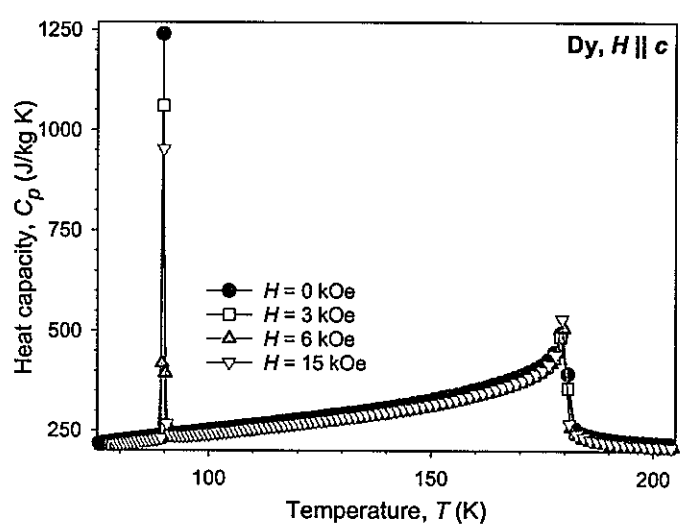

Fig. 9. The heat capacity of Dy between ~70 K and 250 K measured on heating of a zero field cooled sample in low magnetic fields with the magnetic field vector parallel to the *c*-axis.

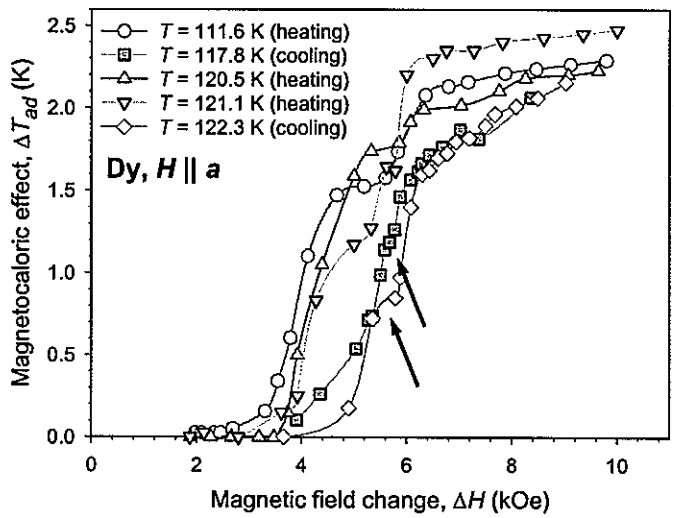

Fig. 10. The magnetocaloric effect of Dy between ~111 K and ~122 K measured directly in low magnetic fields with the magnetic field vector parallel to the *a*-axis. The magnetic field was changed between 0 and the value specified as the abscissa after the sample was either heated in a zero magnetic field from below 90 K or zero-field-cooled from above 180 K to the temperature of the measurement as indicated in the legend. The arrows point to low-field steps observed at $T = 111.6$ K and $T = 117.8$ K.

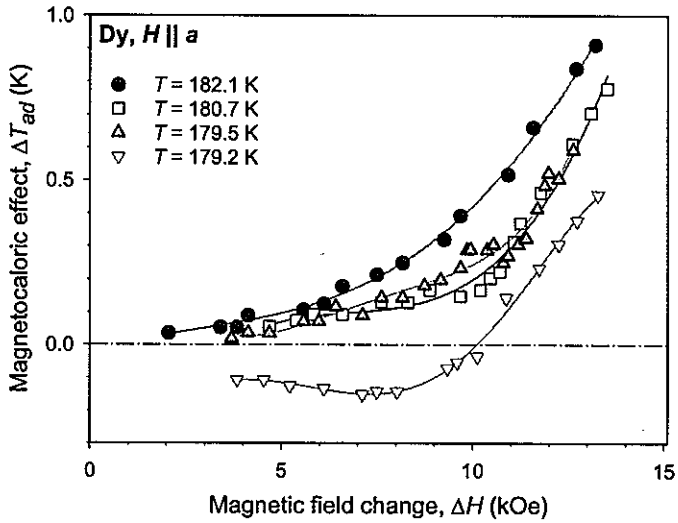

Fig. 11. The magnetocaloric effect of Dy between ~179 K and ~182 K measured directly in low magnetic fields with the magnetic field vector parallel to the *a*-axis. The magnetic field was changed between 0 and the value specified as the abscissa and then back to 0 while the sample was kept at constant initial temperature, as marked in the legend.

The isothermal behavior of the MCE in the vicinity of the Neél point is shown in Fig. 11. At and below 179.2 K, the MCE is negative in low magnetic fields, which is due to the contribution from the AFM phase in this range of magnetic fields. At higher temperatures, the antiferromagnetic order disappears, and the magnetocaloric effect becomes positive in all magnetic fields. It is, therefore, possible to define the Neél point as the temperature where the MCE becomes non negative in weak magnetic fields. The value of thus obtained Neél temperature is 179.4 K. Just below the Neél temperature, the MCE shows plateau-like behavior, i.e., the weakly magnetic field dependent MCE (e.g. from ~4 to ~8 kOe at 179.2 K, from ~10 to ~12 kOe at 179.5 K, and from ~6 to ~8 kOe at 180.7 K). The fine features in the behavior of the MCE as a function of magnetic field change disappear above 182 K, where Dy is in the PM state.

The temperature dependencies of the magnetocaloric effect for a magnetic field change from 0 to 10 kOe between 50 K and 200 K obtained using different techniques are depicted in Fig. 12. All of the data are presented without accounting for the demagnetization factor. Some discrepancies between the MCE values are observed in the temperature interval from 90 K to 160 K. The magnetocaloric effect measured isothermally generally exceeds that obtained from the isofield measurements, possibly due to the presence of an additional phase caused by the commensurability of the magnetic and crystallographic structures. The results computed from heat capacity are generally lower than those measured directly in this temperature range. While a variety of reasons may account for the discrepancies between the computed and the measured MCE values, including different error limits intrinsic to each technique,[39] we believe that the observed differences are partially due to the fact that the heat capacity is measured in a constant magnetic field, while the direct MCE measurements require changing the magnetic field. Normally, this makes little, if any, difference unless the material undergoes a first-order phase transition, as does Dy, where the first-order AFM → FM transformation can be induced by low magnetic fields between 90 K and ~180 K (see Fig. 1 and Fig. 2).

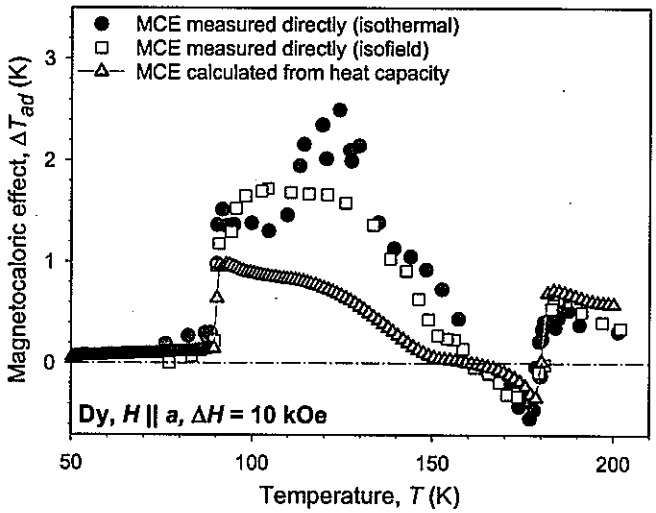

Fig. 12. The magnetocaloric effect of single crystalline Dy between 50 K and 200 K measured directly for a magnetic field change from 0 to 10 kOe and calculated from the heat capacity data collected in 0 and 10 kOe magnetic fields. In all cases, the magnetic field vector was parallel to the *a*-axis of the crystal.

All measured physical properties of Dy, especially those with the magnetic field parallel to the *a*-axis of the crystal, show multiple temperature and magnetic field dependent anomalies. These are included in Fig. 13, which represents a refined *T-H* phase diagram of Dy. In general, most of the experimental results described in this section are in good agreement with those reported earlier. In particular, Dy behaves as a ferromagnet below the Curie temperature and as an antiferromagnet between the Curie and Neél temperatures in a zero magnetic field. We also detect anomalies, which can be associated with the intermediate fan phase during the transition from the AFM to FM phase when temperature exceeds ~125 K and the magnetic field exceeds ~4 kOe. At temperatures above 181.7 K, Dy behaves as a conventional paramagnet. Yet, several additional anomalies have been observed in the course of this study, thus leading to a revision of the magnetic phase diagram of Dy as discussed below.

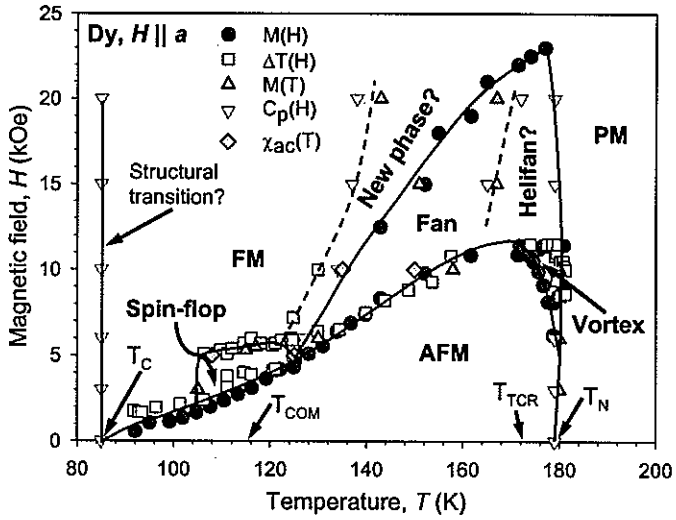

Fig. 13. The magnetic phase diagram of Dy with the magnetic field vector parallel to the easy magnetization direction, i.e., to the *a*-axis of the crystal. Also see Fig. 17 and Fig. 20 for enlarged portions of the magnetic phase diagram in the range of 100 K to 130 K and 3 kOe to 7 kOe, and 170 to 180 K and 6 kOe to 12 kOe, respectively.

AFM → FM phase transition

Magnetization and ac magnetic susceptibility measurements with the magnetic fields applied along the easy magnetization direction are in good agreement with previous investigations.[1-4] The Curie temperature is ~90 K in a zero magnetic field. As temperature increases, a small magnetic field is required to induce the AFM → FM transformation and the value of the critical magnetic field increases with temperature (see Fig. 13 and relevant experimental data in Figs. 1 through 7). Below the Curie temperature, magnetic and thermal properties indicate that the FM phase of Dy is in a uniform state.

The anomalous behavior of the heat capacity observed between 90 K and 180 K when the magnetic field is applied along the *a*-axis (Fig. 8) is related to complex interplay of magnetic and structural transitions between the AFM and FM phases. The lowest temperature anomaly is a sharp peak, which resides at ~90 K in magnetic fields up to 20 kOe. The second, next higher temperature anomaly, is a small cusp that in *T-H* coordinates (e.g., ~124 K at 6 kOe and ~135 K at 15 kOe)) corresponds to the location of the magnetic field induced AFM → FM transition obtained from the magnetization data. It is, therefore,

reasonable to assume that magnetic field applied along the easy magnetization direction leads to a two-step transformation in the elemental Dy. The first is the orthorhombic to hexagonal distortion, which appears to be magnetic field independent and it always occurs at ~90 K on heating. In a non-zero magnetic field this is likely to be a structural transition between two ferromagnetic phases of Dy. The second step is the *c*-axis discontinuity (according to Ref. 10 the discontinuity is observed at temperatures as high as 169 K), which is coupled with the FM → AFM change of the magnetic structure as temperature and field increase. Thus, the AFM ↔ FM transition in Dy involves an anisotropic change of the magnetoelastic interactions along the 6-fold crystallographic axis,[19] and it appears that two structural (an orthorhombic – hexagonal distortion and the *c*-axis discontinuity) and one magnetic (AFM – FM) phase transitions coexist at T_C in a zero magnetic field. Thus, T_C may be considered as the lowest temperature tricritical point in the magnetic phase diagram of Dy.

Commensurability effects

The magnetocaloric effect data collected between 110 K and 120 K reveal anomalous behavior of the isothermal MCE curves in the range of magnetic fields from 3 kOe to 6 kOe (Fig. 10). Similar features have been observed in low magnetic fields in the thermal expansion at 100 K and 110 K, and are thought to be caused by the proximity of the commensurability point at 113 K.[14] To gain further insights on the observed low magnetic field anomalies and to describe the behavior of the critical fields between ~110 K and 120 K, one can employ the Landau-Ginsburg theory. Although the theory is phenomenological, it provides a qualitative understanding of the different magnetic phase transitions irrespective of their nature.

Theoretical analysis

Consider the helical antiferromagnetic structure of Dy as a set of ferromagnetic planes stacked perpendicular to the *c*-axis. From one plane to the next, the in-base components of the magnetic moments rotate by a specific angle ϕ, the so called helix angle. According to neutron scattering,[14] the commensurability sets at T_{com} = 113 K, in agreement

with anomalies of the magnetic and thermal properties between 110 K and 120 K described above. At T_{com}, the non-zero c-component of the magnetic wave vector **q** and the helix angle φ become, respectively, $1/6\tau$ and 30° (where τ is the length of the reciprocal lattice vector). The magnetic moment, therefore, completes the full rotation over 12 sequential planes and one can consider these planes as an antiferromagnetic cluster consisting of 6 pairs of planes, each with mutually opposite magnetic moments. The investigation of how the commensurability point affects magnetic properties of a material was carried out in Refs. 40, 41 and 42. The case of a spiral structure with AFM ordering in the basal plane was described in Ref. 42.

For Ho and Dy, the Landau-Lifshitz function, expanded in the vicinity of the rational value of $\mathbf{q} = [0, 0, 1/6\tau]$, is as follows:[41]

$$\Phi = \frac{1}{V}\int d\mathbf{r}\left\{r(\xi\eta) + u\left(\xi^2\eta^2\right) + w\left(\xi^6 + \eta^6\right) + i\sigma\left(\eta\frac{d\xi}{dz} - \xi\frac{d\eta}{dz}\right) + \gamma\left(\frac{d\eta}{dz}\frac{d\xi}{dz}\right)\right\}. \qquad (4)$$

In Eq. 4, ξ and η are the order parameters corresponding to clockwise and counter-clockwise rotations of the magnetic moment in the basal plane, respectively; r, u, σ, and γ are the temperature dependent coefficients; w represents the basal plane anisotropy, and V is the volume of a system. Equation (4) was obtained using full symmetry of the system at $\mathbf{q} = [0, 0, 1/6\tau]$.

The order parameters ξ and η represent a superposition of the left-handed and right-handed spirals. Therefore, the two variables can be reduced to one complex order parameter:[41]

$$\xi = \rho e^{i\varphi}, \eta = \xi^* = \rho e^{-i\varphi}, \qquad (5)$$

where ρ is the modulus (amplitude) of the order parameter. In case of an undistorted helix structure of Dy, $\varphi = qz$, where $q = |\mathbf{q}|$ and z is the coordinate along the c-axis.

After substituting the new variable into the functional (4), neglecting the fourth-order term, assuming that $\rho(\mathbf{r})$ is constant, and $\varphi(\mathbf{r}) = \varphi(x, y, z) = \varphi(z)$ depends only on the z-coordinate,[41] one can obtain the following simplified function:

$$\Phi = \frac{1}{V}\int d\mathbf{r}\left\{r\rho^2 + \gamma\rho^2\left(\frac{d\varphi}{dz}\right)^2 + 2\sigma\rho^2\frac{d\varphi}{dz} + w\rho^6\cos 6\varphi\right\}. \tag{6}$$

Equation (6) does not account for the presence of 12-plane antiferromagnetic clusters caused by the commensurability of the crystal and magnetic structures of Dy. Thus, one must introduce an antiferromagnetic spiral, where the cluster is treated as an antiferromagnetically ordered slab. The density of magnetic moments inside the material in case of the AFM spiral can be expressed as:[42]

$$\mathbf{M}(\mathbf{r}) = M(\mathbf{m} + \mathbf{l}e^{-i\mathbf{q}_A\mathbf{r}}), \tag{7}$$

where M is the modulus of the magnetization, $\mathbf{q}_A$ is the vector of the AFM structure inside the slab, and $\mathbf{m}$ and $\mathbf{l}$ are auxiliary vectors that satisfy the following conditions to keep the density of the magnetic moments independent of the coordinate:[42]

$$\mathbf{m}^2 + \mathbf{l}^2 = 1 \text{ and } (\mathbf{m}\cdot\mathbf{l}) = 0. \tag{8}$$

If the magnetic field is applied along the easy magnetization a-axis (x-direction) and $\mathbf{q}_A$ is located along the c-axis (z-direction), then vectors $\mathbf{m}$ and $\mathbf{l}$ should have the following components:[42]

$$\begin{aligned} &m_x = m\cos\varphi, \quad m_y = m\sin\varphi, \quad m_z = 0, \\ &l_x = l\sin\varphi, \quad l_y = -l\cos\varphi, \quad l_z = 0, \end{aligned} \tag{9}$$

where $m = |\mathbf{m}|$ and $l = |\mathbf{l}|$ are the amplitudes of the vectors $\mathbf{m}$ and $\mathbf{l}$.

Considering the density of magnetic moments as the order parameter, one can obtain the function:[42]

$$\frac{\Phi}{M^2} = \frac{1}{V}\int d\mathbf{r}\left[rl^2 + \gamma l^2\left(\frac{d\varphi}{dz}\right)^2 + 2\sigma l^2\frac{d\varphi}{dz} + mh\cos\varphi + wl^6\cos 6\varphi\right], \tag{10}$$

where l substitutes for ρ in (6).

Taking into account that $m^2 + l^2 = 1$, minimization of the following equation models the phase transitions of the system:[42]

$$\frac{\Phi}{M^2} = \frac{1}{V}\int d\mathbf{r}\left[rl^2 + \gamma l^2\left(\frac{d\varphi}{dz}\right)^2 + 2\sigma l^2\frac{d\varphi}{dz} + mh\cos\varphi + wl^6\cos 6\varphi \right] - \lambda\left(m^2 + l^2 - 1\right) \tag{11}$$

After differentiating (11) with respect to ϕ, l, m, and λ, one obtains the following series of Euler equations:

$$\begin{aligned}
&\frac{\delta\left(\Phi/M^2\right)}{\delta\varphi} = 0 \Rightarrow \quad \frac{d^2\varphi}{dz^2} + \frac{mh}{2\gamma l^2}\sin\varphi + 6w\frac{l^4}{2\gamma}\sin 6\varphi = 0,\\
&\frac{\delta\left(\Phi/M^2\right)}{\delta l} = 0 \Rightarrow \quad l\left\{ r + \frac{1}{V}\int d\mathbf{r}\left[\gamma\left(\frac{d\varphi}{dz}\right)^2 + 2\sigma\frac{d\varphi}{dz} + 3wl^4\cos 6\varphi\right] - \lambda \right\} = 0,\\
&\frac{\delta\left(\Phi/M^2\right)}{\delta m} = 0 \Rightarrow \quad h\frac{1}{V}\int d\mathbf{r}\cos\varphi - 2m\lambda = 0,\\
&\frac{\delta\left(\Phi/M^2\right)}{\delta\lambda} = 0 \Rightarrow \quad m^2 + l^2 - 1 = 0,
\end{aligned} \tag{12}$$

where l and m are treated as constants, and γ, σ, r, and w depend only on temperature.

Employing the perturbation theory for small values of the basal plane anisotropy (w) and taking into account only the terms that are linear with respect to w, we obtain the following approximate solutions for Eqs. 12:

$$\begin{aligned}
&\text{(I)} \quad \varphi = kz + \frac{w}{12\gamma}\sin 6kz, \quad l = 1, m = 0 \quad (h < h_2)\\
&\text{(II)} \quad \cos\varphi = -1 \quad l = \sqrt{1-(h/2r)^2}, m = -h/2r \quad (h_1 < h < h_3)\\
&\text{(III)} \quad \cos\varphi = 1 \quad l = 0, m = -1 \quad (h > h_3)\\
&\text{(IV)} \quad \varphi = 2\cdot\mathrm{am}\left(\sqrt{\frac{mh}{2\gamma l^2}}\frac{z}{\chi}, \chi\right) + O\left(\frac{wl^{10}}{(mh)^3}\right) \quad m \cong 1, l \ll 1 \quad (h_2 < h < h_1)
\end{aligned} \tag{13}$$

where the limiting values of the magnetic field are:

$$h_1 = 2|r|\left(\frac{16|r|}{\pi^2\left(\sigma^2/\gamma\right)}+1\right)^{-1/2} + O\left(wl^2\right), \tag{14}$$

$$h_2 = \left[2\frac{\sigma^2}{\gamma}\left(\frac{\sigma^2}{\gamma}+|r|+O(w)\right)\right], \tag{15}$$

$$h_3 = 2|r|, \tag{16}$$

and the modulus χ of the amplitude of the Jacobian elliptic function, am(z/χ, χ), can be found by using the energy conservation equation:

$$\frac{E}{\chi} = \left(\frac{1}{8}\pi^2\left(\sigma^2/\gamma\right)\frac{l^2}{mh}\right)^{1/2}, \; E = \text{const}. \tag{17}$$

Solution (13.I) corresponds to a helix phase slightly distorted in the basal plane; solution (13.II) is an additional spin-flop phase that transforms to the ferromagnetic phase (13.III) when the magnetic field exceeds the critical value $h_3 = 2|r|$. Solution (13.IV) corresponds to a distorted helix. Relying on this phenomenological model, the region where the helix and the spin-flop phases co-exist is defined in terms of the critical fields, i.e., when $h_2 > h_1$. Phase (13.IV), therefore, should not exist on the H-T phase diagram of Dy. As a result, the transition from the helix to the spin-flop phase is a first-order, while that from the helix to the ferromagnetic state is a second-order transformation. After substituting these solutions into the equation (11) and integrating over the volume of a sample one can calculate the free energies:

$$\begin{aligned}
\frac{\Phi_I(h,T)}{M^2} &= -|r(T)| - \frac{\sigma^2(T)}{\gamma(T)} \\
\frac{\Phi_{II}(h,T)}{M^2} &= -|r(T)|\left(1-\left[\frac{h}{2|r(T)|+O(w)}\right]^2\right) - \frac{h^2}{2|r(T)|+O(w)} \\
\frac{\Phi_{III}(h,T)}{M^2} &= -h
\end{aligned} \tag{18}$$

After comparing the free energies of different phases, the temperature dependencies of the critical magnetic fields related to the corresponding transitions are as follows:

$$h_{I-II} = h_{\text{H-SF}}(T) = 2\sqrt{|r(T)|\left(B(T)+O(w)\right)} \quad \Rightarrow \qquad \text{for Helix} \rightarrow \text{Spin-flop} \tag{19}$$

$$h_{II-III} = h_{\text{SF-FM}}(T) = 2\,|r(T)| \quad \Rightarrow \qquad \text{for Spin-flop} \rightarrow \text{FM} \tag{20}$$

$$h_{I-III} = h_{\text{H-FM}}(T) = |r(T)| + B(T) + O(w). \quad \Rightarrow \qquad \text{for Helix} \rightarrow \text{FM} \tag{21}$$

In Eqs. 19 – 21, $B(T) = \dfrac{\sigma^2(T)}{\gamma(T)}$ is introduced for convenience only because the actual temperature dependencies of the coefficients r, σ and γ are unknown.

Thus, the two boundaries of magnetic transitions $h_{\text{H-SF}}(T)$ and $h_{\text{SF-FM}}(T)$ may merge into a single $h_{\text{H-FM}}(T)$ line on the T-H magnetic phase diagram at a fixed temperature $T = T_{brn}$ (T_{brn} is the branching point at 127 K between spin-flop and FM states on the magnetic phase diagram of Fig. 13) and is defined by the condition:

$$|r(T_{brn})| = B(T_{brn}) + O(w(T_{brn})) \tag{22}$$

By differentiating the free energy of the system with respect to the magnetic field, one can obtain the temperature and field dependencies of the magnetization, M:

$$M(H,T) = \begin{cases} 0 & \text{if} \quad H < h_{\text{H-SF}} M_S & \text{Helix} \\ \dfrac{H - 4\pi N M_S}{2\,|r(T)|} & \text{if} \quad h_{\text{H-SF}} M < H < 2\,|r(T)| & \text{Spin-flop}, \\ M_S & \text{if} \quad H > 2\,|r(T)| & \text{FM} \end{cases} \tag{23}$$

where M_S is the mean value of the magnetization, and H is the value of the magnetic field.

To compare the experimental and theoretical curves of the MCE, we may use the magnetization calculated from Eq. 23 and the well-known expression for the MCE:

$$\Delta T = -\int_0^H \frac{T}{C_p}\left(\frac{dM}{dT}\right) dH, \tag{24}$$

where C_p is the heat capacity at constant pressure. In Eq (24), we used the experimental value of heat capacity (C_p=278 J/kg K) at fixed temperature (120 K), assuming it does not depend on magnetic field, and the magnetization data $M(H,T)$ calculated using Eq (23).

Comparison with the experiment

Using the experimentally determined temperature dependencies of the critical magnetic fields (see the magnetic phase diagram in Fig. 13), we first examine the correctness of our main assumption, i.e., that the basal plane anisotropy is small. The value of the basal plane anisotropy constant is $w = 0.04\frac{\text{Tg}}{\text{emu}}$ (see Ref. 14). The average values of $|r| \approx h_{\text{H-SF}}/2 \cong 0.3\frac{\text{Tg}}{\text{emu}}$, $B \approx h_{\text{H-SF}} - |r| \cong 0.3\frac{\text{Tg}}{\text{emu}}$ were estimated in the vicinity of the branching point T_{brn} = 127 K, where all the critical fields coincide and are approximately equal to $h_{\text{H-SF}} = 0.6\frac{\text{Tg}}{\text{emu}}$. We use the units of $\frac{\text{Tg}}{\text{emu}}$ to represent the basal plane anisotropy energy for convenience of the calculations. The corresponding ratios are, therefore, $\left|\frac{w}{r}\right| \cong \left|\frac{w}{B}\right| \cong 0.1$ and in the first approximation, the basal plane anisotropy is indeed only a small perturbation.

The temperature dependence of the magnetization in a 6 kOe magnetic field is shown together with the theoretically predicted behavior in Fig. 14. The minor anomaly at ~100 K (better seen in the inset) corresponds to a second-order FM → spin-flop phase transition. The distinct step around 123 K is associated with a first-order spin-flop → AFM transformation. The calculated $M(T)$ curve was determined from Eq. 23 by using the theoretically predicted temperature dependence of $|r(T)|$. The computed values of the magnetization were corrected for demagnetization factor, $N = 0.15$, which is close to $N = 0.2$ used to correct experimental data. The theory and experiment agree satisfactory, facilitating calculations of the isothermal dependencies of the magnetization and MCE.

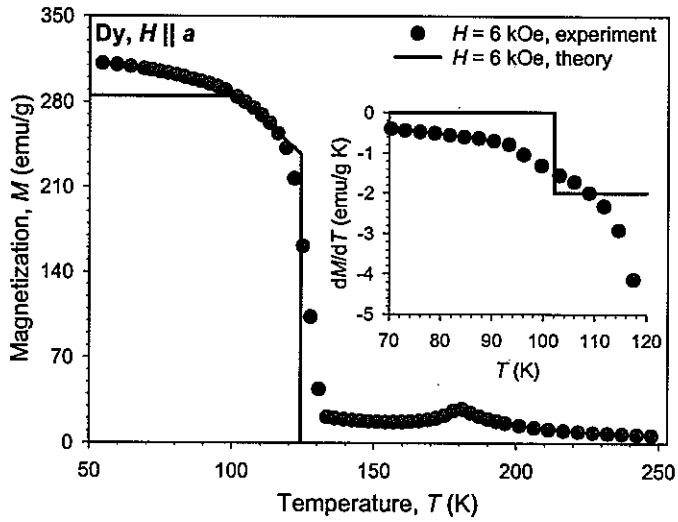

Fig. 14. The temperature dependence of the magnetization measured along the *a*-axis in the magnetic field of 6 kOe compared with calculated values (see Eq. 23). The inset shows the derivative of the magnetization with respect to temperature in the vicinity of the commensurability point.

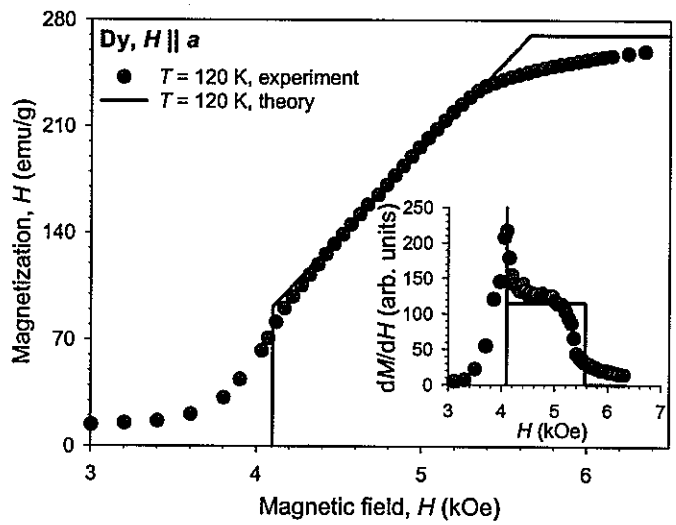

Fig. 15. Magnetization of single crystal Dy measured at 120 K between 3 and 6.4 kOe with the magnetic field applied along the *a*-axis compared to that calculated using Eq. 23. The inset shows the derivative of the magnetization with respect to field.

Another example comparing the measured and calculated (Eq. 23) $M(H)_T$, is illustrated in Fig. 15. Two critical fields are seen at $T = 120$ K. The first one corresponds to the inflection point during the jump of the magnetization around 4.1 kOe, and it manifests a first-order magnetic transition from a simple AFM spiral to a spin-flop phase. The second critical field (~5.6 kOe) is the change of slope due to a second-order phase transition from the spin-flop to the FM phase. Both features are seen as discontinuities of the derivative of the magnetization with respect to the magnetic field, as shown in the inset of Fig. 15, illustrating qualitative agreement between the experimental data and the model.

We also compare (Fig. 16) the measured calculated (Eqs. 23 and 24) isothermal magnetic field dependencies of the MCE at $T = 120$ K. Once again, one can see a reasonable agreement between the theory and the experiment. It is important to note that the anomalous MCE is both observed and reproduced theoretically in the temperature interval from 110 K to 130 K (see Figs. 10 and 12), i.e., where the simplification postulated above are applicable. The enhanced value of the magnetocaloric effect is, therefore, achieved due to the presence of the intermediate spin-flop phase.

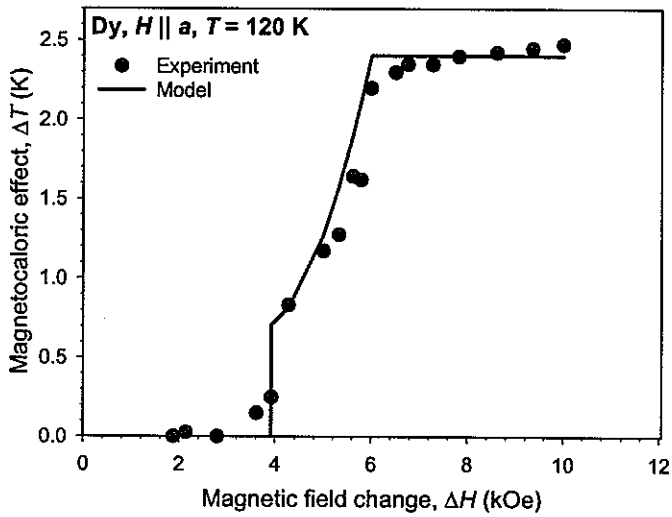

Fig. 16. The comparison of the isothermal magnetocaloric effect of the single crystal of Dy at $T = 120$ K measured experimentally with the same predicted using Eqs. 23 and 24.

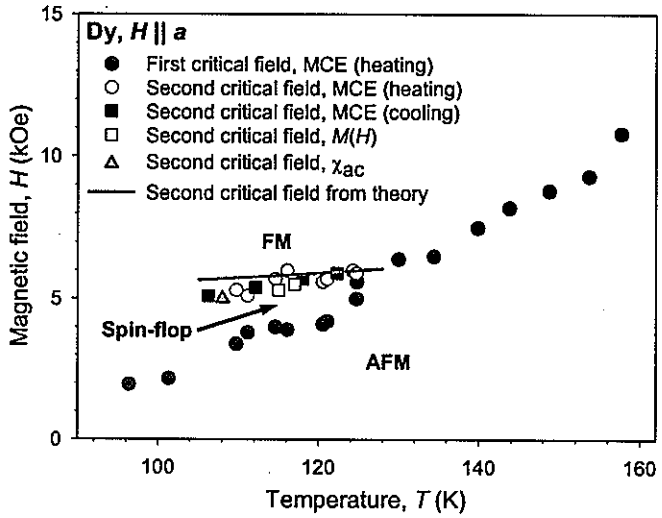

Fig. 17. Details of the magnetic phase diagram of Dy with the magnetic field applied along the *a*-axis in the vicinity of the commensurability point and the theoretically predicted boundary delineating the second critical field (see Eq. 20).

Finally, in Fig. 17 we illustrate the part of the magnetic phase diagram between ~90 K and ~160 K with the magnetic fields under ~11 kOe applied along the easy magnetization axis. The experimental critical fields, obtained from magnetization, MCE and ac magnetic susceptibility data are shown together with the second critical field boundary delineating the transition from the spin-flop to the FM state as calculated from the temperature dependence of the parameter $|r(T)|$. The agreement in this range of temperatures is nearly quantitative.

The fan phase

An intermediate fan phase exists in the temperature interval from ~125 K to ~180 K in the range of magnetic fields from ~5 kOe to ~23 kOe when the magnetic field is applied along the easy magnetization direction (see Fig. 13). Its occurrence has been confirmed experimentally by using magnetization,[4] MCE,[5] ultrasonic measurements,[17] and a variety of other experimental data.[19] The theoretical discussion of the origin of the fan phase has been presented in Refs. 1 and 40. However, recent ac heat capacity[13] and neutron scattering measurements [31] indicate that the assumed homogeneity of the fan phase region may not reflect reality. Our heat capacity data in this temperature-magnetic fields region (see Fig. 8)

are in good agreement with the results,[13,31] and they confirm the presence of an additional phase between ~172 K and ~180 K and between ~12 kOe and 25 kOe. If one assumes similarity of Dy and Ho, it is possible to speculate that this additional phase is similar to the so-called 'helifan' phase in Ho, theoretically predicted by Jensen and Mackintosh.[1] However, the corresponding calculations for Dy [31] indicate that the helifan phase is unstable at any combination of temperature and magnetic fields.

Considering Kitano and Nagamiya's model described in Ref. 40, one can determine the temperature boundary of the region where the fan structure exists in a fixed magnetic field during the helix → fan → FM phase transitions. The magnetic field dependence of the fan angle φ at low temperatures can be written as:[40]

$$\sin^2\frac{\varphi}{2}=\frac{2[J(\mathbf{q})-J(0)-g_J\mu_B H/2S]}{[3J(\mathbf{q})-2J(0)-J(2\mathbf{q})]}, \qquad (25)$$

where $J(\mathbf{q})$ is the Fourier transformation of the exchange integral $J(\mathbf{R}_{nm})$; the magnetic wave vector $\mathbf{q}$ is directed along the c-axis; $J(0)$ is the value of $J(\mathbf{q})$ at the point $|\mathbf{q}| = 0$; S is the total angular momentum quantum number of a magnetic atom; g_j is the Lande factor, and μ_B is the Bohr magneton.

The numerator of Eq. 25 is non-negative; it decreases with the increasing magnetic field and becomes zero at a fixed value of the magnetic field H_f, which corresponds to the fan → FM phase transition:

$$g_J\mu_B H_f = 2S[J(\mathbf{q})-J(0)]. \qquad (26)$$

It is worth noting that Eq. 26 does not explain the observed temperature dependence of the critical field. In order to do so, contributions from the basal plane anisotropy and the magneto-elastic interactions need to be considered.

For convenience, one can write the denominator of Eq. 25 in the following form:

$$3(J(\mathbf{q})-J(0))-(J(2\mathbf{q})-J(0)). \qquad (27)$$

Since both the left-hand side and the numerator in the right-hand side of the Eq. 25 are non-negative, the denominator in the right-hand side of this equation should be positive. Using

the experimental data for $J(\mathbf{q}) - J(0)$ from Ref. 1, one can analyze the sign of the denominator in order to establish the critical condition when the right-hand side becomes negative and Eq. 25 is no longer valid. As a result, there should be a certain value of the magnetic wave vector, q_{cr}, where for any values of q exceeding q_{cr}, conventional fan structure does not exist. Taking into account almost linearly increasing temperature dependence of the magnetic wave vector obtained from neutron scattering measurements,[31] it is possible to estimate the critical temperature as $T_{cr} = 172$ K corresponding to the value of q_{cr}. Hence, at temperatures exceeding T_{cr}, the fan should disappear in any magnetic field.

The estimates mentioned above are in support of the experimentally established configuration of the magnetic phase diagram of Dy illustrated in Fig. 13. As will be shown below, the critical temperature $T_{cr} = 172$ K also coincides with the location of the experimentally observed tricritical point $T_{tcr} = 172$ K and $H_{tcr} = 11.2$ kOe.

We now discuss some differences in the behavior of the magnetization and heat capacity as functions of temperature. The heat capacity exhibits a maximum at $T \cong 171$ K and a slope anomaly at ~180 K in both 15 kOe (Fig. 8) and 20 kOe magnetic fields. The magnetization, however, displays inflection at ~170 K but has no obvious anomalies around 180 K in magnetic fields of 15 kOe (see Fig. 4 illustrating the same for the nearly identical magnetic field of 14 kOe) and 20 kOe. This discrepancy leads to an uncertainty in the location of the Neél temperature in non-zero magnetic fields.

Taking into account the model of the AFM fan structure of Dy described above, it is easy to realize that both the magnetization and heat capacity should reflect the changes that may occur within the fan as both the magnetic field and temperature vary. Thus, it is possible to assume that the typical paramagnetic dependence of the magnetization following an inflection point in low magnetic fields indicates weakened correlations between the ferromagnetic planes above $T_{cr} = 172$ K. In fact, Dy may become a "two-dimensional paramagnet", where the orientations of the ferromagnetically ordered moments of one plane are only weakly correlated with those in the neighboring plane. At the Neél point, which coincides with the inflection point on the temperature dependence of heat capacity, the in-plane ferromagnetic order is destroyed and Dy becomes conventional three-dimensional

paramagnet. Thus, in the range of magnetic fields between 15 kOe and 20 kOe, the Neél temperature can not be obtained from magnetization data, and it probably should be defined from the location of an inflection point on the temperature dependence of the heat capacity. This interpretation, however, requires further experimental and theoretical study.

The vicinity of Neél and tri-critical points

In order to refine the magnetic phase diagram near the Neél point, we performed detailed low-field isothermal measurements of the magnetization between 172 K and 181 K. These data are shown in Figs. 18 and 19. As noted earlier, the sharp, nearly discontinuous M vs. H behavior is seen at temperatures as high as 174 K. Between ~175 K and ~181 K, the discontinuity evolves into an inflection point and the latter disappears at T_N = ~181 K. The anomalies of $M(H)$ at temperatures closest to the Neél point are better seen on the plots of $(\partial M(H,T)/dH)_T$, shown in the inset of Fig. 19. At T = 178.7 K, the first peak at 6 kOe corresponds to a second-order AFM → intermediate phase transition. The anomaly around 11.5 kOe at the same temperature manifests a second inflection point of $M(H)$ corresponding to a field induced transition from the intermediate phase region into the fan phase.

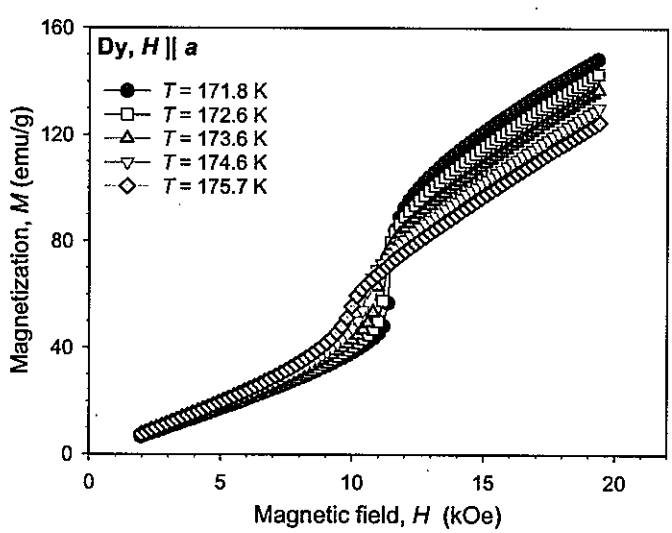

Fig. 18. The isothermal dependencies of magnetization of a single crystal of Dy measured between 171.8 K and 175.7 K with the magnetic field vector parallel to the a-axis of the crystal.

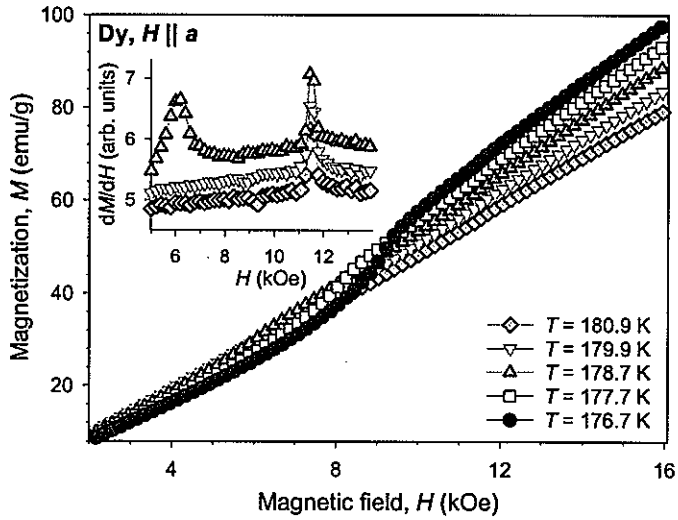

Fig. 19. The isothermal dependencies of magnetization of a single crystal of Dy measured between 176.7 K and 181.9 K with the magnetic field vector parallel to the *a*-axis of the crystal. The inset shows the derivatives of the magnetization with respect to magnetic field at temperatures closest to the Neél point.

Detailed view of the magnetic phase diagram of dysprosium with the magnetic field applied along the easy magnetization axis in the vicinity of Neél temperature is shown in Fig. 20 The intermediate phase field exists around 180 K in the range of magnetic fields from ~6 kOe or lower to ~12 kOe. The critical fields obtained from the magnetization (see Figs. 18 and 19) and direct MCE measurements (see Fig. 11) are in a satisfactory agreement with one another. A similar intermediate phase region has been reported recently by Alkhafaji and Ali,[26] who used magnetization measurements with the magnetic field applied along the $[11\bar{2}0]$ direction. The appearance of the intermediate phase in the vicinity of the Neél temperature can be explained by the presence of the so-called "vortex" state. The formation of the vortex phase with the magnetic field applied along the *c*-axis of a crystal was theoretically investigated by Kosevich *et al*,[24] who also showed that vortex state may even occur in a zero magnetic field.

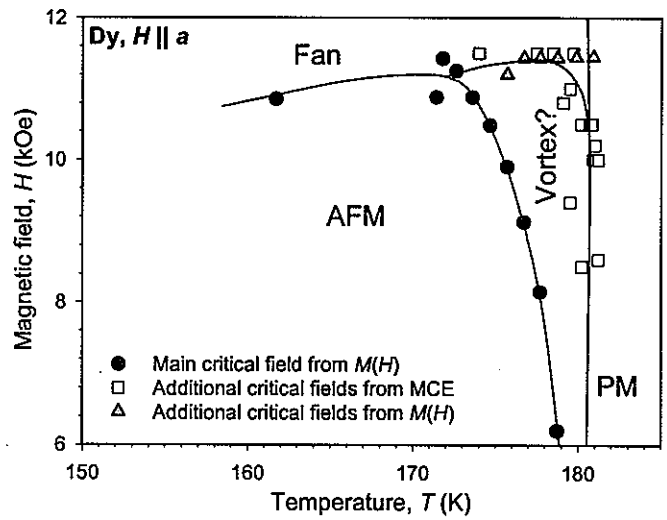

Fig. 20. Details of the magnetic phase diagram of Dy with the magnetic field applied along the *a*-axis in the vicinity of the Neel point.

Impurity effects

Clarifying how the purity of a specimen affects the value of the paramagnetic Curie temperature, θ_p, and the location of the tricritical point, T_{tcr}, on a magnetic phase diagram poses an interesting basic question, especially because of the presence of the intermediate vortex state phase. The tricritical point is a point along a phase boundary where a first-order transition evolves into a second-order transformation. The value of dH_{cr}/dT should be equal to zero at $T = T_{tcr}$. As follows from our magnetization measurements (see Figs. 18 and 20), T_{tcr} of pure Dy is 172 K. This value is higher than the 165 K reported in Refs. 4, 5 and 19, where the purity of Dy was lower. Also, as easily seen from the Curie-Weiss behavior illustrated in Fig. 21, the higher the purity of Dy, the higher its paramagnetic Curie temperature: we obtain θ_p=163.3 K, while the values listed in Refs. 1, 19, 40 are lower by several Kelvin, i.e. θ_p = 159 K.

We now recall several expressions proposed by Kitano and Nagamiya (see Ref. 40) in order to describe the sequence of helix → fan → FM transitions of Dy. The first equation relates Neél and tricritical point temperatures:

$$\frac{T_N - T_{tcr}}{T_N} \cong \frac{8}{11}\frac{J(\mathbf{q}) - J(0)}{2J(\mathbf{q})}, \tag{28}$$

where $J(\mathbf{q})$ is the Fourier transformation of the exchange integral $J(\mathbf{R}_{nm})$, vector $\mathbf{q}$ is directed along the c-axis and $J(0)$ is the value of $J(\mathbf{q})$ at $\mathbf{q} = 0$ and $T_N = 181$ K. The next two define, respectively, the Néel and paramagnetic Curie temperatures as follows:[40]

$$T_N = 2J(\mathbf{q})\frac{S(S+1)}{3k_B} \tag{29}$$

$$\theta_p = 2J(0)\frac{S(S+1)}{3k_B} \tag{30}$$

where S is the total angular momentum quantum number and k_B is the Boltzman constant. Using Eqs. 28 – 30 and the experimentally determined θ_p=163.5 K, the location of the tricritical point should be:

$$T_{tcr} = T_N\left[1 - \frac{8}{11}\frac{T_N - \theta_p}{T_N}\right] \cong 168.4K\,. \tag{31}$$

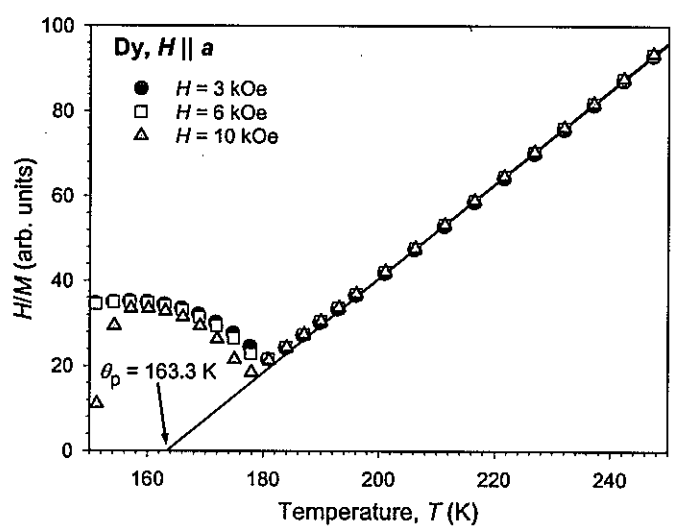

Fig. 21. The inverse magnetic susceptibility of Dy measured in different magnetic fields. The lines correspond to the Curie-Weiss fit of the data above ~210 K.

The theoretically predicted 168.4 K is lower that T_{tcr} = 172 K observed experimentally in a high purity single crystal but it exceeds the 165 K reported for lower purity specimens. The temperature difference between the T_{tcr} and T_N in a relatively pure Dy used in our study is 9 K, which is smaller by about 3 K than the difference between same temperatures in a less pure metal. Therefore, it is possible to speculate that as material's purity improves, the tricritical point may approach T_N. If this assumption is correct, then some of the phase fields in this part of the magnetic phase diagram of Dy may have a different configuration, or there may be even fewer phase fields on the diagram. In the limiting case, the AFM-fan boundary may approach the nearly vertical AFM-PM boundary with zero dH_{cr}/dT. Hence, the point where these boundaries meet becomes a tricritical point. Therefore, it is quite possible that the range where the vortex and other unknown phases were observed near T_N will become much narrower or even disappear in a much higher purity Dy sample.

Magnetocaloric effect

The temperature dependencies of the isothermal magnetic entropy change, ΔS_M, in the temperature interval from ~70 K to ~250 K with the magnetic field applied along the easy magnetization direction in the range of magnetic field changes from 0 to 4 kOe, 8 kOe, 12 kOe, and 15 kOe are shown in Fig. 22. The ΔS_M in the temperature interval from ~4 K to 300 K for much larger magnetic field changes, i.e., from 0 to 20 kOe, 50 kOe, 75 kOe, and 100 kOe is illustrated in Fig. 23. Several features seen in the behavior of the MCE are worth mentioning. First, the discontinuity of $\Delta S_M(T, \Delta H)$ at ~90 K remains independent of both T and ΔH, although the "background" contribution to the MCE below and above 90 K continues to increase as the magnetic field change increases. This behavior of the magnetocaloric effect is typical of first-order phase transition materials and it has been predicted by Pecharsky et al.[43] Second, the amplitude of the discontinuity at ~90 K, $\delta(\Delta S_M)$ = 0.55 J/mol K, is in an excellent agreement with the $\Delta S_{tr} = 0.56 \pm 0.01$ J/mol K ($\Delta H_{tr} = T_C \Delta S_{tr}$ = 50.4 J/mol)at T_C obtained from direct calorimetric measurements of the solid state electrotransport purified Dy by Pecharsky et al.[29] Third, the negative contribution

to $|\Delta S_M|$ observed just below T_N in magnetic fields of 20 kOe and lower is consistent with the AFM state of the metal. Finally, between 20 and 50 kOe, there is a large increase in $|\Delta S_M|$ at ~180 K; the magnetic entropy change in the 100 kOe magnetic field reaches the value of ΔS_M = -29 J/kg K at $T = T_N$ = 180 K, and between ~100 K and 300 K the MCE exhibits a typical caret-like behavior in magnetic fields of 50 kOe and higher. All of these features are consistent with the FM state of Dy, which is realized below ~180 K in magnetic fields exceeding 20 kOe.

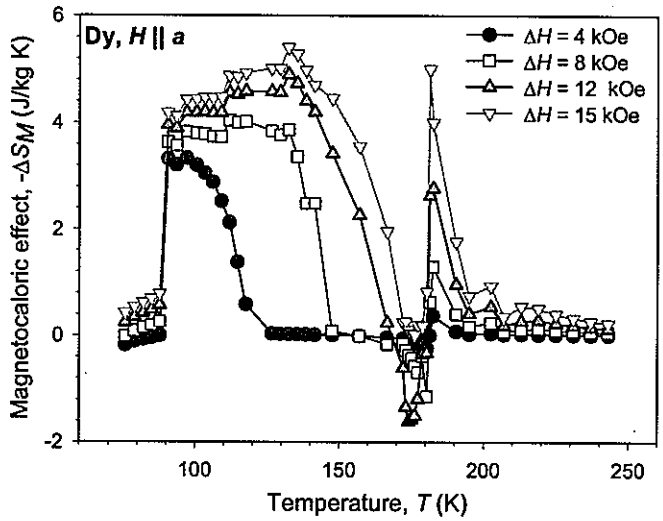

Fig. 22. The temperature dependencies of the low-field isothermal magnetic entropy change calculated from the magnetization data in the temperature interval from ~70 K to ~250 K.

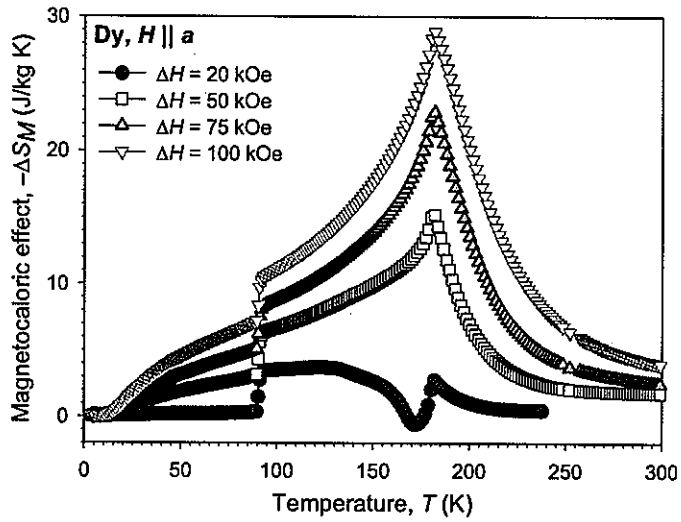

Fig. 23. The temperature dependencies of the high-field isothermal magnetic entropy change calculated from the heat capacity in the temperature interval from ~5 K to ~300 K.

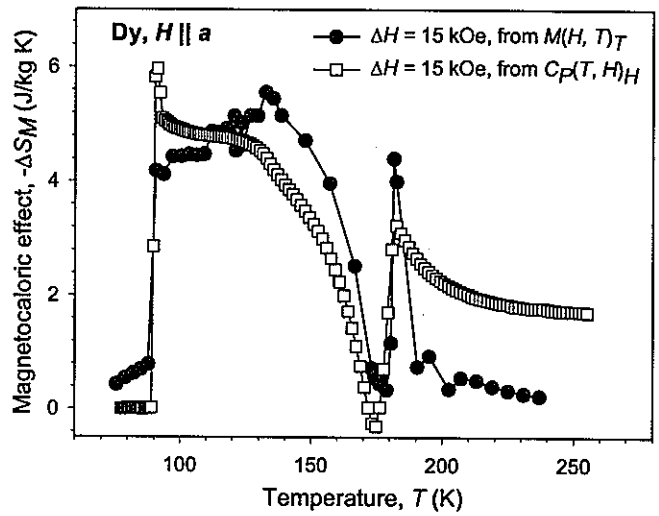

Fig. 24. The comparison of the isothermal magnetic entropy change calculated from the heat capacity and the magnetization data for a magnetic field change of 15 kOe.

The isothermal magnetic entropy changes calculated from the heat capacity and magnetization data for a magnetic field change from 0 to 15 kOe with the *a*-axis of a crystal parallel to the field are compared in Fig. 24. The agreement is generally good, but above the Neél temperature, the MCE obtained from heat capacity deviates systematically from the MCE calculated from magnetization data. This variance in the $-\Delta S_M$ computed from different experimental data in the paramagnetic region is likely related to the fact that a progressively smaller quantity (ΔS_M) is computed by subtracting progressively larger total entropies. As a result, the relative error in determining ΔS_M from heat capacity rises much faster than the corresponding absolute errors. Similar systematic differences have been noted in the ΔT_{ad} of Gd measured directly and calculated from heat capacity data above the Curie temperature.[44]

In Fig. 25, we compare the magnetocaloric effect measured directly during a magnetic field change from 0 to 10 kOe applied along the *a*-axis with the temperature dependencies of the magnetocaloric effect reported earlier.[5,19] In addition to a much sharper rise of the ΔT_{ad} around 90 K, which can be understood because the specimen employed in this study has a higher purity when compared to the crystals used in the past, there is a substantial difference in the MCE's of Dy in the paramagnetic state. The amplitude of the difference is greater than the measurement errors and therefore should not be neglected.

Also important is the fact, that the greatest deviation from the previous measurements is observed in the immediate vicinity of the Neél temperature, i.e. where short range correlations, such as AFM clustering, can be significant.

In order to estimate the influence of clustering on the magnetocaloric effect, we first calculate the MCE of dysprosium assuming the ideal paramagnetic behavior at $T > T_N$. Magnetization, $M(H,T)$, of an ideal paramagnet follows the Curie-Weiss law:

$$M(H,T) = \frac{Np_{eff}^2 H}{3k_B(T-\theta_p)}, \tag{32}$$

where N is the number of paramagnetic atoms, k_B is the Boltzmann constant, θ_p and p_{eff} are 163.5 K and 10.65 μ_B, respectively. Since the heat capacity of Dy in the paramagnetic state is nearly magnetic field independent at 10 kOe and below (see Fig. 8), it can be approximated by the following analytical expression:

$$C(T,H)_{H\leq 10\,\mathrm{kOe}} = 220 + \frac{125}{T-180}\ \mathrm{J/kgK} \tag{33}$$

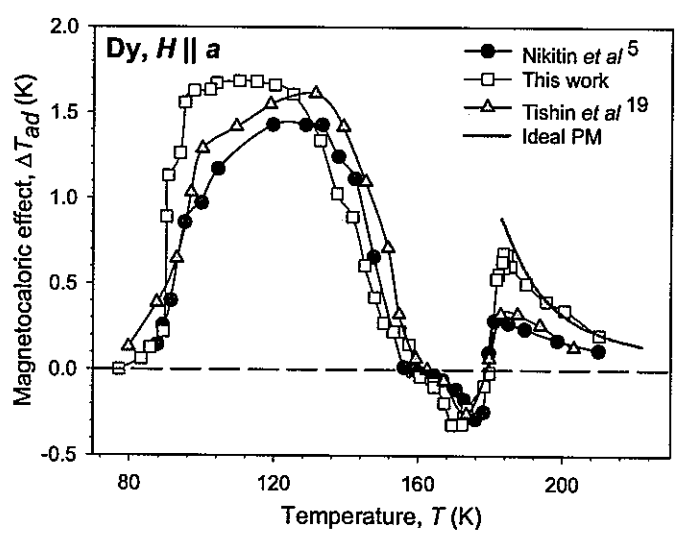

Fig. 25. The temperature dependencies of the magnetocaloric effect for a magnetic field change of 10 kOe in comparison with earlier measurements and the theoretical MCE for Dy assuming an ideal paramagnetic behavior above T_N.

After substituting Eqs. 32 and 33 into Eq. 24 and integrating, we obtain the following temperature dependence of the MCE above T_N for a magnetic field change $\Delta H = 10$ kOe:

$$\Delta T_{ad}(T)_{\Delta H=10\,\mathrm{kOe}} = -\int_0^{10} \frac{T}{C(T,H)} \frac{dM(T,H)}{dT} dH = 2.2 \frac{T(T-180)}{(T-179.4)(T-163.5)^2} \quad (34)$$

The MCE calculated using Eq. 34 is shown in Fig. 25 as a heavy solid line. The estimated MCE values are in excellent agreement with our experimental data at all temperatures above T_N. The earlier ΔT_{ad} values are smaller than the calculated ones, and the deviations are most obvious in the immediate vicinity of the T_N.

The following qualitative model can be proposed to understand the observed differences. Assuming that AFM clustering can occur at $T > T_N$, dysprosium may be considered as a paramagnet with a certain amount of embedded AFM phase (AFM clusters) above the T_N. The concentration of these AFM clusters decreases as temperature increases. Naturally, small magnetic field changes produce a negative ΔT_{ad} for an AFM component and a positive MCE for a fraction of the material that is in the PM state. The experimentally measured ΔT_{ad} is the combined total of the two contributions. Therefore, the higher the concentration of the AFM clusters, the lower the observed total MCE and the greater the negative deviation from the ideal paramagnetic behavior. The results shown in Fig. 25 indicate that impurities enhance the AFM clustering in Dy.

The ΔT_{ad} of Dy in strong magnetic fields applied along the a-axis as calculated from the heat capacity is shown in Fig. 26. The maximum MCE is 19.4 K for the magnetic field change of 100 kOe. Considering both the large values of the isothermal magnetic entropy change (Fig. 23) and the adiabatic temperature change, single crystalline Dy is indeed a promising magnetocaloric material. Its practical use, however, requires that the magnetic field change exceeds 2 T in order to eliminate the negative contributions to the MCE due to the presence of the AFM phase.

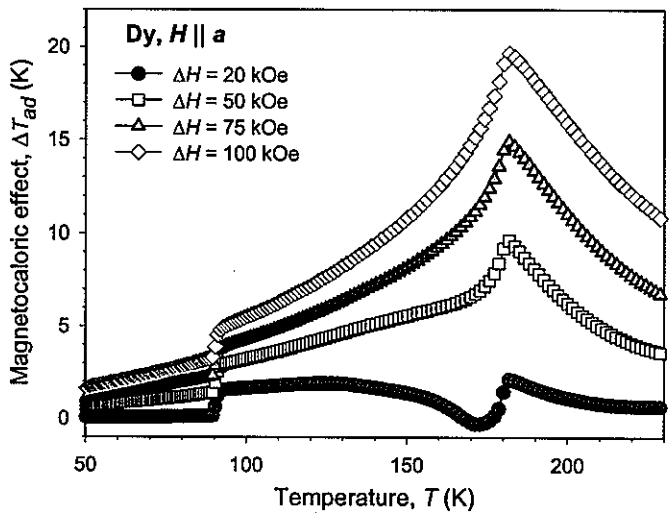

Fig. 26. The temperature dependencies of the magnetocaloric effect of Dy as calculated from the heat capacity data.

Conclusion

As a result of measuring magnetization, ac magnetic susceptibility, heat capacity, and magnetocaloric effect of single crystals of Dy we confirmed the majority of previous findings but also report some notable differences in the behaviors of the magnetothermal properties, especially in the vicinities of Curie, Neél and tricritical temperatures. When the magnetic field vector is parallel to the *a*-axis of a crystal, the refined *H-T* phase diagram of Dy is more complicated than previously thought, and it contains several new phases. The appearance of some of these new phases has been explained by considering the Landau-Ginsburg theory of phase transitions.

Acknowledgements

Authors thank to Mr. M. I. Ilyn, Mr. A. S. Mischenko, Dr. S. Yu. Dan'kov, and Dr. Yu. I. Spichkin for assistance with some of the experimental measurements and useful discussions. Work at Ames Laboratory is supported by the Office of Basic Energy Sciences, Materials Sciences Division of the U. S. Department of Energy, under contract No. W-7405-

ENG-82. Work at Moscow State University is supported by the Russian Foundation for Basic research under grant No. 04-02-16709-A.

References

[1] J. Jensen and A. R. Mackintosh, *Rare earth magnetism: structure and excitations* (Clarendon Press, Oxford, 1991), 12 pp.

[2] S. Legvold, in *Ferromagnetic Materials*, edited by E. P. Wohlfarth (North-Holland, Amsterdam, 1980), Vol. **1**, Chap. 3, p.183.

[3] K. A. McEwen, in *Handbook on the Physics and Chemistry of Rare Earths*, edited by K. A. Gschneidner, Jr. and L. Eyring (North-Holland, Amsterdam, 1978), Vol. **1**, Chap. 6, p.411.

[4] R Hertz and H. Kronmüller, J.Magn. Magn. Mater. **9**, 273 (1978).

[5] S. A. Nikitin, A. S. Andreenko, and V. A. Pronin, Fiz. Tverd. Tela (Leningrad) **21**, 2808 (1979).

[6] V. A. Finkel, *The structure of rare earths* (Metallurgiya, Moscow, 1978), 6 pp.

[7] V. G. Bessergenev, V. V. Gogava, Yu. A. Kovalevskaya, A. G. Mandzhavidze, V. M. Fedorov, and S. I. Shilo, Pis'ma Zh. Eksp. Teor. Fiz. **42**, 412 (1985).

[8] V. G. Bessergenev, V. V. Gogava, A. G. Mandzhavidze, V. M. Fedorov, and S. I. Shilo, Pis'ma Zh. Eksp. Teor. Fiz. **47**, 92 (1988).

[9] V. V. Vorob'ev, M. Ya. Krupotkin, and V. A. Finkel, Sov. Phys. JETP **61**, 1056 (1985).

[10] Y. Kida, K. Tajima, Y. Shinoda, K. Hayashi, and H. Ohsumi, J. Phys. Soc. Jpn. **68**, 650 (1999).

[11] E. B. Amitin, V. G. Bessergenev, and Yu. A. Kovalevskaya, J. Phys. F **14**, 2935 (1984).

[12] Y. Shinoda and K. Tajima, J. Phys. Soc. Jpn. **65**, 2367 (1996).

[13] H. U. Astrom and G. Benediktson, J. Phys. F 18 **18**, 2113 (1988).

[14] R. D. Greenough, G. N. Blackie, and S. B. Palmer, J. Phys. C **14**, 9 (1981).

[15] R. G. Jordan and E. W. Lee, Proc. Phys. Soc. (London) **92**, 1074 (1967).

[16] F. Willis and N. Ali, J. Appl. Phys. **69**, 5694 (1991).

[17] F. Willis and N. Ali, J. Appl. Phys. **70**, 6548 (1991).

[18] A. V. Andrianov, Yu. P. Gaidukov, A. N. Vasil'ev, and E. Fawcett, J. Magn. Magn. Mater. **97**, 246 (1991).

[19] A. M. Tishin and O. P. Martynenko, *Physics of Rare Earth Metals in the Vicinity of Magnetic Phase Transitions* (Nauka, Moscow, 1995), 336 pp.

[20] S. W. Zochowski, D. A. Tindall, M. Kahrizi, J. Genossar, and M. O. Steinitz, J. Magn. Magn. Mater. **54-57**, 707 (1986).

[21] J. Dudáš, A. Feher, and Š Jánoš, J. Less-Common Metals **134**, 9 (1987).

[22] G. I. Kataev, S. V. Red'ko, M. R. Sattarov, and A. M. Tishin, Fiz. Tverd. Tela **31**, 267 (1989).

[23] W. D. Corner, W. C. Roe, and K. N. L. Taylor, J. Phys. Soc. Jpn. **17**, 1310 (1962).

[24] A. M. Kosevich, V. P. Voronov, and I. V. Manzhos, Zh. Eksp. Teor. Fiz. **2**, 148 (1983).

[25] E. B. Amitin, V. G. Bessergnev, and Yu. A. Kovalevskaya, Zh. Eksp. Teor. Fiz. **84**, 205 (1983).

[26] M. T. Alkhafaji and N. Ali, J. Alloys. Comp. **250**, 659 (1997).

[27] S. Yu. Dan'kov, Y. F. Popov, and A. M. Tishin, Vestnik Moskovskogo Universteta **35**, 98 (1994).

[28] N. F. Hettiarachi, R. D. Greenough, D. Fort, and D. W. Jones, J. Magn. Magn. Mater. **25**, 310 (1981).

[29] V. K. Pecharsky, K. A. Gschneidner, Jr., and D. Fort, Scr. Mater. **35**, 843 (1996).

[30] K. A. Gschneidner, Jr., V. K. Pecharsky, and D. Fort, Phys. Rev. Lett. **78**, 4281 (1997).

[31] N. Wakabayashi, J. W. Cable, and J. L. Robertson, Physica B **241-243**, 517 (1998).

[32] K. A. Gschneidner, Jr., J. Alloys Compds. **193**, 1 (1993).

[33] V. K. Pecharsky and K. A. Gschneidner, Jr., Adv. Mater. **13**, 683 (2001).

[34] K. A. Gschneidner, Jr. and V. K. Pecharsky, in *Intermetallic Compounds. Principles and Practice*, edited by J. H. Westbrook and R.L. Fleischer (John Wiley & Sons, New York, 2002), Vol. **3**, p.519.

[35] V. K. Pecharsky, A. P. Holm, K. A. Gschneidner, Jr., and R. Rink, Phys. Rev. Lett. **91**, 197204 (2003).

[36] L. Morellon, Z. Arnold, C. Magen, C. Ritter, O. Prokhnenko, Y. Skorokhod, P. A. Algarabel, M. R. Ibarra, and J. Kamarad, Phys. Rev. Lett. **93**, 137201 (2004).

[37] A. M. Tishin and Y. I. Spichkin, *The Magnetocaloric Effect and its Applications* (Institute of Physics, Bristol and Philadeplphia, 2003), 475 pp.

[38] V. K. Pecharsky, J. O. Moorman, and K. A. Gschneidner, Jr., Rev. Sci. Instrum. **68**, 4196 (1997).

[39] V. K. Pecharsky and K. A. Gschneidner, Jr., J. Magn. Magn. Mater. **200**, 44 (1999).

[40] B. Coqblin, *The Electronic Structure of Rare - Earth Metals and Alloys: The Magnetic Heavy Rare - Earths* (Academic Press, London, 1977).

[41] Yu. A. Izyumov, Usph. Fiz. Nauk **144**, 493 (1984).

[42] Yu. A. Izyumov and V. M. Laptev, Zh. Eksp. Teor. Fiz **143**, 2185 (1983).

[43] V. K. Pecharsky, K. A. Gschneidner, Jr., A. O. Pecharsky, and A. M. Tishin, Phys. Rev. B **64**, 144406 (2001).

[44] S.Yu. Dan'kov, A.M. Tishin, V.K. Pecharsky, K.A. Gschneidner, Jr., Phys.Rev.B, **57**, 3478 (1998).

CHAPTER 3 CRYSTALLOGRAPHIC STUDY OF DYSPROSIUM

This is a manuscript prepared for publication

A.S. Chernyshov,[1,2] Ya.S. Mudryk,[1] V.K. Pecharsky,[1,2] K.A. Gschneidner, Jr.[1,2]

Abstract

This research is concerned with a detailed X-ray powder diffraction study of polycrystalline Dy in the temperature interval 4 - 300 K in applied magnetic fields up to 40 kOe. Our measurements point to a complicated interplay of magnetic and structural transitions. According to our data, a splitting of a structural transformation and a magnetic transition occurs in non zero magnetic fields in the temperature interval from 135 K to 170 K. A discontinuous change along the *c*-axis follows a first order magnetic Helix-Fan transition, whereas a hexagonal-orthorhombic distortion occurs simultaneously with change of the magnetic structure from Fan to ferromagnetic (FM) state. Our measurements also indicate that transition to FM state is always followed by a distortion of the hexagonal lattice, even if it is a transition from the paramagnetic (PM) to the FM state in magnetic fields exceeding 20 kOe.

---

[1] Ames Laboratory, Materials and Engineering Physics Program, Iowa State University, Ames, IA 50011-3020, USA

[2] Department of Materials Science and Engineering, Iowa State University, Ames, IA 50011-2300, USA

Introduction

The rare-earth metal Dy has been extensively studied over the last few decades, because of its high magnetocrystalline anisotropy, large localized magnetic moment (p_{eff}=10.65μ_B) and complex magnetic structure at low temperatures.[1] At room temperature, Dy is paramagnetic (PM). On lowering the temperature in a zero magnetic field,[2] a helix antiferromagnetic (AFM) ordering occurs at T_N = 180 K (Neél point) that is followed by a transformation to the ferromagnetic structure (FM), and when the temperature is lowered below T_C = 90 K (Curie point) a coupled magnetic – structural transition occurs.[3,4]. At temperatures from the Curie point up to 135 K, an applied magnetic field transforms the magnetic structure directly from a helix to a ferromagnetic type, whereas between 135 K and the Neél point, the AFM - FM transition is separated by an intermediate fan magnetic phase in the range of magnetic fields from 7 kOe to 25 kOe, depending on temperature.

According to single crystal x-ray diffraction study at low temperatures [3], Dy which has a close packed hexagonal crystal structure at room temperature, distorts orthorhombically on lowering temperature below the Curie point in a zero magnetic field. The single crystal x-ray diffraction investigation of Dy in low magnetic fields [4] ($H \leq 1$ kOe), carried out in the vicinities of both the Curie and Neél temperatures, showed the presence of a broad region where the AFM and FM phases coexist as judged from splitting of the (006) peak into two (hexagonal AFM and orthorhombic FM) components. Authors of Ref. 4 reported temperature dependencies of the *c*-lattice parameter in applied magnetic field and showed that even low fields applied along the easy *a*-axis shifts the structural transformation to higher temperatures according to H-T magnetic phase diagram reported in Refs. 2,5,6. It was also shown that a second order transition from helix to PM can be identified as a minimum on the temperature dependence of the *c*-lattice parameter, and the critical field data obtained from the X-ray investigation agree well with the H-T phase diagram. [2,5,6] Kida *et al.*[7] reported similar observations for temperature and magnetic field dependence of the *c*-lattice parameter in magnetic fields up to 60 kOe. The x-ray powder diffraction investigation of polycrystalline Dy at 70 K, 145 K and room temperature in applied magnetic fields up to 13.8 kOe was

undertaken by Finkel and Belovol,[8] who directly observed a hexagonal-orthorhombic distortion in applied magnetic field.

The thermal expansion and magnetostriction of Dy single crystals was first reported by Clark et al.[9] These authors reported the temperature dependencies of the thermal expansion along different crystallographic axes in applied magnetic fields up to 14 kOe. The investigation of correlations between commensurability points, where magnetic helix structure becomes commensurate with the crystal structure, and anomalies of thermal expansion was carried out in Ref. [10].

The magnetic moments of Dy atoms lay in the basal plane (Fig. 1, Appendix), that is, perpendicular to the *c*- axis, of the hexagonal close packed structure [1]. So, Dy in the ordered state has a set of ferromagnetically ordered planes interacting via Ruderman-Kittel-Kasuya-Yoshida (RKKY) interaction. The RKKY interaction has an oscillating character depending on the interatomic distances; therefore, the magnetic structure is sensitive to magnetic field and temperature dependencies of the *c*-lattice parameter. This explains why the majority of crystal structure examinations in applied magnetic field were concerned with measurements of the *c*-lattice parameter, although the hexagonal–orthorhombic transformation occurs as a distortion of the hexagonal net in the basal plane.

There are a number of papers where magnetic phase diagram of Dy along the easy magnetization axis was constructed using different experimental techniques, such as magnetization,[2] ultrasonic measurements,[11] *ac*-calorimetry,[12] magnetocaloric effect [5] and Young's modulus [6] measurements. The most recent work [13] presented a detailed investigation of dysprosium single crystal by *dc* magnetization, *ac*-susceptibility, heat capacity and direct measurements of the magnetocaloric effect. The magnetic phase diagram along the easy magnetization *a*-axis was reported and some new interesting anomalies were revealed. A first order transformation in applied magnetic field up to 20 kOe was observed around the Curie point (90 K) from heat capacity measurements. Additional anomalies were reported close to commensurability point at 113 K and a phenomenological model was proposed to explain the observed anomalies. Heat capacity measurements [13] confirmed the observations of Ref. 7 and 12 that area of the fan phase on the magnetic H-T phase diagram splits into two regions: the

low temperature region in the temperature interval 135-165 K (fan I) and the high temperature region (fan II) that spans from 165 K to the Neél point (180 K). A simple model was proposed stating that a fan structure in a classical understanding exists only in the low temperature region and the high temperature limit of the classical fan was estimated and it coincides with line of critical fields dividing the experimentally observed fan I and fan II regions (~170 K). Additional anomalies close to Neel point were observed by magnetization and direct magnetocaloric effect measurements. The magnetocaloric effect measurements also showed values approximately twice as large as compared to previous measurements in the PM region (Ref. 5) due to AFM clustering in low purity samples.

In this paper we report a detailed x-ray powder diffraction study of polycrystalline Dy in the temperature interval 5-300 K in applied magnetic fields up to 40 kOe. The objective of this work was to directly investigate structural changes in Dy in order to resolve observed [13] contradictions between thermal properties (heat capacity) and magnetic properties (magnetization and magnetocaloric effect).

Experimental details

The polycrystalline Dy investigated in this work was prepared by the Materials Preparation Center at the Ames Laboratory. The major impurities in the bulk metal were as follows (in ppm atomic): O – 600, C – 190, F – 110, Fe – 60, N – 50, and the total of other impurities was ~50. Thus, the starting material was 99.89 at.% (99.98 wt.%) pure. Dysprosium powder was prepared by grinding a piece of metal using rough (80 grit) Al_2O_3 sand paper. Even though Dy is paramagnetic at room temperature, particles stick to a high-power Neomax-type magnet due to a high magnetic moment of dysprosium. The non-magnetic Al_2O_3 particles do not stick to the magnet, thus we used magnetic separation to clean Dy powder from the Al_2O_3 dust. The Dy powder was screened through a 75 μm sieve, wrapped in a Ta foil, sealed in a quartz tube, and annealed for 3 hours at 400 °C to minimize strains produced in a sample during grinding. The final product contained around 9 wt.% of Dy_2O_3 oxide (determined from X-ray diffraction measurements at room temperature). The powder was mixed with a diluted solution of GE varnish in methanol and mounted on a

copper sample holder filling a 24.5×21.4×0.5 mm^3 cavity. After drying, a flat surface was formed by using a 380 grit sand paper to minimize preferred orientation and improve resolution of powder diffraction patterns. The X-ray powder diffraction data were collected on a Rigaku TTRAX rotating anode powder diffractometer with Mo Kα radiation in the 2θ Bragg angle interval ranging of 11° to 55°. The sample temperature was controlled within ±0.02 K below 50 K and better than ±0.05 K above 50 K using a helium flow cryostat. A split-coil superconducting magnet was used to create magnetic fields ranging from 0 to 40 kOe coplanar with the plane of the specimen.[14] Multiple sets of diffraction patterns were collected in a step (1 sec/step) scanning mode with 0.01° steps of 2θ. Each pattern was refined using GSAS[15, 16] software to determine the positional parameters of the individual atoms (for orthorhombic phase) and the unit cell dimensions. Profile residuals (R_p) were about 6-8 % and derived Bragg residuals were from 3 to 5 %. Preferred orientation was accounted using cylindrical symmetry spherical harmonics approximation (8th order, 6 harmonic coefficients) implemented into GSAS [15]. The texture index was 1.29. The same coefficients obtained during refinement of hexagonal phase were used for orthorhombic phase refinement. The other coefficients for Cmcm group (orthorhombic) were kept at zero.

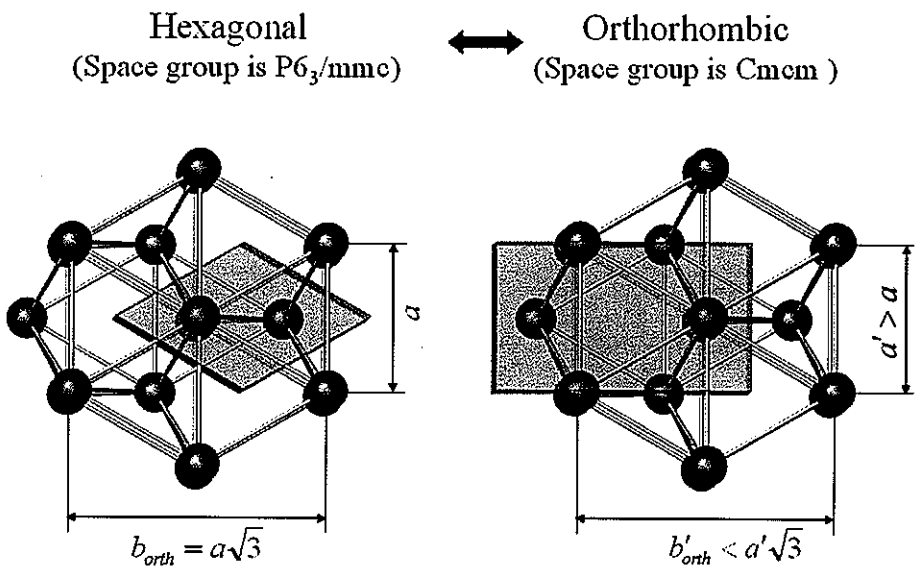

FIG. 1. The comparison of hexagonal (T = 290 K, H = 0) and orthorhombic (T = 60 K, H = 0) unit cells of dysprosium.

Results

At room temperature, dysprosium adopts the hexagonal close packed structure (space group $P6_3/mmc$). Fig. 1 shows the basal plane (perpendicular to the *c*-axis) projection of the crystal structure of Dy and low temperature orthorhombic crystal structure. The gray rhombus and the rectangle represent the basal planes of the unit cells of the two structures. The hexagonal structure with *a* and *c* lattice parameters can be also described as an orthorhombic structure with lattice parameters $a_{orth} = a_{hex}$, $b_{orth} = a_{hex}\sqrt{3}$ and $c_{orth} = c_{hex}$ (see the left hand side of Fig. 1). On cooling dysprosium metal down to $T_C \approx 90$ K the basal plane of the hexagonal structure distorts and the actual lattice parameter b_{orth} deviates from an ideal $a\sqrt{3}$ value (see Fig. 1). This distortion results in a structural transformation from a hexagonal to an orthorhombic lattice symmetry.

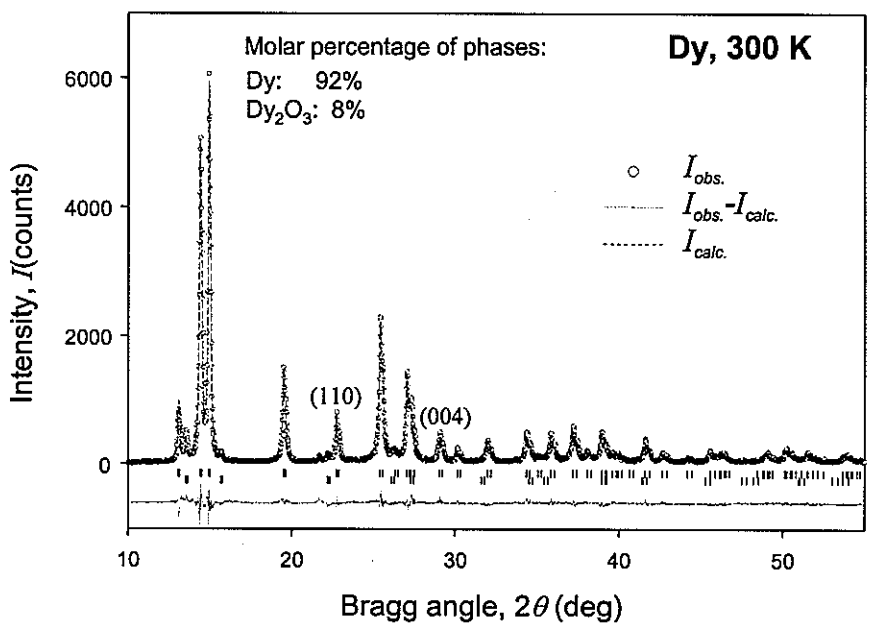

FIG. 2. The x-ray powder diffraction pattern of Dy collected in a zero magnetic field at 300 K. Profile residual (R_p) was about 6 % and derived Bragg residual (R_B) was 3 %. The upper set of vertical bands indicates calculated positions of Bragg peaks of Dy and the lower set represents the same for Dy_2O_3. The Bragg reflections (110) (basal plane) and (004) (*c*-axis) are marked.

The x-ray diffraction pattern, collected at room temperature (300 K) and the results of the Rietveld refinement are presented in Fig. 2. To monitor structural changes at temperatures below 90 K one can use two representative Bragg reflections, the (110) and (004) that are marked in Fig.2. Because the distortion occurs in the basal (*ab*) plane, the splitting of the (hh0) peak is an indicator of the orthorhombic distortion in the hexagonal plane, whereas the shifting of the (00l) peak position is an indicator of changes along the *c*-axis. Fig. 3 and Fig. 4 show the 2θ - temperature maps of scattered intensity collected on heating of the sample in the vicinities of these two reflections. A clear splitting of the hexagonal (110) peak into orthorhombic (200) and (130) peaks and a shift of the (004) peak at temperatures below 90 K are seen in Figs. 3 and 4, respectively. Despite the fact that the splitting is more pronounced at higher Bragg angles (higher values of h), the (110) reflection was chosen because of its high intensity. The maps (Fig. 3 and Fig. 4) represent the actual patterns collected at different temperatures with a step of 5-10 K; dashed lines in Fig. 3 and Fig. 4 follow the intensity maximum positions in the patterns.

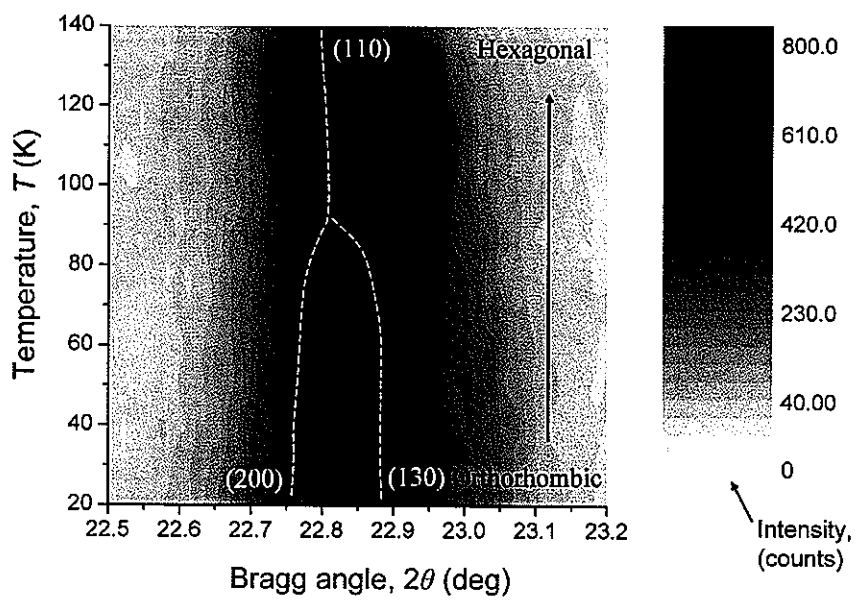

FIG. 3. The contour map of scattered intensity collected on heating in the vicinity of the (110) peak from 20 to 140 K. The dashed lines follow maximum scattered intensity.

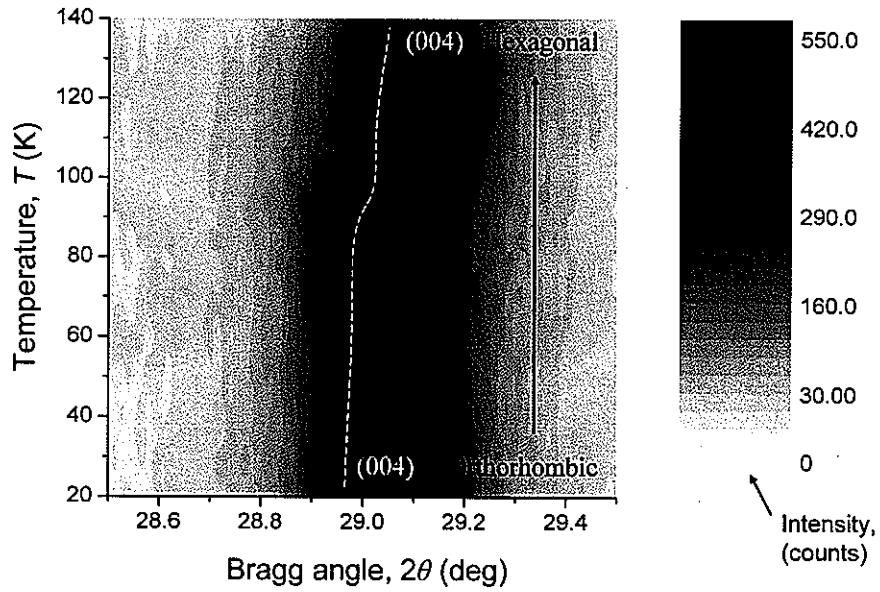

FIG. 4. The contour map of scattered intensity collected on heating in the vicinity of (004) peak from 20 to 140 K. The dashed lines follow the maximums of scattered intensity.

The temperature dependence of the a-lattice parameter of dysprosium in a zero magnetic field is presented in Fig. 5. According to notation of Ref. 8, on lowering temperature, the a-lattice parameter of the hcp structure splits into a- and $b/\sqrt{3}$ orthorhombic parameters as the distortion occurs and the structure changes to the orthorhombic type. The temperatures of transformations on heating and cooling are ~105 K and ~85 K, respectively. Thus, the specimen exhibits a significant hysteresis (~20 K), which is a clear evidence of the first order transformation. The temperature dependencies of the c-parameter (see Fig. 6) show similar values of the transition temperatures and temperature hysteresis.

The temperature dependencies of the a-lattice parameter (hexagonal structure) and/or a- and $b/\sqrt{3}$ parameters (orthorhombic structure) in applied magnetic fields 3 kOe, 12 kOe and 30 kOe are presented in Fig. 7. The curves exhibit structural transitions from hexagonal

to orthorhombic structure type that shifts from 115 K ($H = 3$ kOe) to 145 K and 165 K in 12 kOe and 30 kOe magnetic field, respectively.

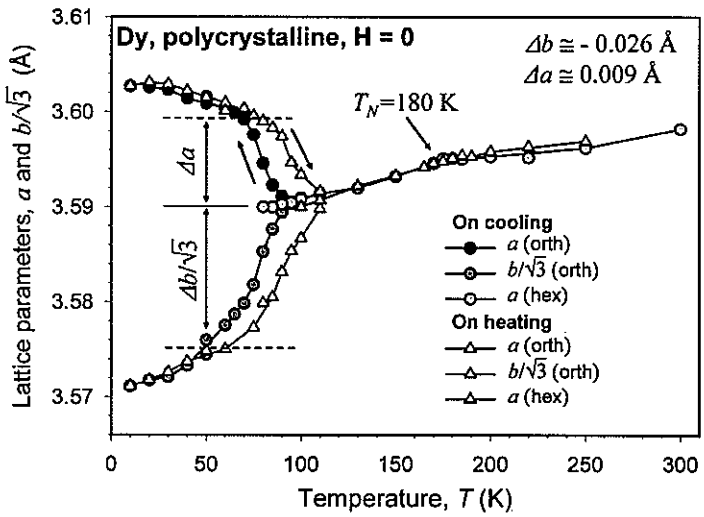

FIG. 5. Temperature dependencies of the hcp a- and of the orthorhombic a- and $b/\sqrt{3}$ lattice parameters of dysprosium in a zero magnetic field between 5 and 300 K.

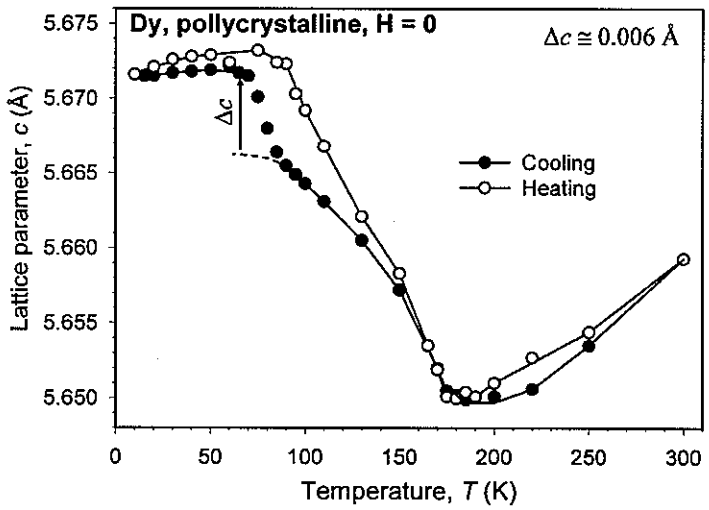

FIG. 6. Temperature dependencies of the c- lattice parameters of dysprosium in a zero magnetic field between 5 and 300 K.

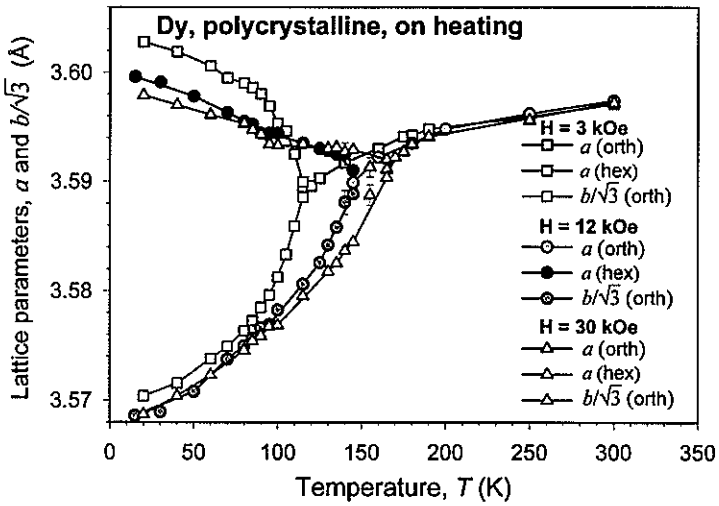

FIG. 7. Temperature dependencies of the hcp a- and of the orthorhombic a- and $b/\sqrt{3}$ lattice parameters in the temperature interval 5 - 300 K, obtained in constant magnetic fields of 3 kOe, 12 kOe and 30 kOe.

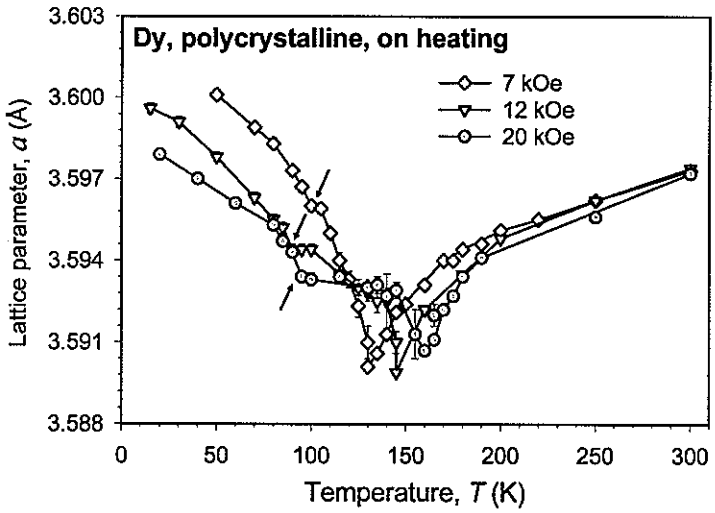

FIG. 8. The temperature dependencies of the hcp and the orthorhombic a-lattice parameter in fixed 7 kOe, 12 kOe and 20 kOe magnetic fields in the temperature interval 5 – 300 K. The arrows indicate the kinks on the curves at low temperatures (orthorhombic structure). The sharp minima correspond to the hcp-orthorhombic distortion.

The 7 kOe, 12 kOe and 20 kOe magnetic field temperature dependencies of the a-lattice parameter are shown in Fig. 8. Sharp singularities between 130 K and 165 K depending on the magnetic field correspond to the structural transition. Weaker kink-like anomalies are also observed around 90 K and these are marked by arrows in Fig. 8.

Fig. 9 represents the temperature dependencies of the *c*-lattice parameter in applied magnetic fields up to 20 kOe. All the curves have a minimum around 180 K that corresponds to the Neél point. A broad maximum around 90 K remains practically unchanged in applied magnetic fields for $H \geq 3$ kOe (see Fig. 9).

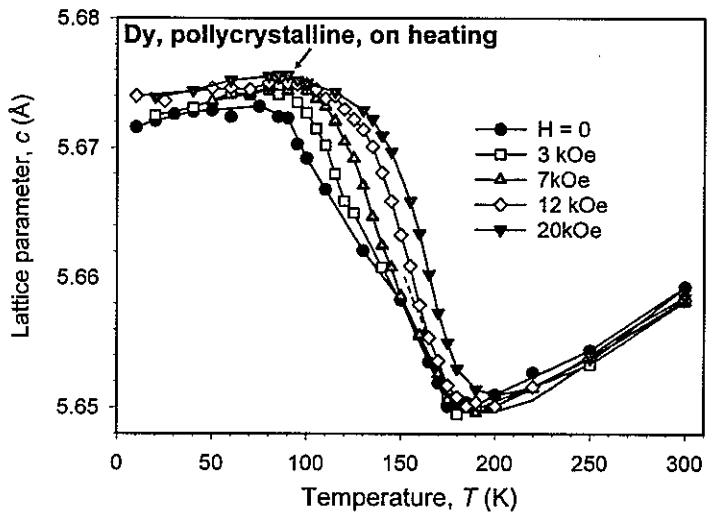

FIG. 9. The temperature dependencies of the *c*-lattice parameter in 0 kOe, 7 kOe, 12 kOe and 20 kOe magnetic fields collected on heating of the sample at fixed magnetic fields. The arrow indicates the broad maxima on the temperature dependence of *c*-lattice parameter.

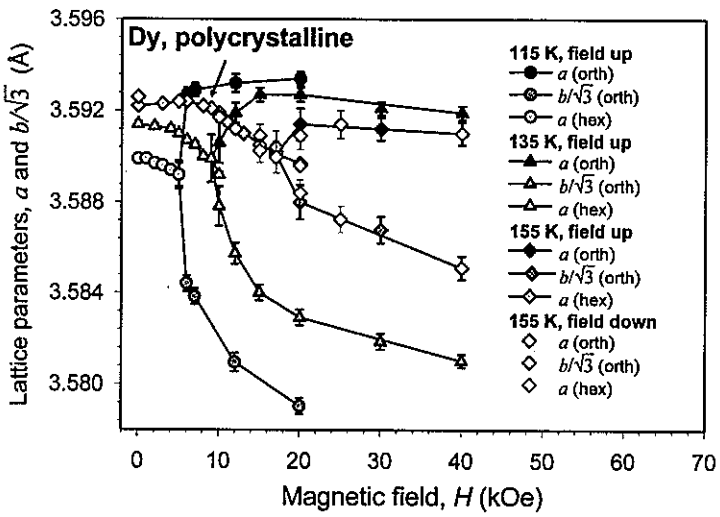

FIG. 10. The isotherms measured at 115 K, 135 K and 155 K representing the hcp *a*- and the orthorhombic *a*- and $b/\sqrt{3}$ lattice parameters as a function of magnetic field. The arrow indicates a kink on the 155 K isotherm.

The isotherms of basal plane parameters for hexagonal and orthorhombic structure in the range of magnetic fields 0 – 40 kOe are presented in Fig. 10. The curves were collected on increasing magnetic field at fixed temperatures. The structural transformation occurs in 5 kOe, 9 kOe and 18 kOe magnetic field at 115 K, 135 K and 155 K correspondingly. One can also note the change of slope on a 155 K isotherm in 10 kOe magnetic field, which is marked by arrow.

The *c*-lattice parameter isotherms in the range of magnetic fields 0 – 40 kOe (see Fig. 11) at 115 K, 135 K, 155 K and 175 K have steps in 5 kOe, 9 kOe, 11 kOe and 10 kOe respectively. There is an inconsistency between the basal plane parameters and the *c*-parameter anomalies, because in Fig. 10 hexagonal-orthorhombic structural transition at 155 K occurs at 18 kOe with kink at 10 kOe, whereas the step of *c*-lattice parameter at 155 K (see Fig. 11) takes place at 11 kOe. We plotted two isotherms at 155 K (see Fig. 11) measured on heating and cooling of the sample to show the presence of a small hysteresis during the AFM-Fan transition around 10 kOe.

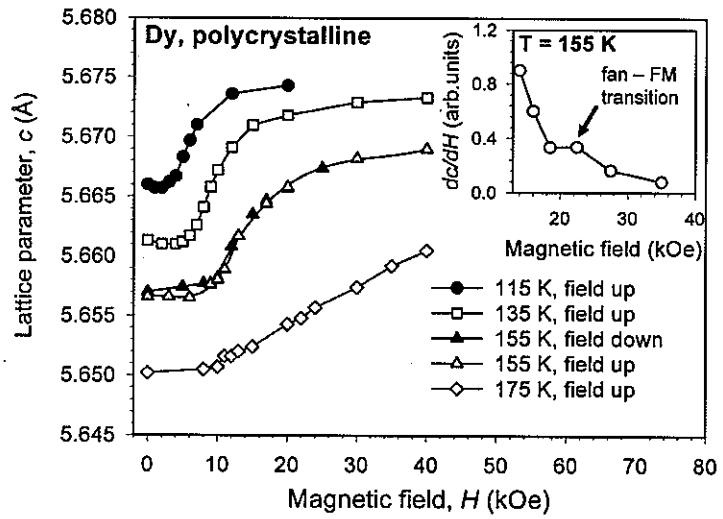

FIG. 11. The isotherms representing the *c*-lattice parameter at 115 K, 135 K, 155 K and 175 K as a function of magnetic field. The inset shows the isotherm at 155 K as the derivative of the *c*-lattice parameter with respect to the magnetic field visualizing a fan - FM transition marked by arrow.

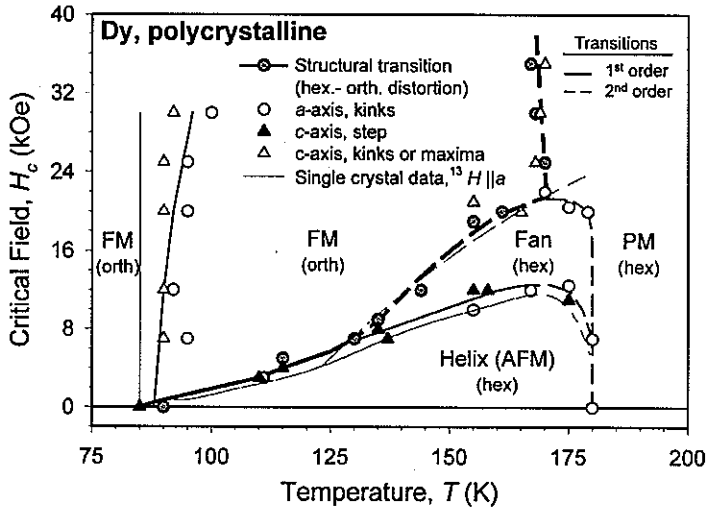

FIG. 12. The structural H-T phase diagram of Dy polycrystal obtained from x-ray powder diffraction data compared to the magnetic phase diagram obtained from single crystal measurements (Ref. 13).

Fig. 12 represents the H-T structural phase diagram of Dy obtained from analyses of basal plane and *c*- lattice parameters behavior described above. The solid circles interpolated by the bold line, solid and dashed follow the boundary of the hexagonal-orthorhombic distortion (see Figs. 5, 7-8 and 10), whereas the solid triangles show the step-like anomalies of the *c*-lattice parameter (see Figs. 9 and 11). The open circles and triangles correspond to minor anomalies of lattice parameters, marked by arrows in Figs. 5 and 8-9. The continuous lines in Fig.12 correspond to a first order transition and the dashed lines correspond to second order transition. The thin lines representing magnetic phase boundaries are taken from Ref. 13, where a study of Dy single crystal with the magnetic field applied along the *a* - axis was carried out using *dc* magnetization, *ac*-susceptibility, heat capacity and direct magnetocaloric effect measurements. Clearly, the magnetic phase diagram of Ref. 13 corresponds quite well with the H-T structural diagram derived from X-ray powder diffraction data.

Discussion

In general, our X-ray powder diffraction measurements are in good agreement with previous magnetic (Refs. 2 and 13), thermal (Refs. 5, 6, 12 and 13) and structural (Refs. 3, 4, 7 and 8) measurements on dysprosium. The structural H-T phase diagram looks similar to the diagrams reported in Refs. 2, 6, 12 and 13. There is also a correspondence between our results and data collected by using single crystal x-ray diffraction technique (Ref. 3, 4, 7). Since there is no sharp step visible during the hexagonal-orthorhombic transition in the data shown in Fig. 5, we tried to estimate changes of the *a*- and *b*- lattice parameters from the maximum height of hysteresis area, marked using dashed lines (see Fig. 5). Thus, Fig. 5 shows the change of parameters $\Delta b = -0.026$ Å, $\Delta a = 0.009$ Å which corresponds to the $\Delta b =$ -0.028 Å and $\Delta a = 0.009$ Å calculated from zero magnetic field data of Ref. 3. The change of the *c*-lattice parameter in a zero magnetic field (see Fig. 6) appears to be $\Delta c = 0.006$ Å, which is lower than $\Delta c = 0.009$ Å, reported in Refs. 3, 4, 7. Thermal expansion measurements [9] along the *a*- and *c*- axes in a zero magnetic field show similar values of the jump of the *c*-lattice parameter (the reported $\Delta c/c = 1.2\times10^{-3}$ corresponds to $\Delta c = 0.007$ Å) and the change a-lattice parameter ($\Delta a/a = 2.8\times10^{-3}$ corresponds to $\Delta a = 0.01$ Å). Since there are no literature data about direct x-ray measurements of basal plane parameters in applied magnetic field, our results were compared to the Dy single crystal thermal expansion and magnetostriction measurements of Ref. 9 along different crystallographic directions in magnetic fields up to 12 kOe applied along the *a*-axis and a qualitative agreement was observed.

There are no distinct discontinuities on the temperature dependencies of lattice parameters (see Figs. 5-11), which can be associated with a first order phase transition, because it was difficult to refine both phases simultaneously due to relatively broad peaks which were caused by residual strain remaining in the powders even after the heat treatment of the powder. One can qualitatively see the coexistence of hexagonal and orthorhombic phases on the X-ray diffraction patterns (e.g. see Fig. 3), but it was impossible to quantify phase contents using Rietveld refinement, meaning that in the two-phase region we are reporting the "average" lattice parameters. The temperature interval of the two-phase

coexistence region amounts to ~20 K and is close to the observed value of the temperature hysteresis during the transition (see Fig. 5).

The present investigation allows us to clarify the connection among magnetic and crystallographic transitions in Dy. According to magnetic measurements of dysprosium (Ref. 2, 5 and 13) there is a first order Helix-FM transition in the temperature interval 90 – 130 K in magnetic fields below 8 kOe (see Fig. 12). At higher temperatures the transformation to FM state occurs through an intermediate fan magnetic phase, which exists in the temperature interval from 130 K to the Neél point (180 K) in the range of magnetic fields 8 – 22 kOe. Dysprosium has a layered magnetic structure consisting of ferromagnetically ordered planes stacked perpendicular to the *c*-axis. So, it is natural to assume that the interplay between Helix, Fan and FM phases is mostly determined by the inter-layer distance (*c*-lattice parameter).

In the temperature interval 80 – 135 K the hexagonal-orthorhombic distortion coincides with the jump along the *c*-axis tied up with magnetic transition (see Fig. 12). At temperatures above 135 K the crystallographic and magnetic transitions split into the first order Helix – Fan transition with the related jump of the *c*-lattice parameter and the second order Fan - FM transition, which is accompanied by the orthorhombic distortion. Hence, the Helix-Fan transition occurs without a change of the symmetry of the lattice, only with a change of the *c*-lattice parameter. The Fan-FM transition can be also identified from magnetic field isotherms of the *c*-lattice parameter (see inset to Fig. 11 and Ref. 7). The inset to Fig. 11 shows a clear second order nature of the coupled Fan – FM and hexagonal - orthorhombic transition. The important conclusion is that a transition to FM state is always coupled with an orthorhombic distortion of the hexagonal lattice (see Fig. 12). So the minimum of free energy of the ferromagnetic phase is reached for the orthorhombic lattice, whereas Helix and Fan magnetic structures exist in the hexagonal lattice only.

According to magnetic measurements (Ref. 2, 5 and 13) and single crystal X-ray diffraction study (Ref. 7) the first order magnetic transformation from Helix to FM and/or Fan structure becomes second order at the so-called tricritical point at 170 K. Our measurements confirm the change of order of the transition. One can see from Fig. 11 that

magnetic field isotherm of the *c*-lattice parameter at 175 K has only a change of slope instead of a characteristic discontinuity, showing up at 115 K, 135 K and 155 K. It is worth noting that change of the order of the AFM-Fan transition also affects the origin of the Fan-FM (PM) transition. According to our data (see Fig. 12) the Fan-FM transition below tricritical point occurs simultaneously with an orthorhombic distortion, whereas the Fan-PM transition in the temperature interval from tricritical (165 K) to Neél point occurs without any structural changes. It is questionable what magnetic structure actually exists in the temperature interval from 165 to 180 K in magnetic fields from 10 kOe to 20 kOe, especially taking into account the results of Ref. 13, where authors show that classical Fan is not stable at temperatures above ~170 K.

Recent measurements of the heat capacity of high-purity dysprosium single crystal (Ref. 13) observed unusual anomalies in the vicinity of Curie point in magnetic fields applied along easy the *a*-axis. According to Ref. 13, a sharp peak observed at the Curie temperature in a zero magnetic field, does not shift to higher temperature as expected from magnetic measurements (Ref. 2, 5 and 13). However, another small anomaly appears on the heat capacity curve in applied magnetic field in addition to the sharp peak. On increasing magnetic field the small anomaly quickly moves towards higher temperatures following the AFM-FM transition until the Fan phase appears at 135 K ($H = 8$ kOe) and then the anomaly follows the Fan-FM transition boundary. This generally agrees with the X-ray powder diffraction data; one can see anomalies in the vicinity of Curie point marked by arrows on temperature dependencies of the *a*-lattice parameter (see Fig. 8). It is worth noting that minor anomaly of the heat capacity from Ref. 13 follows the boundary of the hexagonal – orthorhombic transition, which also follows Fan – FM magnetic transition at temperatures above 135 K (see Fig. 12).

Another open question is whether the orthorhombic-hexagonal distortion is preserved in higher magnetic fields. Our isofield temperature measurements (see Fig. 12) indicate that hexagonal-orthorhombic transition together with slope change of the *c*-lattice parameter still takes place around 160 K in magnetic fields above 20 kOe. Thus, assuming that the FM phase has the minimum energy in a distorted orthorhombic lattice and the PM phase

maintains hexagonal type of crystal structure, the distortion should exist as long as Dy undergoes transition to the ferromagnetic state.

Conclusion

The X-ray powder diffraction study was undertaken in the temperature interval 4 – 300 K in the range of magnetic fields up to 40 kOe. Our measurements confirmed complicated nature of magnetic field - temperature relationships in pure Dy and agree well with the heat capacity observations of Ref. 13. The main conclusion is that ferromagnetic structure is observed together with the orthorhombic distortion of the crystal structure, whereas Helix, Fan and PM magnetic structures have lower energies in an undistorted hexagonal lattice. The hexagonal-orthorhombic distortion and the pronounced anomaly in the *c*-lattice parameter are coupled with AFM-FM transition in magnetic fields below 8 kOe. However, on applying magnetic field above 8 kOe our structural measurements show that these two phenomena are no longer coupled: the change along the *c*-axis occurs between 8 and 12 kOe and the orthorhombic distortion occurs between 8 and 20 kOe, this results in an increase in the number of ordered states of Dy.

Acknowledgements

This work was supported by the Office of Basic Energy Sciences, Materials Sciences Division of the U.S. DOE under contract No. W-7405-ENG-82.

References

[1] J. Jensen and A. R. Mackintosh, *Rare earth magnetism: structure and excitations* (Clarendon Press, Oxford, 1991), 12 pp.

[2] R Hertz and H. Kronmüller, J. Magn. Magn. Mater. **9**, 273 (1978).

[3] F.J. Darnell, E.P. Moore, Suppl. J. Appl. Phys. **34**, 1337 (1963).

[4] V.V. Vorob'ev, M.Ya. Krupotkin, and V.A. Finkel, Sov. Phys. JETP **61**, 1056 (1985).

[5] S.A. Nikitin, A.S. Andreenko, and V.A. Pronin, Fiz. Tverd. Tela (Leningrad) **21**, 2808 (1979).

[6] A.M. Tishin and O.P. Martynenko, *Physics of Rare Earth Metals in the Vicinity of Magnetic Phase Transitions* (Nauka, Moscow, 1995), 336 pp.

[7] Y. Kida, K. Tajima, Y. Shinoda, K. Hayashi, and H. Ohsumi, J. Phys. Soc. Jpn. **68**, 650 (1999).

[8] V.A. Finkel and B.C. Belovol, Soviet Phys. JETP **30**, 424 (1970).

[9] A.E. Clark, B.F. DeSavage and R. Bozorth, Phys. Rev. **138**, A216-24 (1965).

[10] R.D. Greenough, G.N. Blackie and S.B. Palmer, J. Phys. C: Solid State Phys. **14**, 9 (1981).

[11] A.V. Andrianov, Yu.P. Gaidukov, A.N. Vasil'ev, and E. Fawcett, J. Magn. Magn. Mater. **97**, 246 (1991).

[12] H.U. Astrom and G. Benediktson, J. Phys. F **18**, 2113 (1988).

[13] A.S. Chernyshov, A.O. Pecharsky, A.M. Tishin, K.A. Gschneidner, Jr.,[1,2] and V.K. Pecharsky, Phys. Rev. B **71**, 184410 (2005).

[14] A.P. Holm, V.K. Pecharsky, K.A. Gschneidner, Jr., R. Rink and M.N. Jirmanus, Rev. Sci. Instrum. **75(4)**, 1081-8 (2004).

[15] A.C. Larson, and R.B. Von Dreele, Los Alamos National Laboratory Report LAUR 86-748 (1986). Revision: 2005.

[16] B.H. Toby, J. Appl. Cryst. **34**, 210-213 (2001).

CHAPTER 4: STRUCTURAL AND MAGNETO-THERMAL PROPERTIES OF THE $Gd_5Sb_xGe_{4-x}$ SYSTEM

The paper is published in *Journal of Applied Physics* [1]

A.S. Chernyshov,[2,3] Ya.S. Mudryk,[2] V.K. Pecharsky,[2,3] K.A. Gschneidner, Jr.[2,3]

Abstract

The crystallographic and magnetic properties of the $Gd_5Sb_xGe_{4-x}$ pseudo-binary system were studied by x-ray powder diffraction at room temperature, and the heat capacity, magnetization and electrical resistivity in the temperature interval 5-320 K in applied *dc* magnetic fields between 0 and 100 kOe. The $Gd_5Sb_{2.1}Ge_{1.9}$ compound adopts the $Tm_5Sb_2Si_2$-type structure (space group Cmca) and orders magnetically via a second order ferromagnetic-paramagnetic transition at 200 K, whereas the $Gd_5Sb_xGe_{4-x}$ compounds with x = 0.7 and x = 1 crystallize in the Sm_5Ge_4-type structure (space group Pnma) and exhibit first order phase transformations at 45 K and 37 K, respectively, and therefore, the giant magnetocaloric effect. The heat capacity and electrical resistivity measurements of $Gd_5Sb_{0.7}Ge_{3.3}$ indicate a second order antiferromagnetic transition at 60 K in fields 20 kOe and lower.

---

[1] Journal of Applied Physics, 2006, 99, 08Q102

[2] Ames Laboratory, Materials and Engineering Physics Program, Iowa State University, Ames, IA 50011-3020, USA

[3] Department of Materials Science and Engineering, Iowa State University, Ames, IA 50011-2300, USA

Introduction

The magnetic properties of $R_5(Si_xGe_{1-x})_4$ system, where R - is a lanthanide metal, have been extensively studied since 1997 after Pecharsky and Gschneidner[1] discovered the giant magnetocaloric effect in the $Gd_5Si_2Ge_2$ compound. Due to a coupled magneto-structural first-order phase transition in this and other $R_5(Si_xGe_{1-x})_4$ compounds, a number of intriguing magnetic properties, such as the giant magnetostriction[2] and the giant magnetoresistance[3] have been observed in addition to the giant magnetocaloric effect. The crystal structures of $R_5(Si_xGe_{1-x})_4$ compounds consist of ${}^{2}_{\infty}[Gd_5T_4]$ slabs, where T is a statistical mixture of Ge and Si. Specific T-T dimers between the slabs can be reversibly broken or reformed by changing temperature, concentration (x) and/or by applying pressure or magnetic field, leading to magnetostructural transitions. Recent studies of the $Gd_5(Ge_xGa_{1-x})_4$ system[4] showed a sequence of structures changing with x, that mimic the martensitic transition observed in $Gd_5Si_2Ge_2$.[5] The authors of Ref. 4 suggested that lack of one electron in the outer shell of Ga (3 valence electrons for Ga instead of 4 for Si) drives the change of the crystallography in the $Gd_5(Ge_xGa_{1-x})_4$ system via a gradual reduction of the valence electron concentration. Therefore, it is natural to examine how a shift of the valence electron concentration in the opposite direction by substituting pentavalent antimony for tetravalent Si or Ge affects the crystallography and physical properties of the $Gd_5Sb_xGe_{4-x}$ compounds.

A crystallographic study of several $R_5Sb_2(Si,Ge)_2$ compounds,[6] showed the existence of a new structure type, called the $Tm_5Sb_2Si_2$–type structure. The latter is closely related to the Sm_5Ge_4–type, but has a higher symmetry (space group is Cmca instead of Pnma). The authors [6] reported several compounds with heavy rare-earth metals, however they did not observe the $Gd_5Sb_2Ge_2$ compound.

Experimental details

The starting materials for synthesis of $Gd_5(Sb_xGe_{1-x})_4$ samples were pieces of Gd (99.86 at.% or 99.99 wt.%) prepared by the Materials Preparation Center of the Ames Laboratory, and Sb (99.99 wt.%) and Ge (99.99 wt.%) purchased from Meldform Metals

(United Kingdom). Four samples weighting ~5 g each of the $Gd_5Sb_xGe_{4-x}$ alloys with x = 0.5, 1, 2 and 3 stoichiometry were prepared by arc-melting the elements on a copper hearth in an argon atmosphere. Because of low boiling temperature of antimony (1860 K), we used ~5% excess of this metal to make up for evaporation to maintain the necessary stoichiometries. The alloy buttons were remelted 4 times to minimize inhomogeneities. The x-ray powder diffraction studies were performed on an automated Scintag powder diffractometer using Cu-Kα radiation; the crystal structures were refined using Rietveld technique. The magnetization and electrical resistivity data were measured using a Lake Shore magnetometer, model 7225. Magnetic measurements were carried out in the temperature interval from 4.5 K to 300 K in applied magnetic fields up to 56 kOe. Electrical resistivity was measured by a standard four-probe technique in the temperature interval 5-350 K in applied magnetic fields up to 40 kOe. The heat capacity in magnetic fields up to 100 kOe was measured between ~2 K and 350 K in a semiadiabatic heat pulse calorimeter, which has been described elsewhere.[7]

Results

The room temperature x-ray data indicate that when $x \geq 2$, $Gd_5Sb_xGe_{4-x}$ adopts the $Tm_5Sb_2Si_2$–type structure. When $x < 2$, $Gd_5Sb_xGe_{4-x}$ has the orthorhombic Sm_5Ge_4-type structure, same as the binary Gd_5Ge_4. The lattice parameters are listed in Table I. According to the results of the Rietveld refinement, the actual compositions of the $Gd_5Sb_{0.5}Ge_{3.5}$, $Gd_5Sb_2Ge_2$ and Gd_5Sb_3Ge and alloys were $Gd_5Sb_{0.7}Ge_{3.3}$, $Gd_5Sb_{2.1}Ge_{1.9}$ and $Gd_5Sb_{2.7}Ge_{1.3}$, respectively. Based on the results obtained for the latter component, it is quite likely that the largest amount of Sb soluble in Gd_5Ge_4 is x = 2.7.

The magnetization, electronic transport and heat capacity of the three compositions with x = 0.7, 1 and 2.1 were measured. The $Gd_5Sb_{2.1}Ge_{1.9}$ compound exhibits a second order ferromagnetic-paramagnetic (FM-PM) transition at 200 K, whereas $Gd_5Sb_xGe_{4-x}$ with x = 0.7 and x = 1 undergo first order phase transformations at 45 K and 37 K, respectively.

TABLE I The crystallographic properties of alloys in the $Gd_5Sb_xGe_{4-x}$ system. Data for $x = 0$ are taken from Ref. 8.

x	a (Å)	b (Å)	c (Å)	Interslab, $d_{T\text{-}T}$, (Å)	Structure type
0	7.697(5)	14.83(1)	7.785(6)	3.71	Sm_5Ge_4
0.7*	7.786(6)	14.89(1)	7.844(6)	3.77	Sm_5Ge_4
1*	7.865(9)	14.97(2)	7.901(9)	3.82	Sm_5Ge_4
2.1*	15.17(1)	7.968(8)	7.982(9)	4.22	$Tm_5Sb_2Si_2$
2.7*	15.28(1)	8.049(9)	8.072(9)	4.27	$Tm_5Sb_2Si_2$

* As determined from the Rietveld analysis.

Selected magnetization isotherms of Gd_5SbGe_3, shown in Fig. 1, are similar to those observed for $Gd_5Sb_{0.7}Ge_{3.3}$. Although there are no distinct steps of the magnetization on the isotherms, the presence of hysteresis points to a first order nature of the phase transformation that occurs between 45 K and 67 K in magnetic fields below 50 kOe. The magnetization results have been confirmed by heat capacity that shows a sharp first-order phase transition peak moving to higher temperatures with the increasing magnetic field, which is also similar to $Gd_5Sb_{0.7}Ge_{3.3}$, see below. A small anomaly observed at 100 K on the *M(T)* dependencies (not shown) can be interpreted as the Néel point and the first order phase transition at 45 K most likely is of ferromagnetic-antiferromagnetic (FM-AFM) type. It follows from the noticeable FM component observed in low magnetic fields at temperatures as high as 94 K (see Fig. 1) that the AFM structure of this compound may be quite complex. The maximum isothermal magnetic entropy change (ΔS_M), calculated from the heat capacity data for Gd_5SbGe_3, is -23.5 J/kg K at T = 53 K for a 50 kOe magnetic field change, which is somewhat less than the ΔS_M = -37 J/kg K exhibited by $Gd_5Si_{0.33}Ge_{3.67}$ for a 50 kOe magnetic field change at 70 K (Ref. 9), but the former still maintains all the characteristics of the giant magnetocaloric effect.

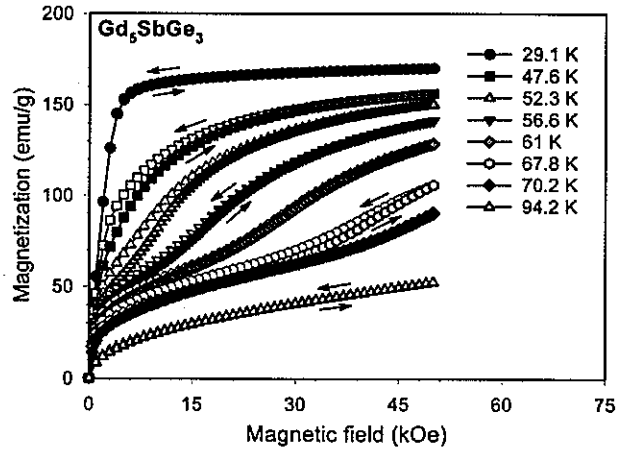

FIG. 1. The magnetization isotherms of Gd_5SbGe_3 in the temperature interval 29-94 K in the range of magnetic fields up to 50 kOe.

The temperature dependencies of magnetization of $Gd_5Sb_{0.7}Ge_{3.3}$ from 4 to 250 K in magnetic fields of 1 kOe, 10 kOe and 20 kOe are presented in Fig. 2. The curves exhibit a sharp step of the magnetization at 37 K in a 1 kOe magnetic field, which shifts to higher temperatures with increasing magnetic field (T = 55 K in a 20 kOe magnetic field). The step in the magnetization corresponds to a first-order magnetic phase transition that is also confirmed by the heat capacity data (Fig. 3). There are also anomalies at ~60 K and ~150 K that can barely be seen in the 1 kOe and 10 kOe curves (inset, Fig. 2). The anomaly at ~150 K may be due to the magnetic ordering of an impurity phase, whose concentration was to low to be detected by x-ray powder diffraction. The heat capacity data only show the presence of a second order transformation at T=60 K in magnetic fields below 20 kOe (see inset in Fig. 3) and no anomaly at 150 K, which is consistent with a small amount of an impurity phase. To clarify the nature of the transformation at T = 60 K, the electrical resistivity measurements were carried out (see Fig. 4). There is a step-like behavior at the first order phase transition and a broad maximum at 60 K that relates to the second order phase transition observed in the heat capacity data. The anomaly at 60 K can be interpreted as a Néel point corresponding to AFM-PM transition. The maximum isothermal magnetic entropy change (-27 J/kg K) for $Gd_5Sb_{0.7}Ge_{3.3}$, calculated from the heat capacity, is observed at 70 K

for a 70 kOe magnetic field change. The corresponding value estimated from *M(H)* data using Clausius-Clapeyron equation for the same magnetic field change is -25 J/kg K.

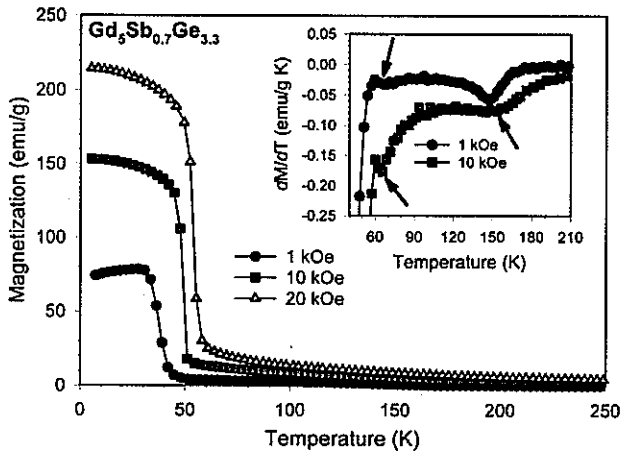

FIG. 2. Temperature dependencies of the magnetization of $Gd_5Sb_{0.7}Ge_{3.3}$ measured in 1 kOe, 10 kOe and 20 kOe magnetic fields. The inset shows the rate of change of the magnetization with field as a function of temperature. The arrows in the inset indicate observed anomalies.

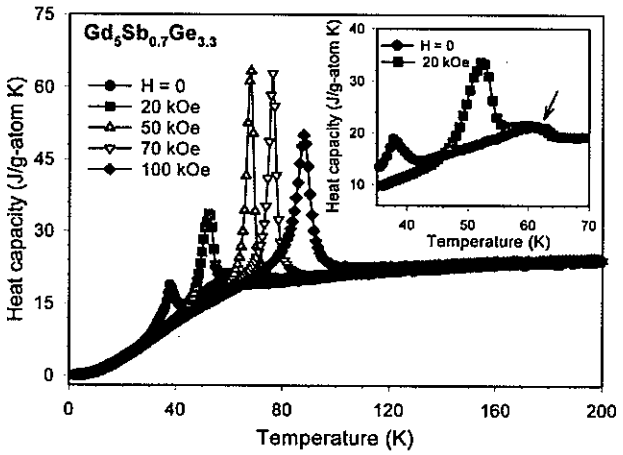

FIG. 3. Temperature dependencies of the heat capacity of $Gd_5Sb_{0.7}Ge_{3.3}$ in magnetic fields up to 100 kOe. The inset shows the details of the second order transition around 60 K.

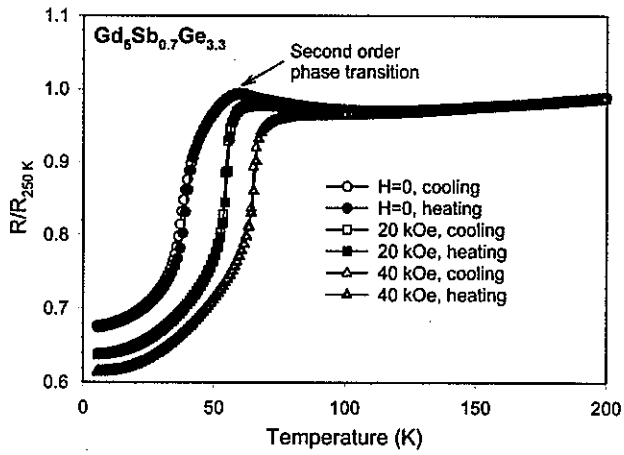

FIG. 4. Temperature dependencies of the electrical resistivity of $Gd_5Sb_{0.7}Ge_{3.3}$ in applied magnetic fields up to 40 kOe.

Discussion

We believe that like in Gd_5Ge_4, where AFM-FM transition is coupled to a martensitic-like structural change,[10] the same happens in both $Gd_5Sb_{0.7}Ge_{3.3}$ and Gd_5SbGe_3. The nature of the structural transition in the $Gd_5Sb_xGe_{4-x}$ system, however, remains open and needs to be studied using x-ray diffraction measurements at low temperatures and in applied magnetic fields. At this point we only know that at room temperature the crystal structure is similar to that of the Gd_5Ge_4 compound, i.e. there are no T-T dimers between the ${}^{2}_{\infty}[Gd_5T_4]$ slabs. Similar to $Gd_5(Si_xGe_{1-x})_4$, one can assume that temperature and/or magnetic field restore some or all of the T-T dimers, causing a structural transition simultaneously with the ferromagnetic ordering. With this assumption and recalling that at room temperature for $x \geq 2$ the T-T interslab distances ($d_{T\text{-}T}$) in $Gd_5Sb_xGe_{4-x}$ are much longer than for $x < 2$ (see Table I), one may explain the absence of a first-order transition when $x \geq 2$ by the inability of the system to restore T-T bonding like in Gd_5Ge_4. One can also notice that 60 K antiferromagntetic transition for $Gd_5Sb_{0.7}Ge_{3.3}$ is magnetic field independent and it disappears in fields above ~20 kOe, where it merges with a structural transformation. In other

words, the AFM-PM transition is found only in the high temperature (low field) Sm_5Ge_4–type phase.

Conclusion

In summary, the $Gd_5Sb_xGe_{4-x}$ system exhibits interesting structural and magnetic properties along with a high value of the isothermal magnetic entropy change. Compared to the $Gd_5(Si_xGe_{1-x})_4$ system, the $Gd_5Sb_xGe_{4-x}$ system exhibits narrower hysteresis during the first order transformation and the samples with antimony are less brittle. Detailed measurements of a single crystal of $Gd_5Sb_{0.7}Ge_{3.3}$ are planned in the near future.

Acknowledgements

This work was supported by the Office of Basic Energy Sciences, Materials Sciences Division of the U.S. DOE under contract No. W-7405-ENG-82.

References

[1] V.K. Pecharsky and K.A. Gschneidner, Jr., Phys. Rev. Lett. **78**, 4494 (1997)

[2] L. Morellon, P.A. Algarabel, M.R. Ibarra, J. Blasco, B. Garcia-Landa, Z. Arnold, and F. Albertini, Phys. Rev. B **58**, R14721-R14724 (1998)

[3] E.M. Levin, A.O. Pecharsky, V.K. Pecharsky, and K.A. Gschneidner, Jr., Phys. Rev. B **63**, 064426/1-064426/10 (2001)

[4] Yurij Mozharivskyj, Wonyoung Choe, Alexandra O. Pecharsky, and Gordon J. Miller, J. Am. Chem. Soc. **125**, 15183 (2203).

[5] W. Choe, V.K. Pecharsky, A.O. Pecharsky, K.A. Gschneidner, Jr., V.G. Young, Jr., G.J. Miller, Phys. Rev. Lett **84**, 4617 (2000)

[6] A.Yu. Kozlov, V.V. Pavlyuk, V.M. Davydov, Intermetallics **12**, 151 (2004)

---

[7] V. K. Pecharsky, J. O. Moorman, and K. A. Gschneidner, Jr., Rev. Sci. Instrum. **68**, 4196 (1997).

[8] A.O. Pecharsky, K.A. Gschneidner, Jr., V.K. Pecharsky and C.E. Schindler, J. Alloys Compd. **338**, 126 (2002).

[9] V. K. Pecharsky and K. A. Gschneidner, Jr., Appl. Phys. Lett. **70**, 3299 (1997)

[10] V. K. Pecharsky, A. P. Holm, K. A. Gschneidner, Jr. and R. Rink, Phys. Rev. Lett. **91**, 197204 (2003)

CHAPTER 5: CRYSTALLOGRAPHIC AND MAGNETIC PROPERTIES OF THE $Gd_5Sb_{0.5}Ge_{3.5}$ SINGLE CRYSTAL

The paper is prepared for publication

A.S. Chernyshov,[1,2] Ya.S. Mudryk,[1] V.K. Pecharsky,[1,2] K.A. Gschneidner, Jr. [1,2]

D. Schlagel [1] and T.A. Lograsso.[1]

Abstract

Crystallographic and magnetic properties of a $Gd_5Sb_{0.5}Ge_{3.5}$ single crystal were investigated using a variety of experimental techniques: *dc* magnetization, ac-susceptibility, electrical resistivity, heat capacity and X-ray powder diffraction. Our measurements indicate that the compound undergoes a coupled magnetic-structural transition at 40 - 70 K and an electronic transition around 60 K. The detailed crystallographic study of $Gd_5Sb_{0.5}Ge_{3.5}$ shows that unlike $Gd_5(Si_xGe_{1-x})_4$, the coupled magnetic structural transition occurs without shear displacements of the $^2_\infty[Gd_5T_4]$ slabs (T is a statistical mixture of Si,Ge or Sb,Ge). The magnetic and structural properties show narrower temperature and magnetic field hystereses associated with a first order transition, when compared to $Gd_5(Si_xGe_{1-x})_4$, which may be important for practical applications. Low magnetic field data clearly show a presence of complicated short range magnetic ordering (Griffiths phase) in the temperature interval from 40 to 250 K. A theoretical model that quantitatively describes the electronic transition in Gd_5Ge_4 and $Gd_5Sb_{0.5}Ge_{3.5}$ and its evolution with addition of Sb is proposed.

---

[1] Ames Laboratory, Materials and Engineering Physics Program, Iowa State University, Ames, IA 50011-3020, USA

[2] Department of Materials Science and Engineering, Iowa State University, Ames, IA 50011-2300, USA

Introduction

The magnetic and crystallographic properties of $R_5(Si_xGe_{1-x})_4$ system, where R – is a rare-earth metal, have been extensively studied since 1997, when Pecharsky and Gschneidner[1] discovered the giant magnetocaloric effect in $Gd_5Si_2Ge_2$ compound. These alloys exhibit a coupled magnetic-structural transition, which not only accounts for the giant magnetocaloric effect, but also the giant magnetostriction[2] and giant magnetoresistance.[3] The system may be utilized for numerous practical applications, because transition temperature, where the giant magnetic responses occur, may be "tuned" by varying Si content.

At room temperature, crystal structure of $R_5(Si_xGe_{1-x})_4$ compounds consists of ${}^{2}_{\infty}[Gd_5T_4]$ slabs, fully or partially bonded by T-T dimers, where T is Si, Ge or their statistical mixture.[4] There are three basic structure types observed in the $R_5(Si_xGe_{1-x})_4$ systems:

1. the orthorhombic Sm_5Ge_4-type (space group is Pnma) with all of the T-T dimers between ${}^{2}_{\infty}[Gd_5T_4]$ broken;
2. the monoclinic $Gd_5Si_2Ge_2$-structure type (space group is $P112_1/a$) with half of the T-T interslab dimers broken;
3. the orthorhombic Gd_5Si_4-structure type (space group is Pnma) . all T-T dimers between ${}^{2}_{\infty}[Gd_5T_4]$ slabs formed.

The formation of T-T dimers strongly affects exchange interaction between ferromagnetically ordered ${}^{2}_{\infty}[Gd_5T_4]$ slabs and the resulting type of magnetic structure. Therefore, on lowering temperature, or changing composition, or applying magnetic field, or pressure the restoration of T-T bonds drives a coupled magnetic – structural transition, which usually starts from orthorhombic Sm_5Ge_4- or monoclinic $Gd_5Si_2Ge_2$- types of structures and ends up as orthorhombic Gd_5Si_4-type with all the T-T dimers formed. It is worth noting that Gd_5Si_4 and Sm_5Ge_4 structure types have the same symmetry of the lattice (space group is Pnma). The difference between those two structure types is a shear displacement of ${}^{2}_{\infty}[Gd_5T_4]$ slabs that restores T-T bonding between the slabs.

Following a series of works devoted to $R_5(Si_xGe_{1-x})_4$ system, a detailed X-ray single crystal and powder diffraction study of $Gd_5(Ga_xGe_{1-x})_4$ was undertaken [5] and a sequence of structures depending on the concentration (x) as in the $Gd_5(Si_xGe_{1-x})_4$ system was observed. The authors [5] showed that substituting Si with Ga, which has 1 electron less in the outer shell (3 valence electrons for Ga instead of 4 for Si), drives a change of crystallography of the $Gd_5(Ga_xGe_{1-x})_4$ system via a gradual reduction of the valence electron concentration, a mechanism similar to the recently reported in $Gd_5Si_2Ge_2$.[6] A crystallographic study of several $R_5Sb_2(Si,Ge)_2$ alloys was undertaken Ref. [7]. The authors reported a new structure type, called the $Tm_5Si_2Sb_2$-type structure, which is closely related to the Sm_5Ge_4-type, but has a higher crystallographic symmetry (space group is Cmca instead of Pnma). Several $R_5Sb_2(Si,Ge)_2$ compounds were reported, however authors [7] did not observe the $Gd_5Sb_2Ge_2$ compound.

Following the idea of substituting Si with Ga, crystallographic, magnetic, electronic and thermal measurements of $Gd_5Sb_xGe_{4-x}$ system were recently reported,[8] where Si was substituted with Sb, which has an additional *p*-electron in the outer shell, compared to Si. The room temperature X-ray powder diffraction study [8] shows that the largest amount of Sb soluble in $Gd_5Sb_xGe_{4-x}$ is $x = 2.7$. For $x < 2$, the system adopts the Sm_5Ge_4 type of crystal structure, which is the same structure as pure Gd_5Ge_4. For $2 < x < 2.7$ the room temperature crystal structure of the $Gd_5Sb_xGe_{4-x}$ alloys is the $Tm_5Si_2Sb_2$-type. Magnetic measurements show that there is a first order magnetic transition for low concentrations of Sb ($x < 2$) and a second order transition from ferromagnetic (FM) to paramagnetic (PM) state for $2 < x < 2.7$. At low temperatures $Gd_5Sb_xGe_{4-x}$ is ferromagnetic. For the $Gd_5Sb_{0.5}Ge_{3.5}$ compound ($x = 0.5$) the transition from ferromagnetic to antiferromagnetic (AFM) state occurs at 37 K and at 60 K the second order joint electronic and AFM-PM transition was observed from the heat capacity and electrical resistivity data. The last transition is similar to the second order transition at 130 K in Gd_5Ge_4. For $x = 1$ there is a first order FM to PM transition, while for $x = 0.5$ the transition is from the AFM to the PM state. The critical temperatures of the observed magnetic transitions of $Gd_5Sb_xGe_{4-x}$ in a zero magnetic field are listed in Table I, for the examined Sb concentrations. Additional anomalies in the *dc* of magnetization and ac-susceptibility were observed at ~150 K and ~100 K for $x = 0.5$ and $x = 1$ respectively [8], and are probably due to short range magnetic ordering, i.e. magnetic clustering.

Table I Magnetic properties of $Gd_5Sb_xGe_{4-x}$ system (Ref. 8); x = 0 data are taken from Ref. [9]

x	***First order transition,*** H *from 0 to 100 kOe*	***Second order transition*** *(H = 0)*	***Additional anomalies,*** *low fields*
0	0 – 75 K	~ 130 K*	–
0.5	37 – 85 K	~ 60 K*	~ 150 K
1	40 – 80 K	–	~ 100 K
1.25	45 K	–	–
2	–	200 K	

* Joint AFM-PM and electronic transition

A qualitative model based on electronic structure calculations was proposed in Ref. 10 to explain the origin of electronic transition in pure Gd_5Ge_4. The authors (Ref 10) proposed that one of fifteen Gd electrons per unit cell does not participate in covalent bonding and may be either localized or belong to the conduction band. A model that quantitatively describes such mechanism of electronic transition of Ce was recently proposed by A.S. Mischenko and A.K.Zvezdin [11]. In this paper the high-temperature electronic transition in Gd_5Ge_4 and $Gd_5Sb_{0.5}Ge_{3.5}$ was modelled by means of Anderson impurity Hamiltonian with the addition of Falikov-Kimball interaction[12]. As a basis of our calculations we used the zero-temperature Green function formalism to explain electronic transition, as described in Refs. 13,14, and the extended finite temperature model used by Ref. 11.

The objective of this research is to investigate the magnetic, electronic and crystallographic properties of $Gd_5Sb_{0.5}Ge_{3.5}$ single crystal. We also used electrical resistivity measurements on $Gd_5Sb_{0.5}Ge_{3.5}$ and the model from Ref. 11 to quantitatively describe the electronic transition $Gd_5Sb_xGe_{4-x}$ at low concentrations of Sb ($x < 0.5$).

Experimental details

The single crystal of $Gd_5Sb_{0.5}Ge_{3.5}$ investigated in this work was grown in a tungsten crucible using the Bridgman technique. The starting materials for the synthesis of the $Gd_5Sb_{0.5}Ge_{3.5}$ compound were pieces of Gd (99.86 at. % or 99.99 wt %) prepared by the Materials Preparation Center of the Ames Laboratory, and Sb (99.99 wt %) and Ge (99.99 wt %) purchased from Meldform Metals (United Kingdom). The $Gd_5Sb_{0.5}Ge_{3.5}$ single crystal specimen for *dc* magnetization measurements was cut by using the spark-eroding technique from large grains and shaped and oriented as cube with the approximate dimensions (in mm) 1×0.98×1.55 with each side of the cube perpendicular to one of the three principal crystallographic direction. The value of demagnetization factors of Gd single crystal in magnetic field applied along *a*-, *b*- and *c*- axis were 0.3, 0.25 and 0.23 respectively (see Ref. 15). The sample for heat capacity and electrical resistivity measurements was cut as a 6 mm diameter and 2 mm high flat cylinder with *a*-axis perpendicular to the plane of the flat plate. The crystallographic directions were determined using the back reflection Laue technique. The combined accuracy of the alignment of the crystallographic axes with the direction of the magnetic field vector was ±5°.

The sample for X-ray powder diffraction measurements were prepared by hand-grinding of a bulk piece of unoriented $Gd_5Sb_{0.5}Ge_{3.5}$ single crystal. The fine $Gd_5Sb_{0.5}Ge_{3.5}$ powder (particle size < 25 μm) was mixed with a methanol diluted GE varnish, air dried, and baked at 120 °C for 1 h in order to solidify the specimen and prevent rotation of individual particles by a magnetic field. The flat surface for the Bragg-Brentano diffraction experiment was created by using a 320-grit sandpaper, thus minimizing preferred orientation near the surface and reducing surface roughness.[16] The x-ray powder diffraction measurements were carried out as functions of temperature between 5 and 300 K in a zero magnetic field and between 5 and 100 K in constant magnetic fields ranging from 0 to 40 kOe on a Rigaku TTRAX rotating anode powder diffractometer employing Mo K_α radiation. The diffractometer was equipped with a continuous flow ^{4}He cryostat controlling the temperature of a sample with ± 0.05 K accuracy, and a split-coil superconducting magnet creating a homogeneous dc magnetic field around the specimen.[16] The scattered intensity was recorded

as a function of Bragg angle (2θ) using a scintillation detector with a step of 0.01° 2θ in a step scan mode with the intensity measured for 2 s at each point. Two patterns at 15 K and 150 K were recorded in a step scan mode with 10 s at each point. The maximum intensity to lowest background intensity ratio was close to ~300 with the strongest Bragg peaks registering nearly 6000 counts at their peak values, which corresponds to ~1.8% statistical spread. The range of measured Bragg angles was from 9° to 49° 2θ, which is equivalent to ~19.5° – 128° 2θ range using Cu Kα radiation ($\sin \theta_{max}/\lambda \approx 0.58$). LHPM RIETICA[17] was employed to carry out the full-profile Rietveld refinement of every recorded pattern. In proximity of the transition an attempt was made to refine both phases simultaneously. However, the program failed to recognize both phases separately (the scale of one phase was negative) due to close positions of their Bragg reflections caused by the similar structures of the high temperature and low-temperature phases. The isotropic thermal displacement parameters of all atoms in each phase were assumed to be the same, in effect, employing the overall isotropic thermal displacement approximation. The profile residuals R_p were from ~0.09 to ~0.12, and the derived Bragg residuals R_B were from ~0.05 to ~0.09. The least-squares standard deviations of the refined lattice parameters were on the order of 20–30 parts per million of the absolute values of the corresponding unit cell dimensions.

The dc magnetization data were collected using Quantum Design SQUID magnetometer (MPMS XL system), which operates in the temperature interval 1.7 – 400 K in the range of magnetic fields up to 70 kOe. The accuracy of magnetic measurements was better than 1 %. Electrical resistivity in an applied magnetic field was measured using a Lake Shore magnetometer, model 7225. Electrical resistivity was measured by a standard four-probe technique in the temperature interval 5–350 K in applied magnetic fields up to 40 kOe. The heat capacity in magnetic fields up to 100 kOe was measured between ~2 and 350 K in a semiadiabatic heat pulse calorimeter, which has been described elsewhere.[18]

Results

Our results are generally consistent with the magnetic and thermal properties measurements of polycrystalline $Gd_5Sb_{0.5}Ge_{3.5}$ (see Ref. 8). However, X-ray powder diffraction study shows that unlike Gd_5Ge_4, where the magnetic – structural transition occur with change of the crystal structure type from Sm_5Ge_4- to Gd_5Si_4 – type, in $Gd_5Sb_{0.5}Ge_{3.5}$ a first order transition occurs without shear displacements of the $^{2}_{\infty}[Gd_5T_4]$ slabs and, therefore, without a crystal structure change. The magnetic measurements along different crystallographic axes generally agree with the data collected on polycrystalline material.[8] However, additional clear steps were observed on the inverse susceptibility (*H/M*) at high temperatures where the compound is assumed to be paramagnetic.

Figs. 1 – 3 represent the temperature dependencies of *a*-, *b*- and *c*- lattice parameters of $Gd_5Sb_{0.5}Ge_{3.5}$, measured on heating and cooling the sample in a zero magnetic field and on heating the sample in 20 kOe and 40 kOe magnetic fields. One can see clear steps of the lattice parameters that shift to higher temperatures in applied magnetic fields. Another minor anomaly (maximum) can also be seen clearly seen in Figs. 1-3 around 70 K in zero and 20 kOe magnetic fields, but it disappears in a 40 kOe magnetic field. The largest relative change of the lattice parameter is observed along the *a*-direction ($\Delta a/a$ = -0.35 %), whereas changes along *c*- and *b*- directions were $\Delta c/c$ = -0.24 % and $\Delta b/b$ = 0.09 % respectively. It is worth noting that changes along the *a*- and *c*- axis are both negative, unlike for Gd_5Ge_4, where the major change occurs along the *a*-axis (-1.8 %) and the change along the *c*- axis is small and positive. The points marked by a gray square correspond to a two-phase region and represent the superposition of the lattice parameters of two different phases. One notices a much narrower value of temperature hysteresis, compared to $Gd_5(Si,Ge)_4$ system (5 K vs. 10-15 K). The shift of the transition temperature with magnetic field is not linear, in other words, for a magnetic field change 0 – 20 kOe the transition temperature shifts more than for 20-40 kOe.

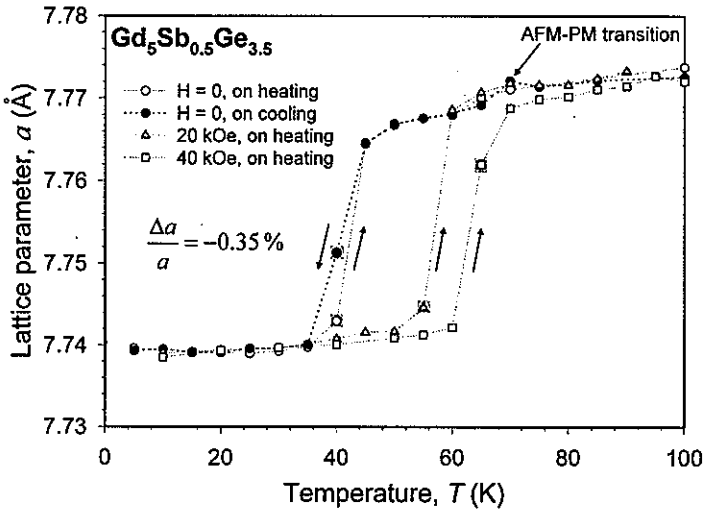

Fig. 1 Temperature dependencies of the *a*-lattice parameter of $Gd_5Sb_{0.5}Ge_{3.5}$ in the temperature interval 5 – 100 K in a zero magnetic field on heating and cooling, and in 20 kOe and 40 kOe magnetic fields on heating.

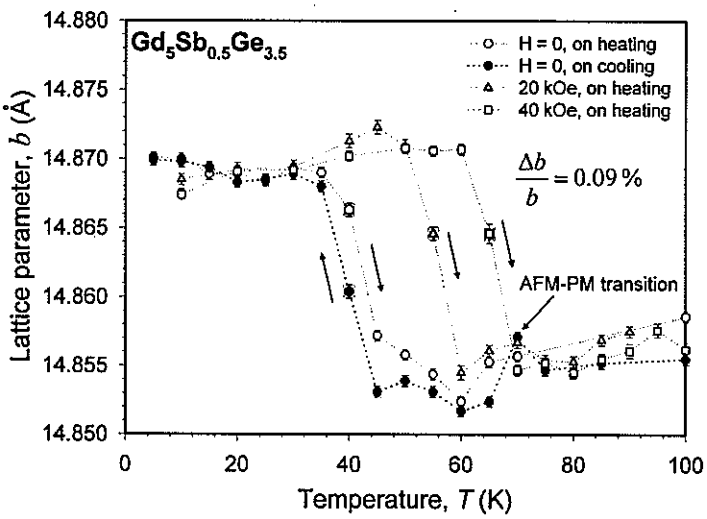

Fig. 2 Temperature dependencies of the *b*-lattice parameter of $Gd_5Sb_{0.5}Ge_{3.5}$ in the temperature interval 5 – 100 K in a zero magnetic field on heating and coolin, and in 20 kOe and 40 kOe magnetic fields on heating.

The unit cell volume of $Gd_5Sb_{0.5}Ge_{3.5}$ calculated from the X-ray powder diffraction patterns collected on heating and cooling in a zero magnetic field and on heating in 20 kOe and 40 kOe magnetic fields as a function of temperature, and on increasing up to 40 kOe magnetic field and decreasing back to zero at 55 K, are presented in Figs. 4 and 5, respectively.

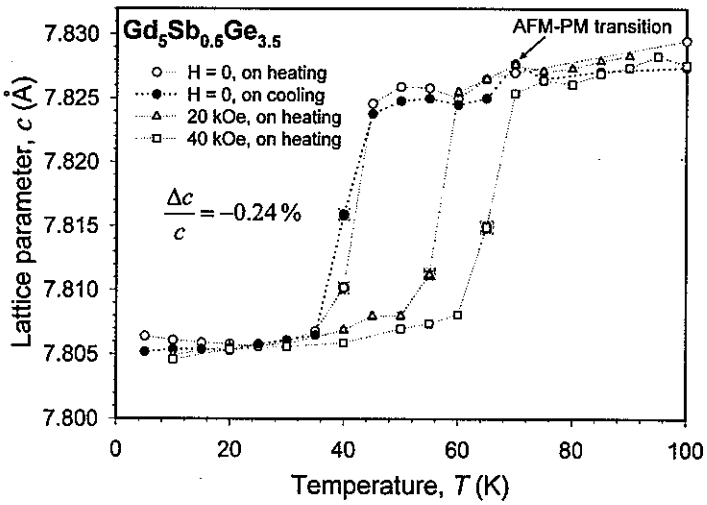

Fig. 3 Temperature dependencies of the *c*-lattice parameter of $Gd_5Sb_{0.5}Ge_{3.5}$ in the temperature interval 5 – 100 K in a zero magnetic field on heating and cooling, and in 20 kOe and 40 kOe magnetic fields on heating.

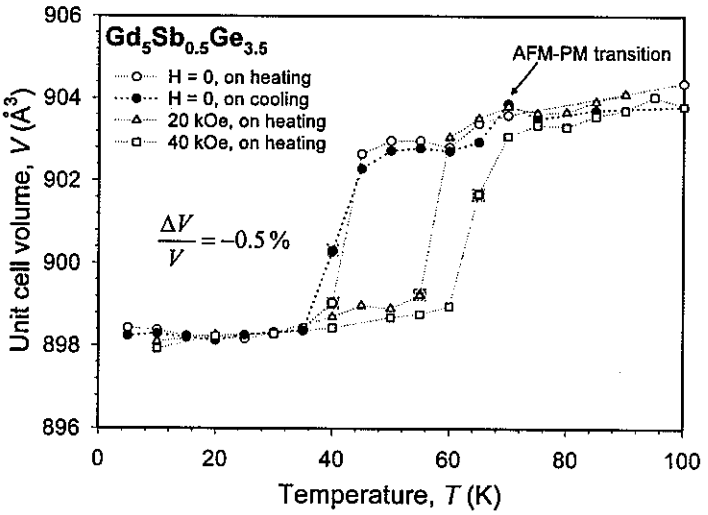

Fig. 4 Temperature dependencies of the unit cell volume of $Gd_5Sb_{0.5}Ge_{3.5}$ in the temperature interval 5 – 100 K in a zero magnetic field on heating and cooling, and in 20 kOe and 40 kOe magnetic fields obtained on heating.

Unlike $Gd_5(Si_xGe_{1-x})_4$, the structural transition observed in Figs. 1-5 is different from a Sm_5Ge_4 – Gd_5Si_4 crystallographic transition with ~ -1 % volume change that takes place in Gd_5Ge_4. In our case despite a relatively large volume change -0.5 %, the crystal structure type does not change, and there are no large shear displacements of the slabs with respect to one another (see discussion below).

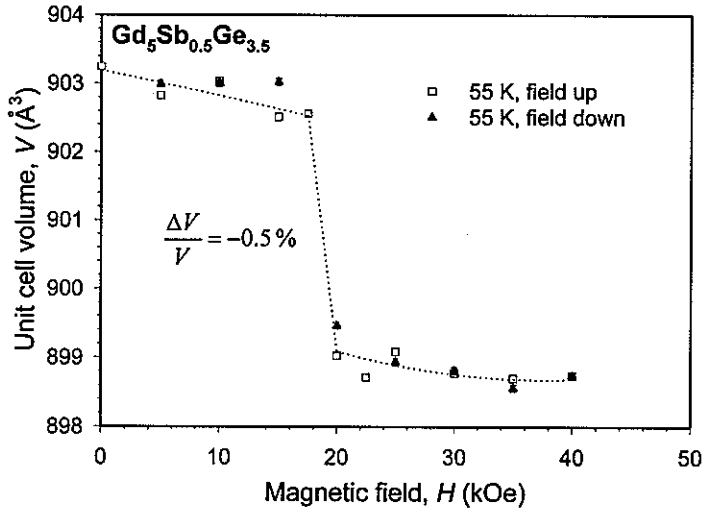

Fig. 5 The isothermal behavior of the unit cell volume of $Gd_5Sb_{0.5}Ge_{3.5}$ at 55 K measured on applying magnetic field from 0 to 40 kOe and then lowering the field back to zero.

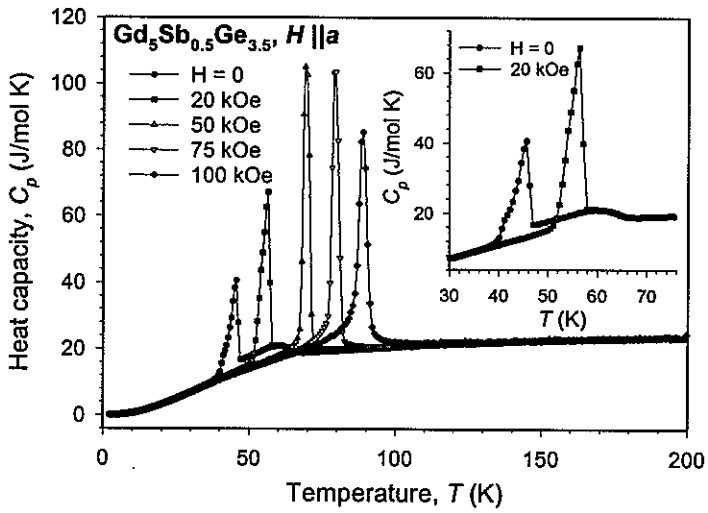

Fig. 6 The temperature dependence of the heat capacity of $Gd_5Sb_{0.5}Ge_{3.5}$ single crystal in the temperature interval 2-200 K in applied magnetic fields up to 100 kOe. The inset shows the additional second order transition observed at 60 K.

The temperature dependencies of heat capacity of $Gd_5Sb_{0.5}Ge_{3.5}$ in the temperature interval 2 - 200 K in magnetic fields ranging from 0 to 100 kOe, applied along *a*-axis are presented in Fig. 6. One can see a sharp peak moving to higher temperatures and, in general, with an increasing peak height on applying a magnetic field. A second order transition was

observed at 63 K and can be clearly seen in the inset of Fig. 6. These results are in a full agreement with previous measurements carried out on a polycrystalline material.[8] It is worth noting that this peak in zero and 20 kOe magnetic fields is broad and asymmetrical, which usually indicates a second order transition.

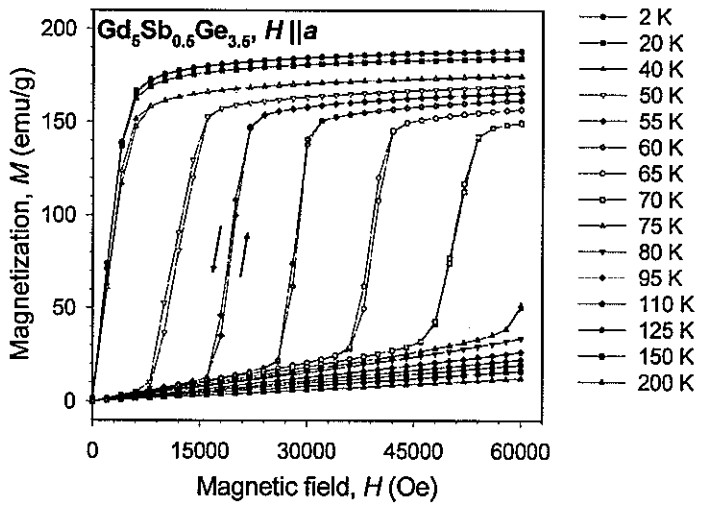

Fig. 7 The isothermal magnetization of $Gd_5Sb_{0.5}Ge_{3.5}$ single crystal in the temperature interval from 2 K up to 200 K in the range of magnetic fields up to 60 kOe, applied along *b*- axis.

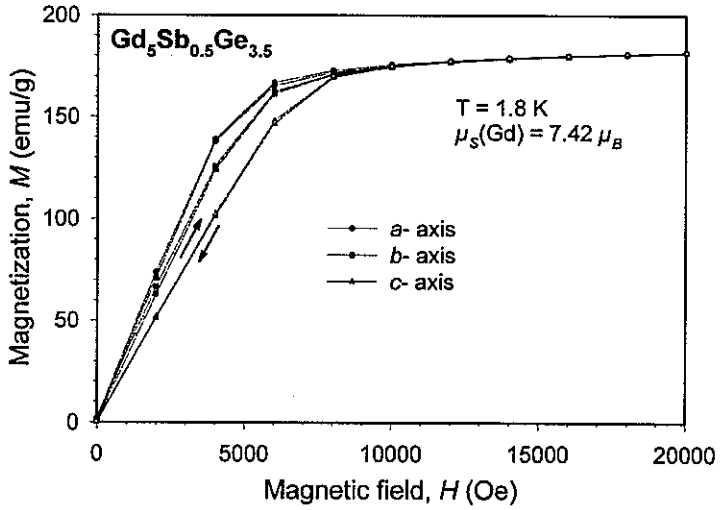

Fig. 8 The isothermal magnetization of $Gd_5Sb_{0.5}Ge_{3.5}$ single crystal at 1.8 K as a function of magnetic field applied along *a*-, *b*- and *c*- axis.

The isothermal magnetization of $Gd_5Sb_{0.5}Ge_{3.5}$ at temperatures from 2 K up to 200 K along the *a*- crystallographic direction is presented in Fig. 7. One can see sharp steps of magnetization shifting to higher magnetic fields on increasing temperature that correspond to a coupled magnetic-structural transition. It is worth noting a much narrower magnetic field hysteresis (<1 kOe) during the first order transition, when compared to $Gd_5(Si_xGe_{1-x})_4$ system (~ 5 kOe). The isothermal magnetization with magnetic fields applied along the *b*- and *c*- axes generally look similar. To determine the easy magnetization direction the 1.8 K isotherms were measured as a function magnetic field applied along *a*-, *b*- and *c*- axes see Fig. 8. One can see from Fig. 8 that unlike Gd_5Ge_4, where the easy magnetization axis is the *b*-direction, the easy axis in $Gd_5Sb_{0.5}Ge_{3.5}$ is the *a*-direction and the *c*-direction is a hard magnetization axis in both Gd_5Ge_4 and $Gd_5Sb_{0.5}Ge_{3.5}$. It is also worth noting that the difference between the three crystallographic directions is smaller in $Gd_5Sb_{0.5}Ge_{3.5}$, compared to Gd_5Ge_4, which means that magnetic anisotropy is weaker in $Gd_5Sb_{0.5}Ge_{3.5}$. The value of the saturation magnetization is 187.1 emu/g or 7.42 μ_B per Gd atom (see Fig. 8). The single crystal isothermal magnetization data agree well with previous polycrystalline measurements [8] and the heat capacity and powder diffraction data.

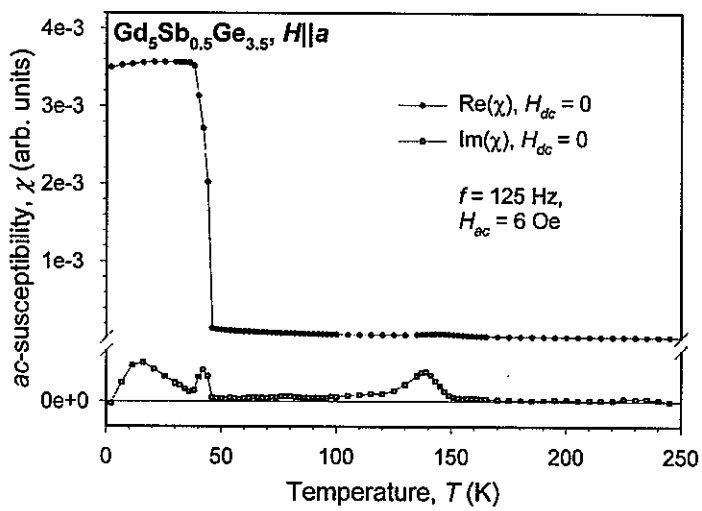

Fig. 9 The temperature dependencies of the real and imaginary components of *ac*- magnetic susceptibility of $Gd_5Sb_{0.5}Ge_{3.5}$ single crystal in the temperature interval 2 – 250 K in a zero *dc* magnetic field. The data were collected at a frequency of 125 Hz and *ac*-field of 6 Oe applied along the *a*- axis.

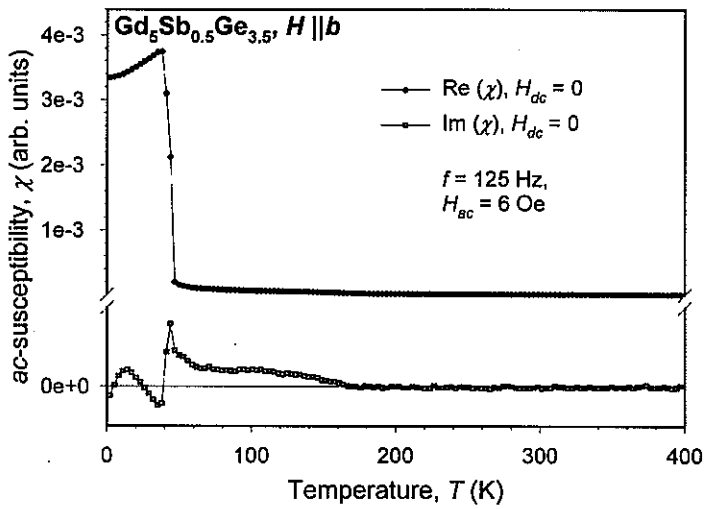

Fig. 10 The temperature dependencies of the real and imaginary components of *ac*- magnetic susceptibility of $Gd_5Sb_{0.5}Ge_{3.5}$ single crystal in the temperature interval 2 – 400 K in a zero *dc* magnetic field. The data were collected at a frequency of 125 Hz and *ac*-field of 6 Oe applied along the *a*- axis.

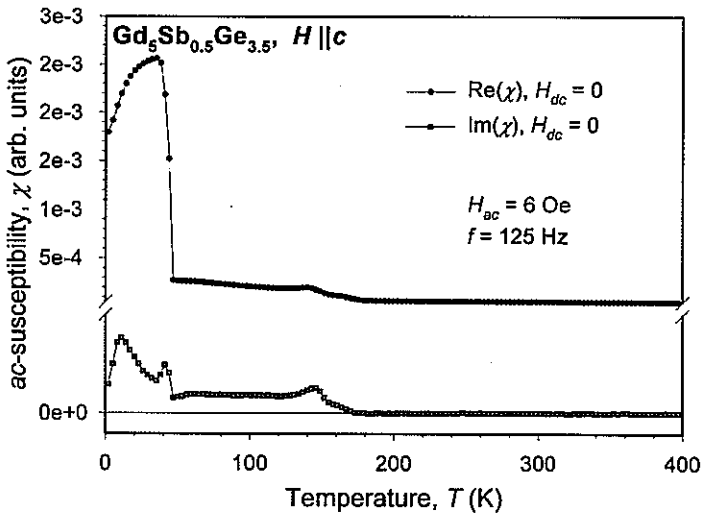

Fig. 11 The temperature dependencies of the real and imaginary components of *ac*- magnetic susceptibility of $Gd_5Sb_{0.5}Ge_{3.5}$ single crystal in the temperature interval 2 – 400 K in a zero *dc* magnetic field. The data were collected at a frequency of 125 Hz and *ac*-field of 6 Oe applied along the *a*- axis.

The zero *dc* magnetic field temperature dependencies of *ac*-susceptibility of $Gd_5Sb_{0.5}Ge_{3.5}$ with *ac*-field applied along the *a*-, *b*- and *c*- axes are presented in Figs. 9-11, respectively. One can see the main transition around 45 K in all three figures and small anomalies of the imaginary part of ac-susceptibility, such as a peak around 140 K in case of

$H \| a$ and $H \| c$ and a step-like anomaly around 160 K in with $H \| b$. It is worth noting that the positive plateau of the temperature dependence of the imaginary part of the susceptibility with $H \| b$ and $H \| c$ of $Gd_5Sb_{0.5}Ge_{3.5}$ in the temperature interval 60 – 160 K relates to magnetic losses in the sample.

The temperature dependencies of the magnetization along the *a*-, *b*- and *c*- axes in the temperature interval 2 - 400 K in the range of magnetic fields up to 10 kOe are presented in Fig. 12 – 14, respectively. One can see a clear first order transition from FM to AFM (at low fields) or PM (at high fields) state around 45 K in all three figures. The insets in Fig. 12 - 14 show calculated temperature dependencies of the inverse susceptibility (*H/M*) in the same magnetic fields. One can see from Fig. 12 that the inverse susceptibility in low magnetic fields along the *a*- axis shows three step deviations from linearity at temperatures from 60 K to 160 K, then from 160 K to 220 K and from 220 K to 290 K. In the latter interval *H/M* shows a linear behavior, which is shifted slightly down from the paramagnetic behavior observed above 290 K. The paramagnetic Curie temperatures (θ_p) and effective magnetic moments (μ_{eff}) of two linear regions of the inversed susceptibility are θ_p = -7 K and μ_{eff} = 8.57 μ_B for the temperature interval from 220 to 290 K and θ_p = -50 K and μ_{eff} = 9.04 μ_B for PM region above 290 K.

The temperature dependence of the inverse susceptibility (*H/M*) along the *b*-axis (see Fig. 13) shows just one deviation from linearity in the temperature interval from 60 K to 160 K and at temperatures above 160 K *H/M* behaves as a paramagnet with the θ_p = -23 K and μ_{eff} = 9.1 μ_B. However, in case of magnetic field applied along the *c*-axis (see Fig. 14) there is an additional deviation from linearity between 160 K and 220 K, when compared to the behavior of the inverse susceptibility along the *b*-axis (see Figs. 13 and 14). The values of the paramagnetic Curie temperature and effective magnetic moment θ_p = -19 K and μ_{eff} = 8.84 μ_B in the PM region above 220 K are close to the values observed along the *b*-axis. One notes that the inverse susceptibility along all three crystallographic directions (Fig. 12 - 14) agrees with the *ac*-susceptibility data (Fig. 9 - 11), which show a peak at 150 K for $H \| a$, a plateau from 60 to 160 K for $H \| b$, and combination of both for $H \| c$.

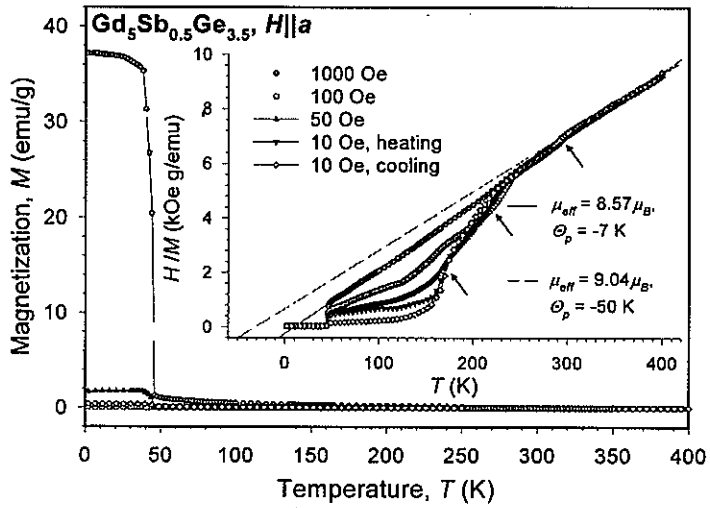

Fig. 12 Temperature dependencies of the magnetization of $Gd_5Sb_{0.5}Ge_{3.5}$ single crystal in the temperature interval 2 – 400 K in the range of magnetic fields from 10 Oe up to 10 kOe, applied along the *a*-axis. The inset shows the temperature dependencies of inverse susceptibility (*H/M*) calculated from the magnetization data.

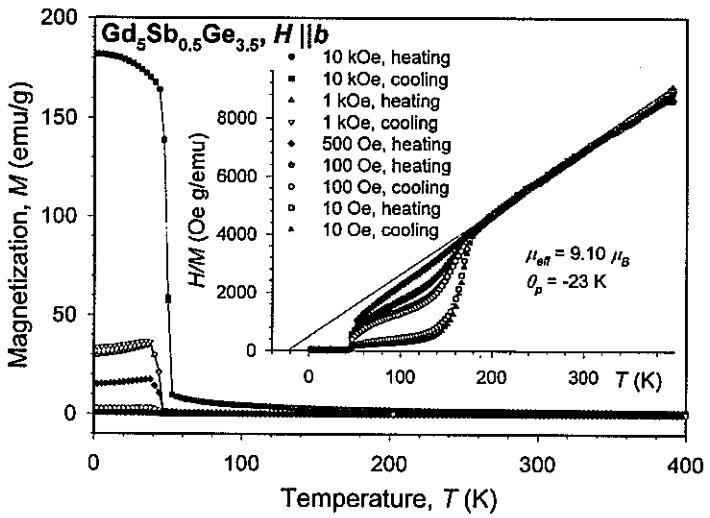

Fig. 13 Temperature dependencies of the magnetization of $Gd_5Sb_{0.5}Ge_{3.5}$ single crystal in the temperature interval 2 – 400 K in the range of magnetic fields from 10 Oe up to 10 kOe, applied along the *b*-axis. The inset shows the temperature dependencies of inverse susceptibility (*H/M*) calculated from the magnetization data.

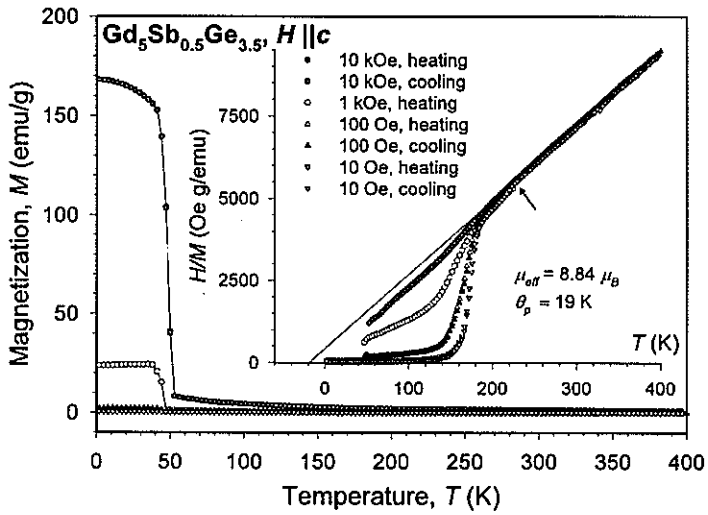

Fig. 14 Temperature dependencies of the magnetization of $Gd_5Sb_{0.5}Ge_{3.5}$ single crystal in the temperature interval 2 – 400 K in the range of magnetic fields from 10 Oe up to 10 kOe, applied along the *c*-axis. The inset shows the temperature dependencies of inverse susceptibility (*H/M*) calculated from the magnetization data.

The above noted deviation of the inverse susceptibility from linearity along all three crystallographic directions may be associated with short range magnetic ordering, i.e. magnetic clustering. It is also worth noting that even in the case of high magnetic fields (10 kOe) the Curie-Weiss behavior of the magnetization along all three crystallographic directions is rather unusual. First, the values of the paramagnetic Curie temperature appear to be negative, despite the fact that the ground state of $Gd_5Sb_{0.5}Ge_{3.5}$ is ferromagnetic, whereas negative value of the paramagnetic Curie temperature usually means the AFM ground state of the compound. Second, the values of calculated effective magnetic moments along all three crystallographic axes exceed theoretical value of 7.94 μ_B by 10-13 %.

Discussion

Our results generally confirm the magnetic and thermal behavior of polycrystalline $Gd_5Sb_{0.5}Ge_{3.5}$, reported in Ref. 8, which were assumed to be somewhat similar to the behaviour found in $Gd_5(Si_xGe_{1-x})_4$ system except for narrower hysteresis values of temperature and magnetic field during the coupled magnetic-structural transition. However, the detailed crystallographic study shows that the nature of the structural transition is significantly different from the transformation in $Gd_5(Si_xGe_{1-x})_4$. Also, detailed low field magnetization data show an unusual behavior of the inverse susceptibility (see Figs. 10 - 12) which may be associated with a so called Griffiths phase, recently reported in $Tb_5Si_2Ge_2$.[19] Following electrical resistivity measurements of Ref. 8 and 10, a theoretical model is proposed to explain electronic transition in Gd_5Ge_4 and $Gd_5Sb_{0.5}Ge_{3.5}$.

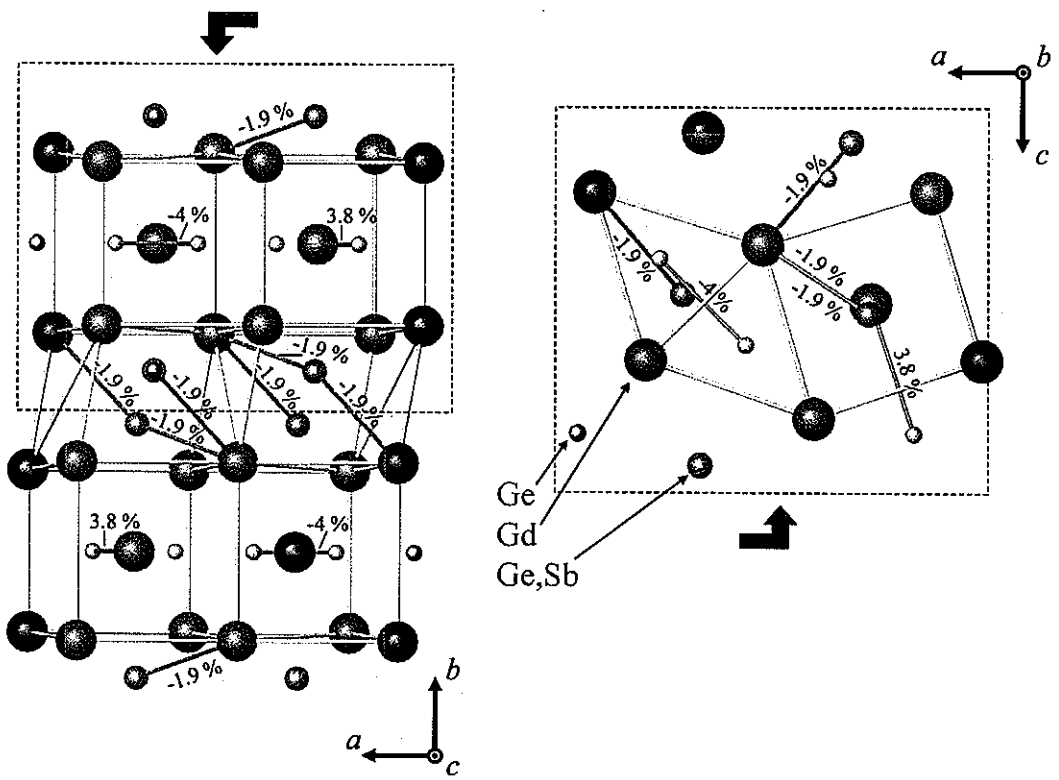

Fig. 15 The *ab*- projection of the unit cell of $Gd_5Sb_{0.5}Ge_{3.5}$ and *ac*-projection of the top Gd- slab marked by dashed rectangles, calculated from the X-ray powder diffraction pattern, collected at 55 K in a zero magnetic field. The numbers represent relative inter-atomic distance changes (in %) of the bonds that undergo maximum changes during the transition.

Coupled magnetic-structural transition in $Gd_5Sb_{0.5}Ge_{3.5}$

According to the magnetic and crystallographic data, $Gd_5Sb_{0.5}Ge_{3.5}$ exhibits a crystallographic transition which is different from that observed in pure Gd_5Ge_4. Despite the fact that at room temperature the crystal structure of $Gd_5Sb_{0.5}Ge_{3.5}$ is the same as in pure Gd_5Ge_4 (the Sm_5Ge_4- type), on applying a magnetic field, no shear displacements of the ${}^{2}_{\infty}[Gd_5Ge_4]$ slabs (see *ab*- and *ac*- projections of the top slab, marked by dashed rectangles in Fig. 15) with respect to one another occur in $Gd_5Sb_{0.5}Ge_{3.5}$ and the lattice does not change its type of structure to Gd_5Si_4 –type as was observed in Gd_5Ge_4.[20]

In pure Gd_5Ge_4 the largest change of lattice dimensions occurs along the a – axis and the relative change ($\Delta a/a$) is equal to -1.8 %, which is larger then $\Delta a/a = -0.35$ %, observed along the a-axis in $Gd_5Sb_{0.5}Ge_{3.5}$ (see Fig. 1). This large change of the a-lattice parameter in Gd_5Ge_4 occurs because of the shear displacements of adjacent ${}^{2}_{\infty}[Gd_5Ge_4]$ slabs and results in drastic shortening of T-T bond distances along the a- axis, (see four medium size atoms between the slabs in Fig. 15). And the shortening of T-T bond distances consequently results in formation of T-T dimers and drives the coupled magnetic-structural transition in Gd_5Ge_4. Such a large negative change (-1.8 %) in Gd_5Ge_4 of the a- lattice parameter causes the minor increasing of b- and c- lattice parameters by ~ 0.14 % and ~ 0.6 %, respectively, to stabilize the lattice, but the giant volume change of Gd_5Ge_4 (-1%) mostly comes from the decreasing of the a- lattice parameter.

In $Gd_5Sb_{0.5}Ge_{3.5}$ the situation is different. Here we have similar changes along the a- and c- axes equal to $\Delta a/a = -0.35$ % and $\Delta c/c = -0.24$ % (see Figs. 1-2), respectively. The ${}^{2}_{\infty}[Gd_5Ge_4]$ slabs in $Gd_5Sb_{0.5}Ge_{3.5}$ do not shift with respect to one another, but shrink nearly equally in the *ac*-plane. It is illustrated in Fig. 15, where one can see approximately -4 % shortening of the Ge-Ge distances (small atoms inside the slab in Fig. 15) accompanied by the 3.8 % increasing of Gd-Ge distances inside the slab. The shrinkage of the ${}^{2}_{\infty}[Gd_5Ge_4]$ slabs in the *ac*-plane affects the b-lattice parameter, which slightly increases by 0.09 % (see Fig. 3). It is shown in Fig. 15 that unlike Gd_5Ge_4, it is not the T-T bond distances that change significantly during the transition in $Gd_5Sb_{0.5}Ge_{3.5}$, but the interslab Gd-T distances, which

decrease by ~1.9 % (see Fig. 15). Thus, one may speculate that structural transition in $Gd_5Sb_{0.5}Ge_{3.5}$ mostly comes from the change of Gd-T interslab bonding instead of the interslab T-T bonding, as in Gd_5Ge_4.

It is also worth noting that the crystal structure and volume change in $Gd_5Sb_{0.5}Ge_{3.5}$ has more symmetrical character that in Gd_5Ge_4. This is may be the origin of the improvement of lattice stability and, consequently, lower values of magnetic field and temperature hystereses, when compared to Gd_5Ge_4 and the $Gd_5(Si_xGe_{1-x})_4$ system as a whole, where the mechanism of the coupled magnetic-structural transition is similar to the one in Gd_5Ge_4.

Appearance of a Griffiths-like phase in $Gd_5Sb_{0.5}Ge_{3.5}$

Following Ref. 19, who first reported the observations of a Griffiths-like phase in $Tb_5Si_2Ge_2$, we made a detailed study of the low field magnetization (see Figs. 12-14). The Griffiths model [21] describes a magnetic system in which a random distribution of the magnetic interactions given by disorder results in different values for the exchange constant at the different sites of the lattice. Then one can introduce a critical temperature, T_C, which is the proper ordering temperature, and the Griffiths temperature, T_G, which accounts for the complete absence of disorder.[19] Considering the temperature interval $T_C < T < T_G$, where the thermodynamic functions become unanalytical, the system lies between the ordered FM and conventional PM states.[19] Such an intermediate regime is called the Griffiths phase and is characterized by a clusterlike system induced by this disordered state.

The calculated inverse susceptibility (H/M) temperature dependencies along the a-, b- and c- axes show low field behavior similar to that observed in Ref. 19. However, our measurements indicate even more interesting details, such as a three and two steps deviations from linearity observed in the PM region along the a- and c- axis (see Fig. 12 and 14), and the negative values of the paramagnetic Curie temperature (θ_p) observed along the all three crystallographic directions. Also the effective magnetic moments in the PM region (see Fig. 12 - 14) exceed theoretical value of 7.94 μ_B by 10-13 %.

The negative value of paramagnetic Curie temperature usually means the AFM ground state of the material, which is inconsistent with the observed FM ordering at low temperatures. Looking at the magnetic H-T phase diagram of polycrystalline $Gd_5Sb_{0.7}Ge_{3.3}$ (see Fig. 16), which is similar to magnetic H-T diagram of the $Gd_5Sb_{0.5}Ge_{3.5}$ single crystal, one can assume that the AFM ordering exists in the temperature interval 45-60 K (see Fig. 16) in analogy with Gd_5Ge_4, where an electronic and AFM-PM transition coexist at 130 K. Our magnetic measurements indicate a weak anomaly at 60 K, which might be an AFM-PM transition. Another possible explanation of the negative value of θ_p is that the short range magnetic ordering (Griffiths phase) in $Gd_5Sb_{0.5}Ge_{3.5}$ is of the AFM type. The three and two steps deviations from linearity of the inverse susceptibility along the *a*-axis and *c*- axes might be interpreted assuming three different length scales of magnetic clustering, which is inconsistent with the fact that we observed a different number of steps along different axes. Another possible explanation of three and two step behavior may be that there are three distinct preferred orientations of AFM short range magnetic ordering in $Gd_5Sb_{0.5}Ge_{3.5}$. However, both statements about the AFM type of short range magnetic ordering and especially about different preferred orientations of the short range AFM ordering are speculations that need to be verified by future X-ray magnetic scattering experiments.

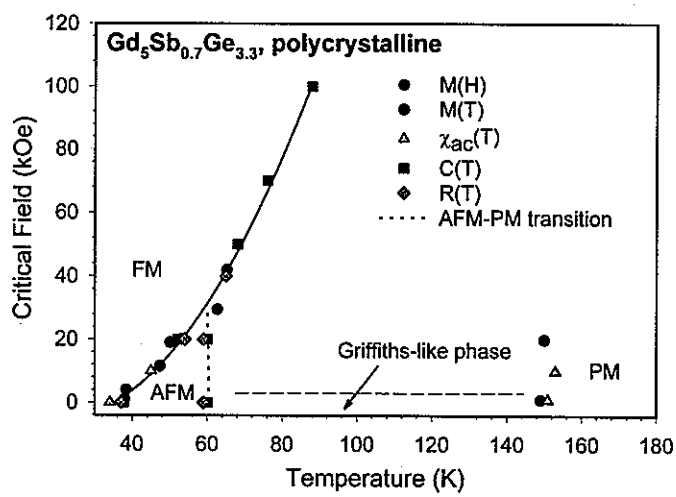

Fig. 16 Magnetic phase H-T diagram of polycrystalline $Gd_5Sb_{0.7}Ge_{3.3}$, constructed using the data of Ref. 8. The dashed line indicates that Griffiths-like phase exists only in magnetic fields below 1 kOe.

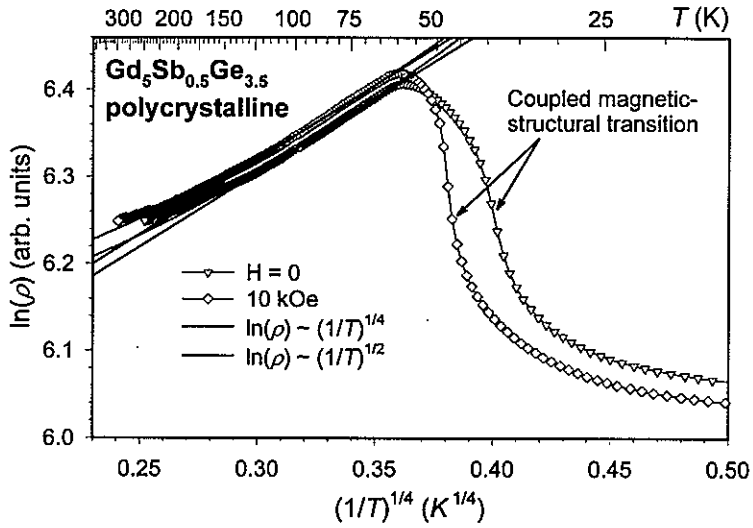

Fig. 17 The dependencies of the logarithm of resistivity ln(ρ) of $Gd_5Sb_{0.5}Ge_{3.5}$ on ¼ and ½ power of inverse temperature $(1/T)^{1/2}$ and $(1/T)^{1/4}$ in a zero and 10 koe magnetic fields. The upper scale indicate real temperatures, corresponding $(1/T)^{1/4}$ scale.

Model of the electronic transition in Gd_5Ge_4 and $Gd_5Sb_{0.5}Ge_{3.5}$

The joint AFM-PM and electronic transition observed at 60 K in $Gd_5Sb_{0.5}Ge_{3.5}$ from heat capacity and electrical resistivity is similar to the transition at 130 K in pure Gd_5Ge_4 (see Refs. 8 and 10). In both compounds the heat capacity exhibits a second order transition (see Fig. 6 and Ref. 10) and electrical resistivity shows a peak at 60 K and 130 K in $Gd_5Sb_{0.5}Ge_{3.5}$ and Gd_5Ge_4, respectively. The natural logarithm of electrical resistivity (ln(ρ)) of polycrystalline $Gd_5Sb_{0.5}Ge_{3.5}$ vs. $(1/T)^{1/4}$ is presented in Fig. 17. The upper scale in Fig. 17 shows the real temperatures corresponding to the $(1/T)^{1/4}$ scale. One can see the steps of ln(ρ), marked by arrows in Fig. 17, at ~40 K and ~50 K and they correspond to the coupled magnetic-structural transition in a zero and 10 kOe magnetic fields. It is also seen from Fig. 17, that a linear behaviour of ln(ρ) vs. $(1/T)^{1/4}$ (straight heavy line in Fig. 17) or $(1/T)^{1/2}$ (curved heavy line in Fig. 17) is observed at temperatures above 60 K. Both temperature dependencies are rather unusual for the intermetallic compound, because this type of temperature dependence is usually observed in amorphous semiconductors, where the

localization of the conduction electrons result in a conductivity provided by electrons "hopping" from one localized state to another and, therefore, it is called hopping conductivity. The electronic transition at 130 K in Gd_5Ge_4 was called as metal-insulator transition by authors of Ref. 10. However, since there is no drastic change of the electrical resistivity during this transition, just change in a temperature dependence behaviour, so we will consider it as an electronic transition.

To introduce a qualitative model of electronic transition in Gd_5Ge_4, proposed in Ref. 10, one can start from the ground state electronic configuration of the Gd atom ($4f^7 5d^1 6s^2$). In compounds, the 3-valent Gd^{3+} ion, which has electronic configuration ($4f^7 5d^0 6s^0$), donates one $5d$ electron and two $6s$ electrons, which participate in forming a band structure of the compound. The authors of Ref. 10 assumed that there are two types of configuration of the Gd-atoms in Gd_5Ge_4: with the $4f^7 5d^1$ and $4f^7 5d^0 + e$ electronic configurations. And for $4f^7 5d^1$ configuration, a $5d$ electron can be either localized or belong to the conduction band. So the observed electronic transition in Gd_5Ge_4 comes from the transition between the mentioned above configurations of Gd atom.

The idea of localized 5d electron comes from a simple electron count in Gd_5Ge_4. The Gd_5Ge_4 compound has 31 valence electrons per formula unit: Ge is 4-valent so it lacks 16 electrons and Gd is 3-valent so it contributes 15 electrons. The valence band below the localized level is formed by 15 valence s -,p -, d – states [10] and it means that there are 30 electrons per formula unit in the valence band. The difference in number of electrons per unit cell comes from formation of Ge-Ge dimers inside the slabs. Using counting formalism for valence compounds, the dimer needs 7 electron pairs instead of 2×4 electron pairs for two isolated Ge atoms. The additional valence electron is utilized to form four Gd-Gd σ-bonding $5d$-z^2 orbitals along the bond axis.[10] In other words, one of the five Gd atoms per unit cell of Gd_5Ge_4 has unpaired electron that does not participate in covalent bonding with Ge atoms. Electron counting in case of Gd_5Ge_4 is illustrated in Fig. 18. The unpaired electron may sit either at the localized $5d$-level below the conduction band created by Gd s, p states or inside the conduction band created by s, p and d states.

$$5\,Gd^{3+} \Rightarrow 15\bar{e} \rightarrow 14\bar{e} + 1\bar{e}(5d)$$
$$4\,Ge^{4} \Leftarrow 16\bar{e} = \underbrace{14\bar{e}}_{\text{Covalent bonding}} + \underbrace{2\bar{e}}_{\text{Ge–Ge dimers}}$$

Fig. 18. The schematic description of a formal electron counting in Gd_5Ge_4.

Mentioned above mechanism in Gd_5Ge_4 is supported by electronic band structure calculations,[10] which show that in the PM region (at high temperatures) the Fermi level falls into a narrow band below the conduction band, whereas at low temperatures the Fermi level lies in the conduction band and Gd_5Ge_4 exhibit metallic behavior.

$$5\ \ Gd^{3+} \Rightarrow 15\,\bar{e} \rightarrow 1.5\bar{e} + 12\bar{e} + 1.5\bar{e}(5d)$$
$$0.5\,Sb^{3} \Leftarrow \underbrace{1.5\bar{e}}_{\text{Covalent bonding}}$$
$$3.5\,Ge^{4} \Leftarrow 14\bar{e} = \underbrace{12\bar{e}}_{\text{Covalent bonding}} + \underbrace{2\bar{e}}_{\text{Ge–Ge dimers}}$$

Fig. 19. The schematic description of a formal electron counting in $Gd_5Sb_{0.5}Ge_{3.5}$.

The same model can be extended to that of $Gd_5Sb_{0.5}Ge_{3.5}$ compound, where we assume Sb to be a 3-electron acceptor. Using the formal electron counting, illustrated in Fig. 19, one obtains one and a half Gd atoms per unit cell, of which the 5d electron can be either a localized or a conduction electron. As we compare our theoretical model to the results of Ref. 8, where the polycrystalline $Gd_5Sb_{0.7}Ge_{3.3}$ was investigated, one adjusts the formal electron counting in case of x = 0.7 instead of x = 0.5 and obtains 1.7 Gd atoms with unpaired electron per unit cell in $Gd_5Sb_{0.7}Ge_{3.3}$.

Taking into account the band structure of Gd_5Ge_4 (Ref. 10) and following the theoretical work of Ref. 11, a simple model can be introduced to explain the electronic transition in Gd_5Ge_4 and $Gd_5Sb_{0.5}Ge_{3.5}$. Considering the individual Gd atom with unpaired electron in a framework of the compound band structure, one can introduce an insulating

state of such a Gd atom, when the unpaired electron belongs to $5d^1$ localized level, and metallic state, when unpaired electron belong to the conduction band. This model is illustrated in Fig. 20. The so-called metallic state occurs at low temperatures, and the so-called insulating state occurs at temperatures above 60 K or 130 K in $Gd_5Sb_{0.5}Ge_{3.5}$ or Gd_5Ge_4, respectively, that is the insulating state corresponds to the $4f^7 5d^1$ configuration of the Gd atom and the metallic state corresponds to the $4f^7 5d + e$ configuration of the Gd atom.

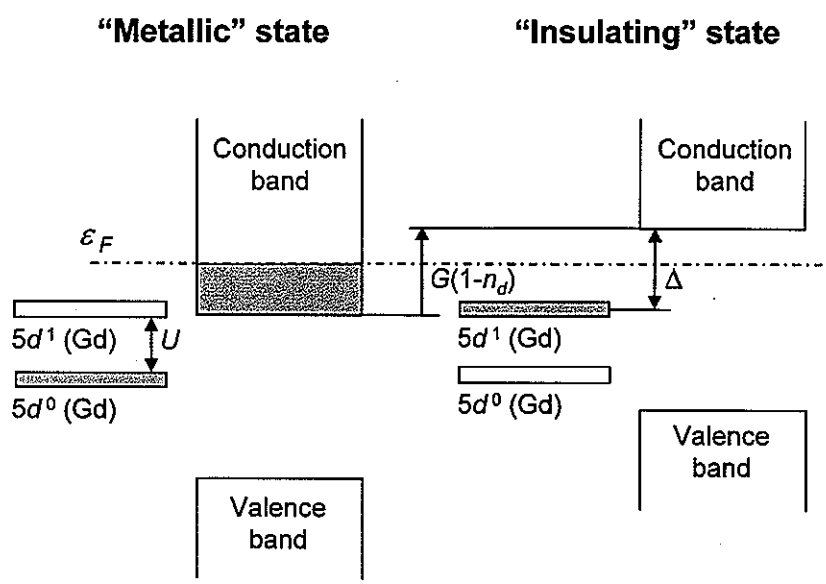

Fig. 20 The schematic of the band structure of an itinerant individual Gd atom in $Gd_5Sb_{0.5}Ge_{3.5}$ with 5d electron that can be either localized or belong to the conduction band.

An important issue illustrated in Fig. 20, is that $5d^0$ configuration of Gd atom has lower energy than the excited $5d^1$ configuration. So the energy gain from losing a $5d$ Gd electron should be equal to work needed to put the unpaired electron in to the conduction band, where it has a higher energy, comparing to localized state. To understand the dynamics of interplay between two states one has to introduce a Falicov-Kimball interaction[12] marked by the symbol "G" in Fig. 20, which is an exchange interaction between the localized and conduction electrons. If we assume that the electron is partially localized with an occupancy of $5d$ level (n_d), it means that the rest of the electron belongs to the conduction band, which

has an occupancy ($n_c = 1 - n_d$). It is also seen from Fig. 20 that due to Falicov-Kimball interaction the gap between the localized 5d level and the conduction band is proportional to the occupancy of the conduction band ($1 - n_d$). Depending on temperature, magnetic field, pressure etc., the $G(1 - n_d)$ term in Fig. 20 may either lower the conduction band, favoring the transfer of electron to the conduction band and a transition to the metallic state, or raise it, favoring the transfer of electron to the localized level, i.e. a transition to the insulating state.

To describe the mentioned above mechanism quantitatively, one can introduce the following Hamiltonian of the interaction of conduction electrons and 5*d*-electrons at the localized level: [11,13]

$$H = \sum_k \varepsilon_k a_k^+ a_k + \sum_{mi} E_{mi} b_{mi}^+ b_{mi} - \sum_{mi} U_m \left(1 - b_{mi}^+ b_{mi}\right) + \sum_{k,mi} \left(V_{k,mi} a_k^+ b_{mi} + V_{k,mi}^* b_{mi}^+ a_k\right) + \frac{G}{N} \sum_{k,mi} b_{mi}^+ b_{mi} a_k^+ a_k \quad (1)$$

where a_k / a_k^+ is an operator to create/annihilate a conduction electron, b_{mi} / b_{mi}^+ is an operator to create/annihilate a 5*d*-localized electron, E_{mi} – the energy of a localized level, ε_k - is the energy of the conduction electron in *k*-representation, G – is a Falicov-Kimball interaction between conduction and *d*- electrons; U – is the energy difference between $5d^0$ and $5d^1$ levels; V – is the hybridization between conduction band and localized 5*d*-level and N is a number of atoms in the system. One notices that by the "*mi*" index in Eq. 1 we mean $2J+1$ ($-J < m < J$) Zeeman splitting of the localized level (with total angular momentum J) of the *i*-th Gd atom.

To understand the dynamics of the system one can use Green function formalism for the above Hamiltonian.[11,13,14] Actually the Hamiltonian (1) is very difficult to deal with because of the last Falicov-Kimball interaction term. The simplest approximation for the last term of Eq. 1 is the a so-called mean field approximation [11,13] in which:

$$\frac{G}{N}\sum_{k,mi} b_{mi}^{+} b_{mi} a_k^{+} a_k \cong G\underbrace{\frac{1}{N}\left\langle \sum_{mi} b_{mi}^{+} b_{mi} \right\rangle}_{n_d} \sum_k a_k^{+} a_k + G\underbrace{\frac{1}{N}\left\langle \sum_k a_k^{+} a_k \right\rangle}_{n_C} \sum_{mi} b_{mi}^{+} b_{mi} - \\ -\frac{G}{N}\left\langle \sum_k a_k^{+} a_k \right\rangle \left\langle \sum_{mi} b_{mi}^{+} b_{mi} \right\rangle , \quad (2)$$

where we introduce the average occupancies of the localized level $n_d = \frac{1}{N}\left\langle \sum_{mi} b_{mi}^{+} b_{mi} \right\rangle$ and the conduction band $n_c = \frac{1}{N}\left\langle \sum_k a_k^{+} a_k \right\rangle$, where the $\langle ... \rangle$ brackets mean that we substituted a quantum mechanical operator with its average value. As already mentioned above the occupancy of conduction band (n_c) is equal to 1 - n_d, because there is only one unpaired electron per Gd atom, which is either a localized or a conduction electron.

Using the above simplifications, the equations of motion for the problem are:

$$G_{mi,m'i'}\left(\omega - E_{mi} - G\frac{1}{N}\left\langle \sum_k a_k^{+} a_k \right\rangle - U\right) - \sum_k V_{k,mi}^{*} G_{k,m'i'} = \delta_{mi,m'i'} \\ G_{k,m'i'}\left(\omega - \varepsilon_k - G\frac{1}{N}\left\langle \sum_{mi} b_{mi}^{+} b_{mi} \right\rangle\right) - \sum_{mi} V_{k,mi} G_{mi,m'i'} = 0 \quad (3)$$

where $G_{mi,m'i'} = \left\langle\left\langle b_{mi} b_{m'i'}^{+} \right\rangle\right\rangle_{\omega}$ and $G_{k,m'i'} = \left\langle\left\langle a_k b_{m'i'}^{+} \right\rangle\right\rangle_{\omega}$ are the Green functions in ω-representation.

After solving Eq. 3, The Green function of the $5d$ electron can be presented as:

$$G_{mi}(\omega) = \frac{1}{\omega - E_{mi} - G(1 - n_d) - U - i\Gamma}, \quad (4)$$

where Γ is:

$$\Gamma = \mathrm{Im}\left(\sum_k \frac{V_{k,mi}^2}{\omega - \varepsilon_k - Gn_d + i0}\right). \quad (5)$$

In this paper we use Γ as a phenomenological parameter and as a reasonable approximation, a value of Γ is equal to 30 meV (see Ref. 22).

Table II the electronic configurations of the Gd atoms in case of the non-localized and localized 5d electron

Notation	*Configuration*	S	L	J	g	μ (μ_B)
"1"	$4f^7\ 5d^1$	3	2	5	8/5	8
"2"	$4f^7\ 5d^0$	7/2	0	7/2	2	7

To quantitatively describe the influence of temperature and magnetic field on the transition one can use the finite temperature formalism of Ref. 11. From the viewpoint of the interaction with a magnetic field, we have three subsystems in Gd_5Ge_4 and $Gd_5Sb_{0.5}Ge_{3.5}$: the Gd atoms with the $4f^7\ 5d^1$ configuration, the Gd-atoms with the $4f^7\ 5d^0$ configuration and the conduction electrons. The two electronic configurations Gd atom, listed in Table II, have different values of the total angular momentum J and total magnetic moment μ and, therefore interact with magnetic field differently. For convenience, we used notations of type 1 and type 2 for the Gd atoms, according to Table II, instead of the full electronic configuration.

From viewpoint of the interaction with the magnetic field, the Gd atoms with all three electrons paired and the Gd atoms with an unpaired electron belonging to the conduction band, are basically the same, because they have same values of the total angular momentum J and the total magnetic moment μ. Introducing the number of the Gd atoms with unpaired electrons per unit cell (f_1) in Gd_5Ge_4 and $Gd_5Sb_{0.5}Ge_{3.5}$ and, respectively, the number the Gd atoms with all paired electrons ($f_2 = 5 - f_1$), one can estimate the number of *Gd* atoms of type 1 and type 2. One also needs to take into account that only a fraction of the Gd atom with an unpaired electron is of type 1 (with localized 5d electron) and this fraction is equal to the occupancy of the localized $5d$ level (n_d) introduced above. Therefore, the total number of the Gd atoms of type 1 (N_1) and type 2 (N_2) atoms per formula unit are:

$$\begin{aligned} N_1 &= f_1 \cdot n_d \\ N_2 &= f_1 \cdot (1 - n_d) + f_2 \end{aligned} \qquad (6)$$

The partition function for the system with the Gd atoms in the simplest approximation of non-interacting Gd atoms with two different values of magnetic moment (type 1 and type 2) has a following form:

$$Z=\left[e^{-\frac{E_{loc}-\Delta}{kT}}\underbrace{\sum_{m=-J_1}^{J_1}\exp\left(\frac{-g_1\mu_B mH}{kT}\right)}_{Z_1}\right]^{N_1}\left[\underbrace{\sum_{m=-J_2}^{J_2}\exp\left(\frac{-g_2\mu_B mH}{kT}\right)}_{Z_2}\right]^{N_2}, \tag{7}$$

where values of $J_{1,2}$ and $g_{1,2}$ are taken from Table II, k is the Boltzman constant, μ_B is the Bohr magneton, and we introduced the sub-partition functions Z_1 and Z_2 for convenience.

The free energy of the system of the Gd atoms (per formula unit) is:

$$F=-kT\ln Z=-f_1 n_d\left(E_{loc}+\Delta+kT\ln Z_1\right)-\left[f_1\left(1-n_d\right)+f_2\right]\cdot kT\ln Z_2. \tag{8}$$

And the chemical potential (per formula unit) is:

$$\mu=-\frac{\partial F}{\partial n_d}=E_{loc}+\Delta+f_1 kT\ln Z_1-f_1 kT\ln Z_2. \tag{9}$$

At equilibrium the chemical potential of the Gd atoms must be equal to the Fermi level (ϵ_F) of the conduction electrons. Thus, the following equality takes place:

$$E_{loc}-\varepsilon_F=-\Delta-f_1 kT\ln Z_1+f_1 kT\ln Z_2. \tag{10}$$

Using the Green function calculated above (Eq. 4), the Green function of an electron at the $5d$ level can be presented as follows:

$$G_{loc}(w)=\frac{1}{w-E_{loc}+G\left(1+n_d\right)-U+i\Gamma}. \tag{11}$$

After substituting the Green functions into the general equation of the occupancy of the excited localized level (n_d) and formal change of variables (see Eq. 12), one obtains the following self-consistent equation for n_d (see Eq. 13):

$$n_d=\frac{1}{\pi}\int_{-\infty}^{+\infty}\operatorname{Im}G_{loc}(\omega)\frac{d\omega}{1+\exp\left(\frac{\omega-\varepsilon_f}{kT}\right)} \quad \Leftarrow \quad x=\frac{1}{\Gamma}\left(\omega-E_{loc}+G\left(1+n_d\right)-U\right) \tag{12}$$

$$n_d=\frac{1}{\pi}\int_{-\infty}^{+\infty}\frac{dx}{x^2+1}\frac{1}{1+\exp\left(\frac{\Gamma}{kT}\left\{x+\frac{U-G\left(1+n_d\right)-\Delta-f_1 kT\ln Z_1+f_1 kT\ln Z_2}{\Gamma}\right\}\right)} \tag{13}$$

The integral (13) can be evaluated by using Euler digamma function $\Psi(x) = \frac{d \ln \Gamma(x)}{dx}$, where $\Gamma(x)$ is Gamma function:[14]

$$n_d = \frac{1}{2} + \frac{1}{\pi} \operatorname{Im} \Psi\left(\frac{1}{2} + \frac{\Gamma}{2\pi kT} - i \frac{1}{2\pi kT} \left\{ \underbrace{(U - G - \Delta)}_{A} - f_1 kT \ln Z_1 + f_1 kT \ln Z_2 - \underbrace{G}_{C} n_d \right\} \right) \Rightarrow$$

$$n_d = \frac{1}{2} + \frac{1}{\pi} \operatorname{Im} \Psi\left(\frac{1}{2} + \frac{\Gamma}{2\pi kT} - i \frac{1}{2\pi kT} \{ A - f_1 kT \ln Z_1 + f_1 kT \ln Z_2 - C n_d \} \right), \qquad (14)$$

where we have introduced the phenomenological parameters A and C.

The numerical solution of Eq. 14 allows us to calculate the temperature and magnetic field dependencies of the occupancy of the localized $5d$ level. The calculated theoretical temperature dependencies of the $5d$ level occupancy and temperature dependence of the critical field of electronic transition compared to the experimental H-T diagram of $Gd_5Sb_{0.7}Ge_{3.3}$ are presented in Fig. 21. The comparison of theoretically calculated temperature dependence of critical field of an electronic transition with the experimentally obtained H-T diagram of the Gd_5Ge_4 (Ref. 10) is shown in Fig. 22. One can see a good correspondence between theory and experiment. The parameters used in the calculations are listed in Table III and they are consistent with the electronic band structure of Gd_5Ge_4.[10] As we apply our theoretical model to the $Gd_5Sb_{0.7}Ge_{3.3}$ instead of the $Gd_5Sb_{0.5}Ge_{3.5}$ one has to adjust the number of the Gd atoms with an unpaired electron in $Gd_5Sb_xGe_{4-x}$ from 1.5 (x = 0.5) to 1.7 (x = 0.7), using a formal electron counting illustrated in Fig. 19. One notes that the parameters A and C are not independent, because $A = U - \Delta - C$, which means that an adjustment of the C parameter automatically affects the A parameter.

Table III Phenomenological parameters used in the calculation of the occupancy of the localized 5d level

	A (eV)	*Γ (eV)*	*C (eV)*	f_1	T_{cr} *(K)*
Gd_5Ge_4	0.0504	0.03	0.0939	1	128 K
$Gd_5Sb_{0.7}Ge_{3.3}$*	0.0504	0.03	0.0939	1.7	76 K*
$Gd_5Sb_{0.7}Ge_{3.3}$	0.0498	0.03	0.0945	1.7	60 K

* The estimation of transition temperature of $Gd_5Sb_{0.7}Ge_{3.3}$ based on band structure parameters of Gd_5Ge_4.

It is noted that the theoretical model explains the shift of the transition temperature when Ge is substituted for Sb. As in pure Gd_5Ge_4 the number of Gd atoms with unpaired electron per unit cell (f_1) is equal to 1 and in case of $Gd_5Sb_{0.7}Ge_{3.3}$ the value of f_1 is equal to 1.7. So if we fixed the phenomenological parameters of calculation in case of Gd_5Ge_4 and then change value f_1 from 1 to 1.7 one obtains a transition temperature of 76 K in a zero magnetic field (see "$Gd_5Sb_{0.7}Ge_{3.3}$*" raw in Table III), which is somewhat higher than experimentally observed 60 K. However, the addition of Sb will definitely affect the band structure and after a slight adjustment of C (see Table III) and, consequently, the A parameter (see Table III), the solution of Eq. 14 gives a transition temperature around 60 K.

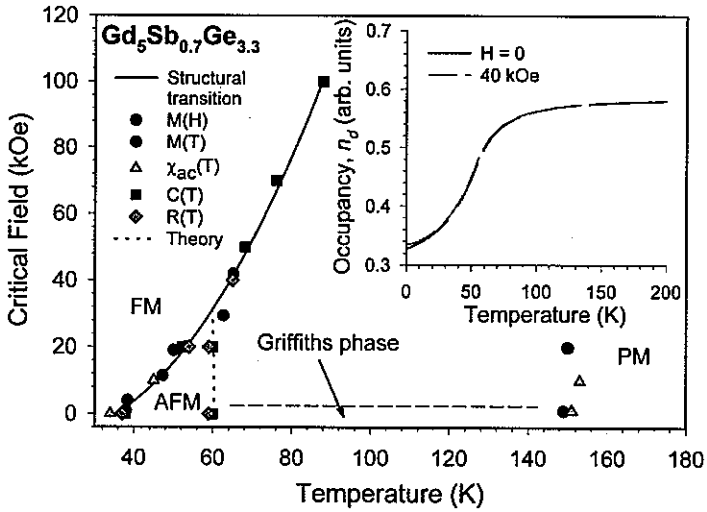

Fig. 21 The magnetic H-T phase diagram of polycrystalline $Gd_5Sb_{0.7}Ge_{3.3}$ constructed from the data of Ref. 8 with the line of the electronic transition fitted by theoretical curve (dotted line). The inset shows the theoretical temperature dependencies of occupancy n_d of 5d level. The dashed line indicates that the Griffiths-like phase exists only in magnetic fields below 1 kOe.

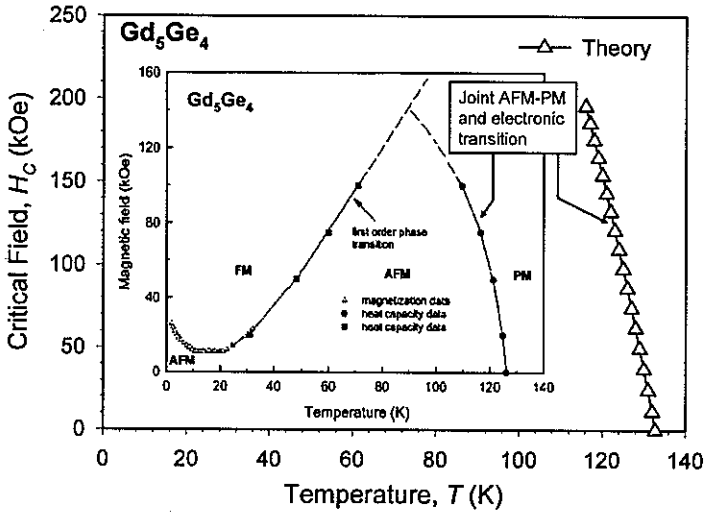

Fig. 22 The theoretically calculated joint AFM-PM and electronic transition boundary on the magnetic *H-T* phase diagram of Gd_5Ge_4 compared to experimental data from Ref. 10, shown in the inset.

Conclusion

In summary, the $Gd_5Sb_{0.5}Ge_{3.5}$ compound exhibits interesting magnetic, thermal electronic and crystallographic properties. The coupled magnetic structural transition in $Gd_5Sb_{0.5}Ge_{3.5}$ in the temperature interval 45 - 85 K and in magnetic fields from zero to 100 kOe exhibits large a volume change ($\Delta V/V$ = -0.5 %) and the giant magnetocaloric effect ΔS_M = -24 J/(kg K) (ΔH = 50 kOe) compared to the ~ -1 % volume change and -37 J/(kg K) (ΔH = 50 kOe) magnetic entropy change of the $Gd_5Si_{0.33}Ge_{3.67}$ compound [23] (transition temperature is ~ 70 K). Despite the smaller values of the volume change and the magnetocaloric effect, the $Gd_5Sb_{0.5}Ge_{3.5}$ compound exhibit smaller values of magnetic field (< 1 kOe vs. 5 kOe) and temperature (< 5 K vs. 10-15 K) hystereses, compared to $Gd_5Si_{0.33}Ge_{3.67}$ and the $Gd_5(Si_xGe_{1-x})_4$ alloys in general. The origin of the small hysteresis values is probably due to the fact that crystallographic transition occurs without change of the crystal structure type. That is a $\Delta V/V$ = -0.5 % volume change is observed and that there are no shear displacements of the slabs with respect to one another, as it is in Gd_5Ge_4 and $Gd_5(Si_xGe_{1-x})_4$.

Detailed low field magnetization measurements revealed the appearance of a Griffiths-like phase similar to the observed in $Tb_5Si_2Ge_2$, which may be of AFM type, as suggested by the observed negative values of paramagnetic Curie temperature. Moreover, inverse susceptibility (H/M) calculated from magnetization measurements along *a*-axis exhibits three distinct steps at 170 K, 220 K and 290 K, whereas the inverse susceptibility along *b*-axis exhibits steps at 170 K and 220 K and inverse susceptibility along *c*-axis as well as of polycrystalline exhibit a plateau only at 170 K. The observed three step behavior of *H/M* may come from the existence of three different scales of AFM clusters formation or three different preferred orientations of AFM axis of individual cluster.

A theoretical model is proposed to explain the observed electronic transition in $Gd_5Sb_{0.5}Ge_{3.5}$ and Gd_5Ge_4 and its evolution depending on antimony concentration. According to the model the electronic transition at low temperatures occurs due to transfer of the Gd atoms localized *5d* electrons not participating in the covalent bonding to the conduction band. The model qualitatively explains the lowering of the transition temperature with increasing Sb concentration due to an increase of the number of localized electrons per unit cell.

Acknowledgements

This work was supported by the Office of Basic Energy Sciences, Materials Sciences Division of the U.S. DOE under contract No. W-7405-ENG-82.

References

[1] V.K. Pecharsky and K.A. Gschneidner, Jr., Phys. Rev. Lett. **78**, 4494 (1997)

[2] L. Morellon, P.A. Algarabel, M.R. Ibarra, J. Blasco, B. Garcia-Landa, Z. Arnold, and F. Albertini, Phys. Rev. B **58**, R14721-R14724 (1998)

[3] E.M. Levin, A.O. Pecharsky, V.K. Pecharsky, and K.A. Gschneidner, Jr., Phys. Rev. B **63**, 064426/1-064426/10 (2001)

[4] V. K. Pecharsky, K. A. Gschneidner Jr., Adv. Mater. 13(9), 683 (2001)

[5] Yurij Mozharivskyj, Wonyoung Choe, Alexandra O. Pecharsky, and Gordon J. Miller, J. Am. Chem. Soc. **125**, 15183 (2203).

[6] W. Choe, V.K. Pecharsky, A.O. Pecharsky, K.A. Gschneidner, Jr., V.G. Young, Jr., G.J. Miller, Phys. Rev. Lett **84**, 4617 (2000)

[7] A.Yu. Kozlov, V.V. Pavlyuk, V.M. Davydov, Intermetallics **12**, 151 (2004)

[8] A.S. Chernyshov, Ya. S. Mudryk, V. K. Pecharsky and K. A. Gschneidner, Jr., J. Appl. Phys. **99**, 08Q102 (2006)

[9] A.O. Pecharsky, K.A. Gschneidner, Jr., V.K. Pecharsky and C.E. Schindler, J. Alloys Compd. **338**, 126 (2002).

[10] E.M. Levin, V.K. Pecharsky, K.A Gschneidner, Jr., G.J. Miller, Phys. Rev. B **64**, 235103 (2001).

[11] A.S. Mischenko and A.K. Zvezdin. Poster No 27PO-13-15, Moscow International Symposium on Magnetism MISM – 2005, (June 25 – 30, 2005, Moscow, Russia)

[12] L. M. Falikov and J. C. Kimball, Phys. Rev. Lett. **22**, 997(1969).

[13] M. Avignon and S.K. Ghatak, Sol. State Commun. **16**, 1243(1975).

[14] B. Coqblin and A. Blandin, Phys. Rev. **17**, 281 (1968).

[15] A. Aharoni, J. Appl. Phys. **83**, 3432 (1998).

[16] A. P. Holm, V. K. Pecharsky, K. A. Gschneidner, Jr., R. Rink, and M. N. Jirmanus, Rev. Sci. Instrum. **75**, 1081 (2004).

[17] B. Hunter, Rietica-A Visual Rietveld Program, International Union of Crystallography Commission on Powder Diffraction Newsletter No. 20, (Summer, 1998) http://www.rietica.org.

[18] V. K. Pecharsky, J. O. Moorman, and K. A. Gschneidner, Jr., Rev. Sci. Instrum. **68**, 4196 (1997).

[19] C. Magen, P.A. Algarabel, L. Morellon, J. P. Araujo, C. Ritter, M. R. Ibarra, A.M. Pereira and J. B. Sousa, Phys. Rev. Lett. **96,** 167201 (2006).

[20] Ya. Mudryk, A. P. Holm, K. A. Gschneidner, Jr., and V. K. Pecharsky, Phys. Rev. B **72,** 064442 (2005)

[21] R. B. Griffiths, Phys. Rev. Lett. **23,** 17 (1969).

[22] R. Ramirez and L. M. Falikov, Phys. Rev. B. **3,** 2425 (1971).

[23] V.K. Pecharsky and K.A. Gschneidner, Jr., Appl. Phys. Lett. **70,** 3299 (1997)

GENERAL CONCLUSIONS

Dysprosium

As a result of measuring the magnetization, *ac* magnetic susceptibility, heat capacity, and magnetocaloric effect of single crystals of Dy, and also the temperature and magnetic field dependent X-ray powder diffraction experiments we confirmed the majority of previous findings but also report some notable differences in the behaviors of the magnetothermal properties, especially in the vicinities of Curie, Neél and tricritical temperatures. When the magnetic field vector is parallel to the *a*-axis of a crystal, the refined *H-T* phase diagram of Dy is more complicated than previously thought, and it contains several new phases.

A peak of heat capacity at the Curie point in applied magnetic fields up to 20 kOe was observed and it is accompanied by minor anomalies on the temperature dependencies of *a*-lattice parameter. Then, an additional spin-flop phase appeared in the temperature interval 100 – 125 K and it has been explained by considering the Landau-Ginsburg theory of phase transitions. A theoretical model has been proposed to explain additional anomalies observed during the Fan-PM transition. It has also been shown that Fan magnetic structure becomes unstable at 170 K, whereas Dy becomes paramagnetic at 180 K. The anomalies of the magnetization and magnetocaloric effect were observed in the vicinity of Neél point and they may be caused by formation of vortex state in FM phase. A model has been proposed to explain the twice as large values of the magnetocaloric effect in PM region in a vicinity of Neel point due to due to formation of AFM clusters on impurities in samples of low purity.

An X-ray powder diffraction study was undertaken in the temperature interval 4 – 300 K in magnetic fields up to 40 kOe. Our measurements confirmed the complicated nature of magnetic field - temperature structural relationships in pure Dy and agree well with the heat capacity observations of our earlier paper. The main conclusion is that ferromagnetic structure is stable in the orthorhombically distorted crystal structure, whereas Helix, Fan and PM magnetic structures have lower energy in case of undistorted hexagonal lattice. The hexagonal-orthorhombic distortion and the pronounced anomaly in the *c*-lattice parameter are coupled with AFM-FM transition in magnetic fields below 8 kOe. However, on applying

magnetic field above 8 kOe our structural measurements show that these two phenomena are no longer coupled: the change along the *c*-axis occurs between 8 and 12 kOe and the orthorhombic distortion occurs between 8 and 20 kOe, this results in an increase in the number of ordered states of Dy.

$Gd_5Sb_xGe_{4-x}$

The crystallographic and magnetic properties of the $Gd_5Sb_xGe_{4-x}$ pseudo-binary alloys were studied by x-ray powder diffraction, heat capacity, magnetization and electrical resistivity in the temperature interval 5-320 K in applied *dc* magnetic fields between 0 and 100 kOe. The $Gd_5Sb_{2.1}Ge_{1.9}$ compound adopts the $Tm_5Sb_2Si_2$-type structure (space group Cmca) and orders magnetically via a second order ferromagnetic-paramagnetic transition at 200 K, whereas the $Gd_5Sb_xGe_{4-x}$ compounds with x = 0.7 and x = 1 crystallize in the Sm_5Ge_4-type structure (space group Pnma) and exhibit first order phase transformations at 45 K and 37 K, respectively, and therefore, the giant magnetocaloric effect. The heat capacity and electrical resistivity measurements of $Gd_5Sb_{0.7}Ge_{3.3}$ indicate a second order antiferromagnetic transition at 60 K in fields of 20 kOe and lower.

The $Gd_5Sb_xGe_{4-x}$ system exhibits interesting structural and magnetic properties along with a high value of the isothermal magnetic entropy change. Compared to the $Gd_5(Si_xGe_{1-x})_4$ system, the $Gd_5Sb_xGe_{4-x}$ system exhibits narrower hysteresis during the first order transformation and the samples with antimony are less brittle. The important parameters of the $Gd_5Sb_xGe_{4-x}$ and $Gd_5(Si_xGe_{1-x})_4$ system for practical applications, such as the hystereses, magnetic entropy change, volume change and transition temperature are listed in Table I. One can see that the giant magnetocaloric effect, and giant magnetostriction in $Gd_5Sb_xGe_{4-x}$ are accompanied by low values of temperature and magnetic field hystereses.

Table I The comparison of the $Gd_5Sb_xGe_{4-x}$ and $Gd_5Si_xGe_{4-x}$ systems.

	$Gd_5Sb_xGe_{4-x}$	$Gd_5Si_xGe_{4-x}$
Hysteresis (H)	< 1 kOe	5 kOe
Hysteresis (T)	< 5 K	10 -15 K
$\Delta Smax$ (ΔH = 50 kOe)	24 J/(kg K) (x = 0.5)	37 J/(kg K) (x = 0.33)
$\Delta V/V$ (%)	0.5 %	~ 1 %
Transition temperature	< 45 K	20 - 300 K

A study of crystallographic, magnetic, electronic and thermal properties of $Gd_5Sb_{0.5}Ge_{3.5}$ single crystal has been undertaken. It is seen from Table I that the coupled magnetic structural transition in $Gd_5Sb_{0.5}Ge_{3.5}$ in the temperature interval 45 - 85 K and in magnetic fields from zero to 100 kOe exhibits large a volume change ($\Delta V/V$ = -0.5 %) and the giant magnetocaloric effect ΔS_M = -24 J/(kg K) (ΔH = 50 kOe) compared to the ~ -1 % volume change and -37 J/(kg K) (ΔH = 50 kOe) magnetic entropy change of the $Gd_5Si_{0.33}Ge_{3.67}$ compound (transition temperature is ~ 70 K). Despite the smaller values of the volume change and the magnetocaloric effect, the $Gd_5Sb_{0.5}Ge_{3.5}$ compound exhibit smaller values of magnetic field (< 1 kOe vs. 5 kOe) and temperature (< 5 K vs. 10-15 K) hystereses, compared to $Gd_5Si_{0.33}Ge_{3.67}$ and the $Gd_5(Si_xGe_{1-x})_4$ alloys in general. The origin of the small hysteresis values is probably due to the fact that crystallographic transition occurs without change of the crystal structure type. That is a $\Delta V/V$ = -0.5 % volume change is observed and that there are no shear displacements of the slabs with respect to one another, as it is in Gd_5Ge_4 and $Gd_5(Si_xGe_{1-x})_4$.

Detailed low field magnetization measurements revealed the appearance of a Griffiths-like phase similar to the observed in $Tb_5Si_2Ge_2$, which may be of AFM type, as suggested by the observed negative values of paramagnetic Curie temperature. Moreover, inverse susceptibility (H/M) calculated from magnetization measurements along *a*-axis exhibits three distinct steps at 170 K, 220 K and 290 K, whereas the inverse susceptibility along *b*-axis exhibits steps at 170 K and 220 K and inverse susceptibility along *c*-axis as well as of polycrystalline exhibit a plateau only at 170 K. The observed three step behavior of

H/M may come from the existence of three different scales of AFM clusters formation or three different preferred orientations of AFM axis of individual cluster.

A theoretical model is proposed to explain the observed electronic transition in $Gd_5Sb_{0.5}Ge_{3.5}$ and Gd_5Ge_4 and its evolution depending on antimony concentration. According to the model the electronic transition at low temperatures occurs due to transfer of the Gd atoms localized 5*d* electrons not participating in the covalent bonding to the conduction band. The model qualitatively explains the lowering of the transition temperature with increasing Sb concentration due to an increase of the number of localized electrons per unit cell.

Recommendations for future work

(1) Although a study of Dy single crystal was undertaken and most of the anomalies were at least qualitatively explained, there are a few features that still need further explanation. One of them is the appearance of the heat capacity peak at 90 K in applied magnetic fields, whereas only a minor anomaly of the heat capacity occurs at the coupled magnetic – structural transition.

(2) The proposed phenomenological model of the influence of the commensurability point in magnetic phase diagram needs to be confirmed by detailed neutron scattering experiments in a vicinity of commensurability point (113 K). Further experimental investigations of other systems that exhibit helix magnetic ordering should be carried out.

(3) The main disadvantage of $Gd_5Sb_xGe_{4-x}$ system is its low transition temperature, which limits potential applications of the material. So the next step will be to increase the transition temperature together with important properties, such as the conservation of the crystal structure symmetry during the coupled magnetic-structural transition that decreases the temperature and magnetic field hystereses.

(4) The appearance of Griffiths phase in $Gd_5Sb_{0.5}Ge_{3.5}$ is based on macroscopic observation, and it needs to be verified by direct neutron scattering experiments.

(5) A model of the electronic transition in $Gd_5Sb_{0.5}Ge_{3.5}$ and Gd_5Ge_4 is mostly based on electrical resistivity measurements of polycrystalline materials, so the next step will be to carry out single crystal electrical resistivity measurements along three different crystallographic directions and further development of the model to fit experimental data.

ACKNOWLEDGEMENTS

I would like to express my sincere gratitude to all the people who became involved with this work. Especially I am very thankful to my major professors Vitalij K. Pecharsky and K.A. Gschneidner, Jr. for a wonderful and productive time I spent at Ames Laboratory. This work would not be done without great help of assistant scientist Yaroslav S. Mudryk throughout all my work in the lab. Also I would like to thank my committee members for useful discussions, especially professor Gordon J. Miller, who unfortunately, was not able to attend my final defense. And I would like to thank all the graduate students and postdocs in the group for their help in experiments and useful discussions.

This work was supported by the Office of Basic Energy Sciences, Materials Sciences Division of the U.S. DOE under contract No. W-7405-ENG-82.

APPENDIX: MAGNETIC STRUCTURES OF DYSPROSIUM

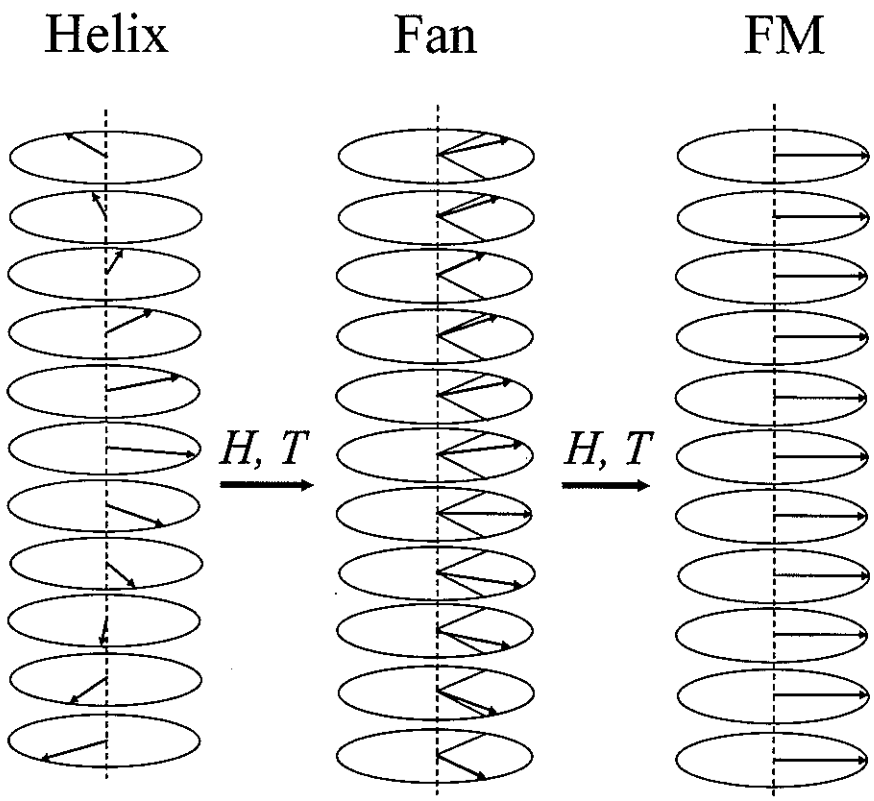

Fig. 1. The magnetic structures of Dy: from left to right helix, fan, ferromagnetic (FM)